Dissertation

submitted to the
Combined Faculties of the Natural Sciences and Mathematics
of the Ruperto Carola University of Heidelberg, Germany,
for the degree of
Doctor of Natural Sciences

Put forward by
Pascal Humbert

Born in Wiesbaden, Germany
Oral examination: July 21, 2016

This page is intentionally left blank

Alternative Electroweak Symmetry Breaking based on Conformal Extensions of the Standard Model

Referees:
Prof. Dr. Manfred Lindner
and
Prof. Dr. Joerg Jaeckel

This page is intentionally left blank

Abstract

In order to address the hierarchy problem and to simultaneously explain small neutrino masses, we study conformal extensions of the Standard Model (SM), which realize an inverse seesaw mechanism. Furthermore, we give a systematic discussion of the neutrino mass matrix in a generalized type-I seesaw set-up.

We study the conformal inverse seesaw mechanism (CISS), in which the conformal symmetry is spontaneously broken via the Coleman-Weinberg mechanism at a few TeV. We confirm that in this set-up the electroweak vacuum expectation value and the Higgs mass are obtained within experimental uncertainties. The scalar sector in the broken phase contains, besides the Higgs, a massive scalar with a mass in the TeV-range and the pseudo-Goldstone boson of broken scale invariance with a mass of the order of hundreds of GeV. The CISS also features a hidden Abelian gauge symmetry. We show that the CISS generates active neutrino masses and mixings in agreement with oscillation data. Additionally, the neutrino spectrum contains a warm dark matter (DM) candidate with mass in the keV-range and tiny mixing of the order of 10^{-10} or smaller to the active neutrinos. Furthermore the CISS comprises sterile neutrinos with pseudo-Dirac masses, which can be as large as several TeV. The active-sterile mixing obtained in the model is naturally sizable.

In the extended conformal inverse seesaw (ECISS), the new gauge group is identified with $\mathrm{U}(1)_{B-L}$. The scalar and neutrino sectors of the CISS are altered to allow for a large Majorana mass for the right-handed neutrinos leading to ample lepton number violation (LNV). Besides LNV, the phenomenology of the CISS is maintained. We show that the contributions of the heavy sterile neutrinos to the effective Majorana mass of neutrinoless double beta decay can saturate current limits on the half-life. In both the CISS and ECISS the new particles lead to collider signatures above SM backgrounds, which should leave a clear signal in Run 2 at the Large Hadron Collider (LHC). In particular, the Z' associated with $\mathrm{U}(1)_{B-L}$ and the sterile neutrinos in the ECISS produce LNV signals. For a luminosity of 300 fb^{-1} at a center-of-mass energy of 14 TeV the ECISS predicts a signal at the LHC of about 400 events in the same-sign di-lepton channel plus two hadronic jets, which is induced by sterile neutrinos with a mass of 500 GeV.

In the last part of the thesis we systematically analyze the neutrino mass matrix obtained in a generalized type-I seesaw. The set-up contains two different neutrino species with arbitrary numbers of generations that are connected via a Dirac mass. One species is assumed to possess an arbitrary Majorana mass term. This includes Majorana masses much larger or much smaller than the Dirac mass, vanishing Majorana mass or a singular structure. In this set-up, a general prediction for the number of vanishing eigenvalues is derived. We discover that many scenarios are related to others, thereby, simplifying the analysis. The eigenvalue spectra of the mass matrices for all non-singular scenarios and for one scenario with a singular set-up are obtained.

This page is intentionally left blank

Zusammenfassung

Um uns des Hierarchieproblems anzunehmen und gleichzeitig kleine Neutrinomassen zu erklären, studieren wir konforme Erweiterungen des Standardmodells (SM), die einen inversen Seesaw realisieren. Außerdem legen wir eine systematische Auseinandersetzung mit der Neutrinomassenmatrix in einer verallgemeinerten Typ-I Seesaw-Anordnung dar.

Wir studieren den konformen inversen Seesaw(CISS)-Mechanismus, in dem die konforme Symmetrie bei einigen TeV spontan durch den Coleman-Weinberg-Mechanismus gebrochen wird. Wir bestätigen, dass der elektroschwache Vakuumerwartungswert und die Higgsmasse in diesem Aufbau innerhalb der experimentellen Ungenauigkeiten erhalten werden. Der skalare Sektor enthält in der gebrochenen Phase neben dem Higgs einen massiven Skalar mit einer Masse im TeV-Bereich und das Pseudo-Goldstone-Boson der gebrochenen Skaleninvarianz mit einer Masse in der Größenordung von hunderten von GeV. Der CISS führt auch eine versteckte Abelsche Eichsymmetrie mit sich. Wir zeigen, dass der CISS aktive Neutrinomassen und -mischungen im Einklang mit Oszillationsdaten erzeugt. Zusätzlich beinhaltet das Neutrinospektrum einen warmen Dunkle-Materie(DM)-Kandidaten mit einer Masse im keV-Bereich und winziger Mischung in einer Größenordnung von 10^{-10} oder weniger zu den aktiven Neutrinos. Darüber hinaus umfasst der CISS sterile Neutrinos mit Pseudo-Dirac-Massen, die bis zu einigen TeV groß sein können. Die im Modell erhaltene aktiv-sterile Mischung ist naturgemäß groß.

Im erweiterten konformen inversen Seesaw (ECISS) wird die neue Eichgruppe mit $\mathrm{U}(1)_{B-L}$ identifiziert. Der Skalar- und Neutrinosektor des CISS werden verändert, um eine große Majorana-Masse für die rechtshändigen Neutrinos zu erlauben, was zu einer reichhaltigen Leptonzahlverletzung (LNV) führt. Bis auf die LNV bleibt die Phänomenologie des CISS erhalten. Wir zeigen, dass die Beiträge der schweren sterilen Neutrinos zur effektiven Majorana-Masse des neutrinolosen Doppel-Beta-Zerfalls die derzeitigen Grenzen für die Lebensdauer sättigen können. Sowohl im CISS wie auch im ECISS führen die neuen Teilchen zu Kollidierer-Signaturen über dem SM-Hintergrund, die ein deutliches Signal in Run 2 am Large Hadron Collider (LHC) hinterlassen sollten. Insbesondere das der $\mathrm{U}(1)_{B-L}$ zugehörige Z' und die sterilen Neutrinos erzeugen LNV Signale. Für eine Luminosität von 300 fb^{-1} und bei einer Energie im Ruhesystem von 14 TeV sagt der ECISS ein Signal am LHC voraus von etwa 400 Ereignissen im same-sign di-lepton Kanal mit zwei hadronischen Jets, das von sterilen Neutrinos mit einer Masse von 500 GeV hervorgerufen wird.

Im letzten Teil der Arbeit analysieren wir die aus einem verallgemeinerten Typ-I Seesaw erhaltene Neutrinomassenmatrix systematisch. Der Aufbau enthält zwei verschiedene Neutrinoarten mit beliebigen Anzahlen von Generationen, die über eine Dirac-Masse verbunden sind. Von einer Art wird angenommen, dass sie einen willkürlichen Majorana-Massenterm besitzt. Das schließt Majorana-Massen mit ein, die viel größer oder viel kleiner als die Dirac-Masse sind, verschwindende Majorana-Massen oder eine singuläre Struktur. In dieser Anordnung wird eine allgemeine Vorhersage über die Anzahl der verschwindenden Eigenwerte hergeleitet. Wir entdecken, dass viele Szenarios mit anderen in Verbindung stehen, was die Analyse vereinfacht. Die Eigenwertspektren der Massenmatrizen für alle nicht-singulären Szenarios und für ein Szenario mit einem singulären Aufbau werden gewonnen.

This page is intentionally left blank

Disclaimer

The results of this work presented in Chapters 3 and 4 have already been published and were done in collaboration with others: Chapter 3 is based on Reference [1] in collaboration with M. Lindner and J. Smirnov; Chapter 4 is based on Reference [2] together with M. Lindner, S. Patra and J. Smirnov. The research presented in Chapter 5 has not been published yet and represents original work by the author.

This page is intentionally left blank

Acknowledgements

First of all, I wish to express my gratitude to my supervisor, Prof. Manfred Lindner, for accepting me as his PhD student and for giving me the opportunity to study physics in such a nice atmosphere. In these past three years I have been able to learn a lot from his wisdom and excellent guidance.

I am also indebted to Juri Smirnov for all the time he spent deepening my insights about physics and sharing his knowledge with me. I owe my gratitude to Alexander Helmboldt, Moritz Platscher and Kai Schmitz for carefully proofreading this thesis and for the many helpful discussions, valuable suggestions and honest advices. I am grateful to Julia Haser for her motivational support and to Miguel "Herr Bismarck" Campos for his creative ideas. I thank Michael Dürr for his mentoring in the first phase of my PhD. I also thank all the seniors, the postdocs, the PhD students, the master and bachelor students and the rest of the division for creating such an inspiring and equally fun environment.

Finally, I am grateful to Janina Kirsch and to my parents Karin and Gerhard Humbert for being there for me and for the love they give.

This page is intentionally left blank

Contents

Chapter 1

Introduction

> ... after all, our purpose in theoretical physics is not just to describe the world as we find it, but to explain – in terms of a few fundamental principles – why the world is the way it is.
>
> *Steven Weinberg*

The triumphal march of the Standard Model of particle physics was finally completed by the discovery of the theory's last missing piece, the Higgs boson, in the year 2012 [3, 4]. However, the smallness of that particle's mass requires a severe fine-tuning known as the gauge hierarchy problem [5–9]. In essence, the problem states that if the Standard Model is embedded into another gauge theory, whose symmetry is spontaneously broken at some high energy scale, the Higgs mass, due to quantum effects, will receive corrections, which are quadratically sensitive to the scale of the high-energy quantum field theory. This high energy scale and, accordingly, the Higgs mass are expected to be extremely large. Typical examples for such large scales are the scale of grand unification, or the Planck scale associated with gravity. In contradiction to this expectation the observed value of the Higgs mass is of the order of the relatively small electroweak scale of the Standard Model [10]. So how can the hierarchy problem be solved?

The most famous attempt to overcome the gauge hierarchy problem is supersymmetry [11, 12]. In that framework each Standard Model particle possesses a superpartner with opposite statistics. In presence of the superpartners the quadratic corrections are systematically cancelled and the hierarchy problem cannot emerge. But, as to date no supersymmetric particles have been discovered at the Large Hadron Collider [13, 14], an increasing tension is placed on the viable parameter space of supersymmetric models with a symmetry breaking scale close to the electroweak scale. Supersymmetry breaking at a certain distance to the electroweak scale, however, reintroduces the hierarchy problem. Other theories that are able to solve the hierarchy problem include technicolor [15–17] and composite-Higgs models [18–20], extra-dimensions [21, 22], and theories based on

a scale-invariant Lagrangian [23]. In this thesis we will focus on the latter class of theories, which we will (in slight abuse of terminology) refer to as conformal theories.

In a conformal theory no dimensional couplings and, in particular, no masses are allowed in the Lagrangian by the conformal symmetry. However, in a generic quantum field theory the conformal symmetry is anomalous. As argued by Bardeen, this conformal anomaly can only lead to logarithmic divergences, but not to quadratic ones [23]. A further justification for Bardeen's argument was given in [24] in the context of the Wilsonian approach to renormalization theory [25]. Consequently, the gauge hierarchy problem does not appear in conformal theories.

The spontaneous breaking of the electroweak symmetry [26–28] within the Higgs mechanism [29–31] represents one of the cornerstones of the Standard Model. But, actually, it has to face several difficulties besides the aforementioned hierarchy problem. First, the assumption that the mass parameter of the Higgs potential in the unbroken phase is negative in order to create a non-trivial minimum is merely of technical nature. The origin of spontaneous symmetry breaking, however, remains obscure. Second, studies related to triviality [32] and the stability [33–35] of the Higgs potential, which are sensitive to the Higgs mass and the top-quark mass, suggest that the ground state of the Universe happens to reside in a very special region of the available parameter space that allows for a renormalization group evolution of the Standard Model up to the Planck scale without encountering Landau poles or instabilities. As the particles' masses are not predicted by the theory, the Standard Model gives no explanation for such a 'convenient' parameter choice. Third, the electroweak theory cannot incorporate the emergence of the Planck scale. Nevertheless, the *future* Standard Model of high-energy physics ultimately needs to include the effects of gravity. Because of these shortcomings, we argue that it is vital to investigate alternatives to the electroweak symmetry breaking in the Standard Model. The fact that the Standard Model with a vanishing Higgs mass parameter becomes scale invariant may be interpreted as a hint at an underlying conformal symmetry in Nature.

The spontaneous breakdown of a conformal symmetry can be triggered by radiative corrections as described in the Coleman-Weinberg mechanism [36]. Soon, it was realized that the Coleman-Weinberg mechanism does not work for the scalar sector of the Standard Model, since the Coleman-Weinberg effective potential is unbounded from below, when the top quark is heavier than the Z boson [37]. Consequently, the scalar sector in the Standard Model needs to be extended by new degrees of freedom in order to allow for spontaneous conformal symmetry breaking. This necessity can be turned into a merit. If more scalar particles are included in the theory, this naturally allows for a richer phenomenology. With the additional particles one always obtains new couplings in the scalar potential. The couplings, however, are not arbitrary, but possess a strong interdependence, which is caused by spontaneous symmetry breaking. This gives conformal theories considerable predictive power. In this context, the aforementioned convenient values that allow for a consistent extrapolation up to the Planck scale of

the parameters in the scalar potential may be understood as a consequence of the requirements for successful spontaneous conformal symmetry breaking. Another prediction of the Coleman-Weinberg mechanism is that there can be only one symmetry breaking scale, which must lie close to the electroweak scale. This means that the new particles required by the conformal symmetry are in principle accessible at the Large Hadron Collider. As was pointed out in [38], the Planck scale might emerge from a non-renormalizable theory of quantum gravity, which gives rise to an effective conformal theory at energies below the Planck scale. We note that similar ideas (but without the explicit referral to conformal theories) were discussed in [39]. The positive prospects of conformal theories have drawn a substantial amount of attention in recent years [40–69].

A different issue of the Standard Model is how to accommodate small but finite neutrino masses in the theory. Almost a century after Pauli "... postulated a particle that cannot be detected"[1] [71], and 60 years after its first detection due to Cowan *et al.* [72], the neutrino still remains an elusive particle at the present day. Originally, neutrinos were assumed to be massless and, consequently, there was no need to include right-handed neutrinos into the particle content of the Standard Model. However, the observation of neutrino oscillations in solar, atmospheric, reactor and accelerator beam neutrino experiments [73–76] have shown that neutrinos are in fact massive. Hence, neutrino oscillations constitute a first direct evidence for physics beyond the Standard Model. However, compared to the other fermions the neutrinos must have extremely small masses. This raises two questions: How do neutrinos become massive? And why are their masses so small?

As for the other fermions, the masses for neutrinos could also be generated in the Higgs mechanism provided the Standard Model's particle content is extended by right-handed neutrino fields. This, however, does not answer the second question as it would require neutrino Yukawa couplings many orders of magnitude smaller than those for the charged leptons. A different possibility was realized by Weinberg [77]. He suggested that neutrino masses could be obtained from an effective dimension-5 operator (now called the Weinberg operator), which can already be constructed using Standard Model fields only. The interaction behind this operator is assumed to be mediated by a super-heavy particle, whose mass effectively suppresses the neutrino mass, thereby, explaining the smallness of the latter. Note that the neutrino mass generated in this way violates lepton number.

The most popular way of generating naturally small neutrino masses is the seesaw mechanism, which was first formulated in [78–81]. The basic idea of the seesaw relies on augmenting the theory by right-handed neutrinos, which do not participate in the interactions of the Standard Model. As these new neutrinos are gauge singlets they can possess a bare Majorana mass. Since this mass has no connection to the electroweak symmetry breaking scale, it can in principle be arbitrarily large. Eventually, the seesaw mechanism leads to a suppression of the Standard Model neutrino masses, which is found to be inversely proportional to

[1] As quoted by F. Reines in the foreword to [70].

the potentially large Majorana mass. As the seesaw mechanism represents a tree-level realization of the Weinberg operator, the small neutrino masses generated this way violate lepton number.

It was pointed out in [60] that the inverse seesaw mechanism [82–84] in the context of a conformal theory could possibly lead to an interesting phenomenology including electroweak precision tests, collider signatures and dark matter. In order to address the hierarchy problem and to explain small neutrino masses we are led to study the conformal inverse seesaw mechanism. Additionally, we will systematically analyze the neutrino mass matrix in a generalized seesaw mechanism set-up to gain further insight into neutrino masses.

The outline of this thesis is as follows. In Chapter 2 we briefly review electroweak symmetry breaking in the Standard Model. There, we will also discuss physics beyond the Standard Model in correlation with this work. The model of the conformal inverse seesaw mechanism is introduced in Chapter 3. After deriving the neutrino mass spectrum and mixing pattern as well as the spontaneous conformal symmetry breaking of the model, we will discuss the predicted phenomenology in connection with electroweak precision test, collider signatures and dark matter. In Chapter 4 the so-called conformal inverse seesaw is extended in order to allow for large lepton number violation. We will discuss how this can be achieved without altering the established phenomenology of active neutrino masses and mixing, of electroweak precision tests and of dark matter. Then, we will examine the possibilities for neutrinoless double beta decay and same-sign di-lepton signals in the extended conformal seesaw. The systematic examination of the neutrino mass matrix in the generalized seesaw scenario is presented in Chapter 5. There, we will predict how many vanishing eigenvalues exist in the generalized set-up of the neutrino mass matrix. Furthermore, we will derive the eigenvalue spectra of several different structures of the neutrino mass matrix. Finally, we will summarize our results and provide an outlook in Chapter 6.

Chapter 2

The Standard Model and beyond

The Standard Model (SM) of particle physics is the quantum field theory (QFT) of the strong, weak and electromagnetic interactions. The description of the latter two is combined in the electroweak theory [26–28]. Within the Higgs mechanism [29–31] the electroweak gauge symmetry is spontaneously broken by the vacuum, leaving only the strong and electromagnetic gauge groups as remaining symmetries of the theory. The mechanism of electroweak symmetry breaking (EWSB) is induced when the potential of a scalar particle, the Higgs boson, develops a non-trivial minimum at a finite vacuum expectation value (vev). The vev, in turn, generates masses for the SM fermions, for the weak gauge bosons associated with the spontaneously broken symmetry groups and, finally, for the Higgs itself. The dynamics of the fermions in the broken phase of the electroweak theory are described by the charged- and neutral-current interactions, and by quantum electrodynamics.

We will briefly review EWSB in the SM in Section 2.1. Afterwards, in Section 2.2, we will take up the aspects of physics beyond the SM (BSM) in correlation with this work, namely, neutrino masses and the seesaw mechanism, lepton number violation, dark matter and conformal theories.

2.1 The Standard Model of particle physics

The outline of this section is as follows. First, the SM gauge group and particle content will be introduced. Then we will discuss the spontaneous breaking of the electroweak gauge symmetry in the SM by the vev of the Higgs. Following this, we will see how, by virtue of EWSB, gauge-invariant fermion mass terms are obtained. Finally we will discuss the charged-current interactions between the charged weak gauge bosons and the fermions in the presence of neutrino masses. There, the lepton mixing matrix will be introduced. The information, on which this section is based on, can be found in any introductory QFT textbook, see e.g. [85, 86].

Table 2.1: The fermion and scalar field content of the Standard Model. The $\mathrm{SU(3)_c}$ and $\mathrm{SU(2)_L}$ rows show to which representation of the corresponding gauge group the fields belong, and the $\mathrm{U(1)_Y}$ row specifies the Abelian hypercharge quantum number of the fields. The indices α and β label the flavor of the quarks and leptons, respectively. Note the absence of a right-handed neutrino field in the Standard Model.

field	$Q_{\mathrm{L}}^{\alpha} = \begin{pmatrix} u_{\mathrm{L}}^{\alpha} \\ d_{\mathrm{L}}^{\alpha} \end{pmatrix}$	u_{R}^{α}	d_{R}^{α}	$L_{\mathrm{L}}^{\beta} = \begin{pmatrix} \nu_{\mathrm{L}}^{\beta} \\ \ell_{\mathrm{L}}^{\beta} \end{pmatrix}$	ℓ_{R}	$H = \begin{pmatrix} H^{+} \\ H^{0} \end{pmatrix}$
$\mathrm{SU(3)_c}$	**3**	**3**	**3**	**1**	**1**	**1**
$\mathrm{SU(2)_L}$	**2**	**1**	**1**	**2**	**1**	**2**
$\mathrm{U(1)_Y}$	$1/6$	$2/3$	$-1/3$	$-1/2$	-1	$1/2$

The SM is a gauged QFT with the local symmetry group

$$G_{\mathrm{SM}} = \mathrm{SU(3)_c} \times \mathrm{SU(2)_L} \times \mathrm{U(1)_Y}\,,$$

where the indices label the groups as color, weak isospin, and hypercharge, respectively. The gauge bosons belonging to the groups are called gluons for $\mathrm{SU(3)_c}$ and electroweak gauge bosons for $\mathrm{SU(2)_L} \times \mathrm{U(1)_Y}$. We will denote them by

$$\begin{aligned} \mathrm{SU(3)_c} &: \quad g_{\mu}^{i} \quad i = 1, \ldots, 8\,; \\ \mathrm{SU(2)_L} &: \quad W_{\mu}^{i} \quad i = 1, 2, 3\,; \\ \mathrm{U(1)_Y} &: \quad B_{\mu}\,. \end{aligned}$$

The properties of the SM scalar and fermionic particles with respect to the gauge groups are listed in Table 2.1.

2.1.1 Electroweak symmetry breaking

In the SM the Higgs possesses a mass parameter μ^2 and quartic self-interactions λ. Accordingly, the SM scalar potential is given by

$$V(H) = \mu^2 H^{\dagger} H + \lambda (H^{\dagger} H)^2\,, \tag{2.1}$$

where the Higgs doublet $H = (H^{+},\, H^{0})^{\intercal}$ has been introduced in Table 2.1. In order to be stable, the potential in Eq. (2.1) must be bounded from below for large field values, which requires $\lambda \geq 0$. Then for $\mu^2 \geq 0$ it only possesses a trivial minimum. However, under the assumption that the mass parameter is negative, $\mu^2 = -|\mu^2| < 0$, the potential develops a non-trivial minimum at the field value

$$v_{\mathrm{ew}} \equiv \sqrt{|\mu^2|/\lambda}\,. \tag{2.2}$$

This field value defines the vev in the SM.[1] We illustrate the Higgs or "Mexican hat" potential, which is obtained for a negative mass parameter μ^2, in Figure 2.1.

[1] Note that in theories with more involved symmetry breaking patterns, as is the case in conformal theories, which are the subject of this study, there can emerge vevs that are distinct from the one in the SM. To make this distinction apparent we denote the vev of EWSB *in the SM* by v_{ew}. The numerical value of v_{ew} is given in Eq. (2.13).

Figure 2.1: Higgs potential in the complex plane of the Higgs boson's neutral component H^0 in the SM obtained for a negative mass parameter. The subspace of the charged component is suppressed. The minimum of the potential lies at a non-zero field value. Note the angular degeneracy of the potential's minimum.

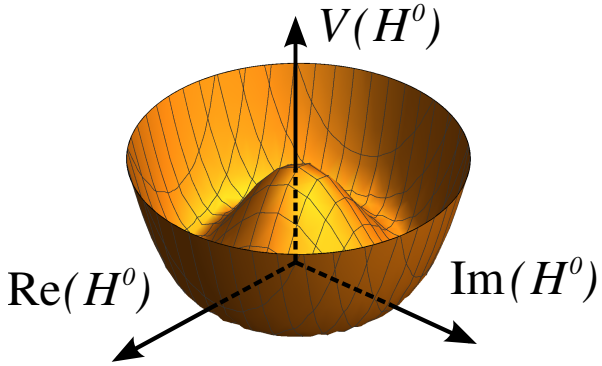

In the figure the potential is restricted to the complex plane of the Higgs boson's neutral component H^0. Note that the Mexican hat potential possesses a rotational symmetry with respect to the phase of H^0, which in particular holds for the minimum. Accordingly, a possible phase of the vev can always be absorbed and is not physical. Furthermore, we can use the three gauge degrees of freedom of the generators that get spontaneously broken by the Higgs vev to gauge away the Goldstone modes of the Higgs. A particularly convenient choice is the unitary gauge, in which only physical particles remain in the Lagrangian. In this gauge the Higgs takes on the following simple form

$$H = \begin{pmatrix} H^+ \\ H^0 \end{pmatrix} = \frac{1}{\sqrt{2}} \begin{pmatrix} h_1 + \mathrm{i}h_2 \\ h_3 + \mathrm{i}h_4 \end{pmatrix} \overset{\text{u.g.}}{=} \frac{1}{\sqrt{2}} \begin{pmatrix} 0 \\ h_3 \end{pmatrix} , \tag{2.3}$$

where the last expression is obtained after imposing the unitary gauge. We can expand the Higgs field around its minimum, which was given in Eq. (2.2), by replacing

$$h_3(x) \to v_{\text{ew}} + h_3(x) . \tag{2.4}$$

When we insert the above expansion into the kinetic term for the Higgs, we obtain the expressions and masses for the physical gauge bosons in the broken phase of electroweak theory. The weak gauge bosons are defined as

$$W_\mu^\pm = \tfrac{1}{\sqrt{2}} \left(W_\mu^1 \mp \mathrm{i} W_\mu^2 \right) , \tag{2.5}$$

$$Z_\mu = \frac{g W_\mu^3 - g' B_\mu}{(g^2 + g'^2)^{1/2}} = \cos\theta_{\text{W}} W_\mu^3 - \sin\theta_{\text{W}} B_\mu , \tag{2.6}$$

$$\sin\theta_{\text{W}} = \frac{g'}{(g^2 + g'^2)^{1/2}} , \qquad \cos\theta_{\text{W}} = \frac{g}{(g^2 + g'^2)^{1/2}} . \tag{2.7}$$

In the last of the above equations we have introduced the Weinberg angle θ_{W}. The other linear combination of the gauge fields, namely

$$A_\mu = \frac{g' W_\mu^3 + g B_\mu}{(g^2 + g'^2)^{1/2}} = \sin\theta_{\mathrm{W}} W_\mu^3 + \cos\theta_{\mathrm{W}} B_\mu \,, \tag{2.8}$$

is the photon field. Since the physical Higgs is electrically neutral, the photon does not couple to it and remains massless. In fact, the charged degrees of freedom of the Higgs, which would in principle couple to the photon, get eaten by the $W^\pm$ bosons and become their longitudinal degree of freedom. A third degree of freedom of the Higgs gets eaten by the Z boson. Note that we can express W_μ^3 and B_μ through Z_μ and A_μ according to

$$\begin{pmatrix} W_\mu^3 \\ B_\mu \end{pmatrix} = \begin{pmatrix} \cos\theta_{\mathrm{W}} & \sin\theta_{\mathrm{W}} \\ -\sin\theta_{\mathrm{W}} & \cos\theta_{\mathrm{W}} \end{pmatrix} \begin{pmatrix} Z_\mu \\ A_\mu \end{pmatrix} . \tag{2.9}$$

After EWSB, the weak gauge bosons and the Higgs become massive. From the kinetic term and the potential of the Higgs their masses can be derived according to

$$m_W^2 = \frac{g^2 v_{\mathrm{ew}}^2}{4} \,, \tag{2.10}$$

$$m_Z^2 = \frac{g^2 v_{\mathrm{ew}}^2}{4\cos^2\theta_{\mathrm{W}}} = \frac{m_W^2}{\cos^2\theta_{\mathrm{W}}} \,, \tag{2.11}$$

$$m_{\mathrm{Higgs}}^2 = 2\lambda v_{\mathrm{ew}}^2 \,. \tag{2.12}$$

The value of the SM vev is related to Fermi's constant G_{F} according to

$$v_{\mathrm{ew}}^2 = \tfrac{1}{\sqrt{2}} G_{\mathrm{F}}^{-1} = (246.221\ \mathrm{GeV})^2 \qquad \text{with} \qquad G_{\mathrm{F}} = \frac{\sqrt{2}}{8}\frac{g^2}{m_W^2} \,. \tag{2.13}$$

The numerical value for Fermi's constant is given by $G_{\mathrm{F}} = 1.1663787 \times 10^{-5}\ \mathrm{GeV}^{-2}$ [87] to very good precision. We also quote the numerical value of the Weinberg angle, which at m_Z in the $\overline{\mathrm{MS}}$ scheme is given by $\sin^2\theta_{\mathrm{W}} = 0.23126$ [87].

2.1.2 Fermion mass terms

So far we have not considered mass terms for the fermions. We define the Dirac mass term for a spinor $\psi^\alpha = \psi_{\mathrm{L}}^\alpha + \psi_{\mathrm{R}}^\alpha$, where α is a flavor index, according to

$$\mathcal{L}_{\mathrm{mass}}^{\mathrm{Dirac}} = -m_{\alpha\beta}\, \overline{\psi_{\mathrm{L}}^\alpha} \psi_{\mathrm{R}}^\beta + \mathrm{h.c.} \quad \text{with} \quad m_{\alpha\beta} = m_{\beta\alpha}^* \,. \tag{2.14}$$

For the charge conjugation of a left-handed spinor field we first define the unitary charge conjugation matrix C through the following relation with the Dirac γ-matrices

$$C^\dagger \gamma_\mu C = -\gamma_\mu^{\intercal} \,, \tag{2.15}$$

and then choose as convention

$$\psi_{\mathrm{L}}^{\mathrm{c}} \equiv (\psi_{\mathrm{L}})^{\mathrm{c}} = P_{\mathrm{R}}\, C\, \overline{\psi}^{\mathsf{T}}\,, \tag{2.16}$$

where P_{R} denotes the right-handed projection operator. Note that with this convention the index L/R of a particle, at first, is to be understood as a *label* and not as an indicator of the chirality. In particular, the charge conjugate of a field has opposite chirality as indicated by the label. However, we naturally preserve the relations $P_{\mathrm{L}}\psi_{\mathrm{L}} = \psi_{\mathrm{L}}$ and $P_{\mathrm{R}}\psi_{\mathrm{L}} = 0$ for the original spinor. A particle ψ is called a Majorana particle if it satisfies the Majorana condition given by

$$\psi = \psi^{\mathrm{c}} \tag{2.17}$$

up to a complex phase. Note that the above equation implies that $\psi = \psi_{\mathrm{L}} + \psi_{\mathrm{L}}^{\mathrm{c}}$ is a Majorana particle. We define the Majorana mass term for a left-handed spinor as [88]

$$\mathcal{L}_{\mathrm{mass}}^{\mathrm{Majorana}} = -\tfrac{1}{2} m_{\alpha\beta}\, \overline{\psi_{\mathrm{L}}^{\alpha}} \psi_{\mathrm{L}}^{\beta,\,\mathrm{c}} + \mathrm{h.c.} \text{ with } \; m_{\alpha\beta} = m_{\beta\alpha}\,. \tag{2.18}$$

Note, however, that in the SM the bare mass terms in Eqs. (2.14) and (2.18) are not gauge-invariant and hence forbidden. Then again, the Yukawa interactions with the Higgs

$$\mathcal{L}_{\mathrm{Yukawa}} = -y_{\alpha\beta}^{(u)}\, \overline{Q_{\mathrm{L}}^{\alpha}}\, \widetilde{H} u_{\mathrm{R}}^{\beta} - y_{\alpha\beta}^{(d)}\, \overline{Q_{\mathrm{L}}^{\alpha}}\, H d_{\mathrm{R}}^{\beta} - y_{\alpha\beta}^{(\ell)}\, \overline{L_{\mathrm{L}}^{\alpha}}\, H \ell_{\mathrm{R}}^{\beta} + \mathrm{h.c.}\;, \tag{2.19}$$

where $\widetilde{H} = \mathrm{i}\sigma_2 H^*$, are gauge-invariant. When the Higgs develops its vev v_{ew} and breaks the electroweak symmetry as described in Section 2.1.1, it generates Dirac mass terms of the form of Eq. (2.14) for the quarks and the charged leptons from Eq. (2.19) according to

$$\mathcal{L}_{\mathrm{Yukawa}} = -m_{\alpha\beta}^{(u)}\, \overline{u_{\mathrm{L}}^{\alpha}} u_{\mathrm{R}}^{\beta} - m_{\alpha\beta}^{(d)}\, \overline{d_{\mathrm{L}}^{\alpha}} d_{\mathrm{R}}^{\beta} - m_{\alpha\beta}^{(\ell)}\, \overline{\ell_{\mathrm{L}}^{\alpha}} \ell_{\mathrm{R}}^{\beta} + \mathrm{h.c.}\;, \tag{2.20}$$

where

$$m_{\alpha\beta}^{(f)} \equiv \frac{y_{\alpha\beta}^{(f)}}{\sqrt{2}}\, v_{\mathrm{ew}} \quad \text{with} \quad f = u,\, d,\, \ell\,. \tag{2.21}$$

Note that there is no mass term for the neutrinos in the SM due to the absence of right-handed neutrino fields.

2.1.3 Charged-current interactions

The interactions of the weak gauge bosons and of the photon with the fermions is contained in the covariant derivatives of the latter. Here we will focus on the interactions of the W bosons with the fermionic charged current. These are the charged-current (CC) interactions, which in the electroweak theory are given by

$$\mathcal{L}_{\mathrm{CC}} = \frac{g}{\sqrt{2}} W_{\mu}^{+} \left\{ \overline{u_{\mathrm{L}}^{\alpha}} \gamma^{\mu} d_{\mathrm{L}}^{\alpha} + \overline{\nu_{\mathrm{L}}^{\beta}} \gamma^{\mu} \ell_{\mathrm{L}}^{\beta} \right\} + \mathrm{h.c.} \tag{2.22}$$

Note that they are diagonal with respect to the fermion flavors. We take this property of the CC interactions to *define* the flavor basis of the fermions. Accordingly, the Yukawa couplings and mass terms in Eqs. (2.19) - (2.21) have been written in the flavor basis. The fermion mass matrices $m^{(f)}$ defined in Eq. (2.21) are in general not diagonal. In order to find the physical masses of the SM fermions we need to diagonalize these matrices. This can always be done with a bi-unitary transformation

$$m^{(f)}_{\text{diag}} = \text{diag}(m^{(f)}_1,\, m^{(f)}_2,\, m^{(f)}_3) \equiv U^{(f)\dagger}_{\text{L}} m^{(f)} U^{(f)}_{\text{R}}\,, \tag{2.23}$$

where $U^{(f)}_{\text{L}}$ and $U^{(f)}_{\text{R}}$ denote unitary matrices. The new basis obtained after this transformation

$$\tilde{f}^i_{\text{L}} = U^{(f)*}_{\text{L},\,\alpha i}\, f^\alpha_{\text{L}}\,, \tag{2.24}$$

$$\tilde{f}^i_{\text{R}} = U^{(f)*}_{\text{R},\,\alpha i}\, f^\alpha_{\text{R}}\,, \tag{2.25}$$

with $\tilde{f} = u,\, d,\, \ell$, is called the *mass* basis.[2] To keep the discussion compressed, we will also allow for the possibility of neutrino masses in the following. Accordingly, we define the unitary transformation relating the flavor and mass bases of the neutrinos according to

$$\tilde{\nu}^i_{\text{L}} = U^{(\nu)*}_{\text{L},\,\alpha i}\, \nu^\alpha_{\text{L}} \tag{2.26}$$

as for the other fermions. With the unitary transformations defined via Eqs. (2.23) - (2.26) we can express the charged-current interactions of Eq. (2.22) in terms of the mass basis as

$$\mathcal{L}_{\text{CC}} = \frac{g}{\sqrt{2}} W^+_\mu \left\{ \overline{\tilde{u}_{\text{L}}} \gamma^\mu\, V_{\text{CKM}}\, \tilde{d}_{\text{L}} + \overline{\tilde{\nu}_{\text{L}}}\, U^\dagger_{\text{PMNS}}\, \gamma^\mu \tilde{\ell}_{\text{L}} \right\} + \text{h.c.}\ , \tag{2.27}$$

The matrices V_{CKM} and U_{PMNS} introduced above denote the quark mixing or CKM matrix (for Cabibbo, Kobayashi, Maskawa) and, respectively, the lepton mixing or PMNS matrix (for Pontecorvo, Maki, Nakagawa, Sakata). They are defined as

$$V_{\text{CKM}} = U^{(u)\dagger}_{\text{L}} U^{(d)}_{\text{L}} \qquad \text{and} \qquad U_{\text{PMNS}} = U^{(\ell)\dagger}_{\text{L}} U^{(\nu)}_{\text{L}}\,. \tag{2.28}$$

From Eqs. (2.27) and (2.28) we see that in the mass basis the CC interactions for the quarks are no longer diagonal. Finally, we remark that if neutrinos were massless, the degrees of freedom for the unitary transformation defined in Eq. (2.26) could be used to obtain $U_{\text{PMNS}} \equiv \mathbb{1}$. Note that the inequality between the neutrino flavor and mass bases leads to flavor oscillations during the propagation of a neutrino. Accordingly, the observation of neutrino oscillations is interpreted as a sign of neutrino masses.

[2] We use Greek indices ($\alpha,\, \beta,\, \ldots$) for the flavor basis and Latin indices ($i,\, j,\, \ldots$) for the mass basis.

2.2 Beyond the Standard Model

In this section we will discuss BSM physics, which will be addressed in this work. First, we will briefly review the seesaw mechanism and the current status of neutrino phenomenology. Other BSM phenomenology addressed here includes baryon and lepton number violation (LNV) and, in particular, neutrinoless beta decay as well as dark matter (DM). At the end of this section we will present the Gildener-Weinberg formalism, which is used to systematically minimize the scalar potential in conformal theories.

2.2.1 Neutrino masses and leptonic mixing

Neutrino masses

In the introduction we have already mentioned that naturally small neutrino masses can be generated by the Weinberg operator and also in the seesaw mechanism. In the following we will elaborate on the second option. For completeness, we note that, to this day, Dirac neutrinos with Yukawa couplings of the order of below 10^{-11}, as would be required for neutrino masses generated via the Higgs mechanism, do not contradict any experimental observation made and also are considered in the literature (see e.g. [89] for a leptogenesis model with Dirac neutrinos).

In the canonical or type-I seesaw mechanism [78–81] the SM is extended by three right-handed neutrino fields N_R with a large Majorana mass term (typically above the order of 10^{14} GeV), which can be introduced as consequence of e.g. some symmetry or by hand. The neutrino mass Lagrangian of the type-I seesaw in the Majorana basis $n_\mathrm{L} = (\nu_\mathrm{L},\, N_\mathrm{R}^\mathrm{c})^\intercal$ is given by

$$\mathcal{L}_\mathrm{mass}^\text{type-I} = -\overline{N_\mathrm{R}} M_\mathrm{D} \nu_\mathrm{L} - \tfrac{1}{2}\overline{N_\mathrm{R}^\mathrm{c}} M_\mathrm{R} N_\mathrm{R} + \text{h.c.} \;= -\tfrac{1}{2}\overline{n_\mathrm{L}^\mathrm{c}}\, \mathcal{M}\, n_\mathrm{L} + \text{h.c.}\;, \tag{2.29}$$

where M_D and M_R denote the 3×3 Dirac and Majorana mass terms, respectively. Accordingly, the neutrino mass matrix in the above equation is defined as

$$\mathcal{M} = \begin{pmatrix} 0 & M_\mathrm{D}^\intercal \\ M_\mathrm{D} & M_\mathrm{R} \end{pmatrix}. \tag{2.30}$$

After diagonalization, the neutrino mass matrix possesses three very heavy eigenstates mainly given by the right-handed neutrino fields, and three very light eigenstates, which mainly consist of the left-handed neutrino fields. While the mass matrix of the heavy eigenstates is approximately given by M_R, the mass matrix of the light eigenstates is obtained in the seesaw formula [90], which to leading order reads

$$m_\nu = -M_\mathrm{D}^\intercal\, M_\mathrm{R}^{-1}\, M_\mathrm{D}\,. \tag{2.31}$$

The above equations shows that the light neutrino mass m_ν is suppressed by the large Majorana mass introduced for the right-handed neutrinos.

The type-II seesaw extends the canonical mechanism in order to include Majorana mass terms also for the left-handed neutrinos. Type-II seesaw models are usually based on higher symmetry groups, which are eventually broken down to the SM gauge group (see e.g. [91] based on an SO(10) GUT, and [92] for a left-right-symmetric model). Typically, a scalar $\mathrm{SU}(2)_\mathrm{L}$ triplet Δ is introduced with Yukawa couplings to the lepton doublet according to

$$\mathcal{L}_\mathrm{mass}^\text{type-II} \supset -\tfrac{1}{2}\, y_\Delta\, \overline{L_\mathrm{L}^\mathrm{c}}\, \mathrm{i}\sigma_2 \Delta\, L_\mathrm{L} + \mathrm{h.c.} \tag{2.32}$$

When the triplet upon spontaneous symmetry breaking develops a vev, it can induce a Majorana mass term for the left-handed neutrinos. The left-handed Majorana mass terms to leading order do not change the diagonalizing transformation for the neutrino mass matrix [90] and lead to an additional contribution to the light neutrino masses. Interestingly, this contribution can be suppressed and of the same order of magnitude as the type-I contribution from the heavy right-handed Majorana masses. However, the suppression of the left-handed Majorana masses has its origin in the minimization of the scalar potential. In particular, the suppression resides in the vev of the neutral component of the scalar, Δ^0, which generates the left-handed Majorana masses. Note that, in principle, the Majorana mass for the left-handed neutrinos alone could already suffice to obtain phenomenologically correct neutrino masses.

Yet another version of neutrino mass generation is the type-III seesaw mechanism [93]. In this seesaw mechanism a fermionic $\mathrm{SU}(2)_\mathrm{L}$ triplet Σ with heavy Majorana mass and Yukawa coupling to the lepton doublet and the Higgs doublet is introduced. Its neutral component Σ^0 plays the role of the right-handed $\mathrm{SU}(2)_\mathrm{L}$ singlet neutrinos N_R of the type-I seesaw and in consequence yields light neutrino masses suppressed by the heavy Majorana mass of the triplet.

We remark that according to [94] the three different seesaw types described above are the only renormalizable, tree-level realizations of the effective Weinberg operator. We illustrate the corresponding Feynman diagrams for the tree-level seesaw types in Figure 2.2. Besides these three canonical seesaws a wide spectrum of altered seesaw mechanisms has been proposed, which include the inverse [82–84], double [95], singular [96–98], linear [99–101], schizophrenic [102] and split [103] seesaw. For completeness, we mention that neutrino masses can also be generated radiatively (see e.g. [94, 104] for discussions of loop-generated neutrino masses).

After this discussion of the seesaw mechanism, let us now describe the known phenomenology of neutrino masses and mixing.

Absolute mass scale and mass ordering

Until today three different kinds of neutrinos, namely, ν_e, ν_μ and ν_τ have been observed [72, 105, 106]. The number of light neutrino species coupled to the Z boson has been measured in high-precision experiments at LEP as $N_\nu = 2.9840 \pm$

Figure 2.2: Feynman diagrams for the different tree-level seesaw types. *Left*: Type-I mediated by a heavy fermionic $SU(2)_L$ singlet (N) and type-III by the neutral component of a heavy fermionic $SU(2)_L$ triplet (Σ^0). *Right*: Type-II mediated by the neutral component of a heavy scalar $SU(2)_L$ triplet (Δ^0).

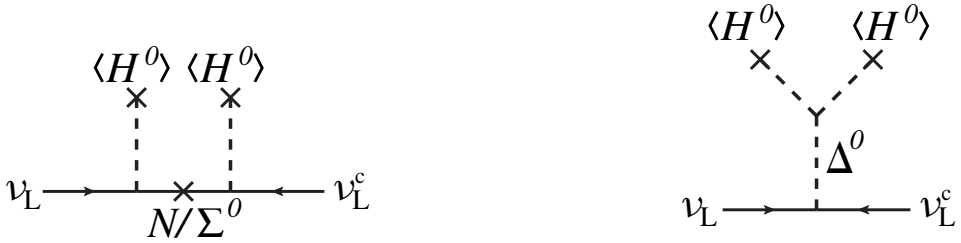

0.0082 in agreement with the expected number of neutrinos [107]. The effective number of relativistic neutrinos related to the radiation energy density in the early universe has been measured as $N_{\text{eff}} = 3.30^{+0.54}_{-0.51}$ at 95% confidence level [108]. All mentioned observations are consistent with the three neutrino generations of the SM. For completeness, we remark that the collected oscillation data can also be consistently fitted to oscillations with more than three neutrino flavors, but the fit suffers from tension between data sets from different experiments [109].

The absolute mass scale of neutrinos has not been measured, yet. However, upper limits on the neutrino mass can be obtained from Kurie plot experiments, neutrinoless double beta decay and from cosmological considerations. The best limit from a direct mass measurement comes from tritium beta spectroscopy and is given by the Mainz experiment as $m_\beta \leq 2.3$ eV at 95% confidence level [110]. The mass observed in the experiment can theoretically be expressed as

$$m_\beta = \left(\sum_{i=1}^{3} |U_{ei}|^2 m_i^2 \right)^{1/2} . \tag{2.33}$$

In the future the current limit from the Mainz experiments is expected improve down to neutrino masses of about 0.2 eV by the KATRIN experiment [111, 112]. Aside from this direct mass measurement, there are two further observables which are sensitive to the absolute mass scale, namely, the effective Majorana mass in neutrinoless double beta decay, $m_{\text{eff}}^{0\nu}$, and the sum of relativistic neutrino species Σ_ν. The discussion of the effective Majorana mass will be postponed until Section 2.2.3. The sum of relativistic neutrino species defined as

$$\Sigma_\nu = \sum_{i=1}^{3} m_i \tag{2.34}$$

can be constrained by cosmological observables. If the temperature fluctuations in the spectrum of the cosmic microwave background (CMB) radiation measured by the Planck satellite and baryon acoustic oscillations are taken into account, the mass sum is limited as $\Sigma_\nu < 0.23$ eV at 95% confidence level [108]. If data

from the Lyman-α forest power spectrum is included, the limit can be tightened down to $\Sigma_\nu < 0.12$ eV at 95% confidence level [113, 114].

Even though there are only upper limits for the absolute neutrino mass scale, the differences of the mass-squares have been measured to quite some precision. The mass-squared differences for the neutrino masses are defined as

$$\Delta m^2_{ij} = m^2_i - m^2_j \quad \text{with} \quad i,\, j = 1,\, 2,\, 3\,. \tag{2.35}$$

Note that there exist only two independent mass-squared differences, which usually are chosen to be Δm^2_{21} and Δm^2_{31}. Since the sign of the latter is still unknown, there exist two possible orderings for the neutrino masses called the "normal ordering" (NO) and "inverted ordering" (IO). They correspond to the following relations between the neutrino masses

$$\begin{aligned} \text{NO:} \quad & m_3 > m_2 > m_1 \equiv m_{\text{lightest}}\,, \quad \Delta m^2_{31} > 0\,, \\ \text{IO:} \quad & m_2 > m_1 > m_3 \equiv m_{\text{lightest}}\,, \quad \Delta m^2_{31} < 0\,, \end{aligned} \tag{2.36}$$

where m_{lightest} denotes the lightest neutrino mass. The mass-squared differences can be derived from neutrino oscillation experiments [73–76]. Their best-fit values with one standard deviation are given by [115]

$$\begin{aligned} \Delta m^2_{21} &= \left(7.50^{+0.19}_{-0.17}\right) \times 10^{-5}\text{eV}^2\,, \\ |\Delta m^2_{31}| &= \left(2.457^{+0.047}_{-0.047}\right) \times 10^{-3}\text{eV}^2\,. \end{aligned} \tag{2.37}$$

Note that the presence of two individual non-vanishing mass-squared differences implies that at least two of the three neutrinos in the SM are massive. The individual neutrino masses can be expressed through m_{lightest} and the two mass-squared differences according to

$$\begin{array}{ll} \text{NO:} \;\; \Delta m^2_{31} > 0 & \text{IO:} \;\; \Delta m^2_{31} < 0 \\ m_1 = m_{\text{lightest}}\,; & m_3 = m_{\text{lightest}}\,; \\ m_2 = \sqrt{m^2_{\text{lightest}} + \Delta m^2_{21}}\,; & m_1 = \sqrt{m^2_{\text{lightest}} + |\Delta m^2_{31}|}\,; \\ m_3 = \sqrt{m^2_{\text{lightest}} + \Delta m^2_{31}}\,; & m_2 = \sqrt{m^2_{\text{lightest}} + |\Delta m^2_{31}| + \Delta m^2_{21}}\,. \end{array} \tag{2.38}$$

In the limit that m^2_{lightest} is much larger than $|\Delta m^2_{31}|$ one enters the "quasi-degenerate" regime (QD), in which the above equations for both mass orderings yield $m_1 \approx m_2 \approx m_3$. From Eq. (2.38) we see that the limit on the sum of neutrino masses of about 0.12 eV reported above is getting closer to the region of the inverted ordering, for which the largest neutrino mass is bounded from below as $m_2 \gtrsim 0.05$ eV, where we have inserted the values of the mass-squared differences given in Eq. (2.37).

Neutrino mixing and oscillations

Neutrino oscillations were first considered by Pontecorvo [116], and Maki, Nakagawa and Sakata [117]. Three-flavor neutrino oscillations (in vacuum) are described by eight parameters. These are the two independent mass-squared differences Δm^2_{ij}, three mixing angles θ_{ij}, one Dirac phase δ_{CP} and two Majorana

phases α and β. In the following we will abbreviate $c_{ij} \equiv \cos\theta_{ij}$ and $s_{ij} \equiv \sin\theta_{ij}$. Then the lepton mixing matrix can be parametrized by three rotations and a phase matrix as

$$\begin{aligned} U &= R_{23}(\theta_{23},\, 0) \cdot R_{13}(\theta_{13},\, \delta_{\mathrm{CP}}) \cdot R_{12}(\theta_{12},\, 0) \cdot P \\ &= \begin{pmatrix} c_{12}\, c_{13} & s_{12}\, c_{13} & s_{13}\, \mathrm{e}^{-\mathrm{i}\delta_{\mathrm{CP}}} \\ -s_{12}\, c_{23} - c_{12}\, s_{23}\, s_{13}\, \mathrm{e}^{\mathrm{i}\delta_{\mathrm{CP}}} & c_{12}\, c_{23} - s_{12}\, s_{23}\, s_{13}\, \mathrm{e}^{\mathrm{i}\delta_{\mathrm{CP}}} & s_{23}\, c_{13} \\ s_{12}\, s_{23} - c_{12}\, c_{23}\, s_{13}\, \mathrm{e}^{\mathrm{i}\delta_{\mathrm{CP}}} & -c_{12}\, s_{23} - s_{12}\, c_{23}\, s_{13}\, \mathrm{e}^{\mathrm{i}\delta_{\mathrm{CP}}} & c_{23}\, c_{13} \end{pmatrix} \cdot P\,, \end{aligned} \tag{2.39}$$

where $P = \mathrm{diag}(1,\, \mathrm{e}^{\mathrm{i}\alpha},\, \mathrm{e}^{\mathrm{i}\beta})$ in the case that neutrinos are Majorana particles, and $P = \mathbb{1}$ in the case that neutrinos are Dirac particles. The Majorana phases α and β do not enter neutrino oscillations. They are, however, present in the effective Majorana mass of neutrinoless double beta decay as we will see in Section 2.2.3. We remark that the matter or MSW effect [118–121] leads to a change in the neutrino oscillation pattern. It describes the effect of the electrons present in matter on the electron neutrino in form of an effective potential due to neutral current interactions.

2.2.2 Inverse seesaw mechanism

To conclude the discussion of neutrino masses we will give an example of neutrino mass generation within the inverse seesaw mechanism [82–84]. Note that in Chapters 3 and 4 we will study an inverse seesaw scenario in the context of conformal theories. In the inverse seesaw mechanism (ISS) the SM is extended by right-handed neutrinos N_{R} and an equal number of left-handed neutrinos S_{L} of another species. Both are introduced as singlets of the SM gauge group. Furthermore, it is assumed that the additional left-handed singlets have a relatively small Majorana mass term μ. On the other hand, a Majorana mass for the right-handed neutrinos is forbidden, e.g. due to a suitable symmetry or due to the absence of a scalar that could lead to a mass term after spontaneous symmetry breaking. In the described scenario the Lagrangian containing the neutrino mass terms is given by

$$\begin{aligned} \mathcal{L}^{\mathrm{ISS}}_{\mathrm{mass}} &= -\overline{N_{\mathrm{R}}}\, m_{\mathrm{D}}\, \nu_{\mathrm{L}} - \overline{N_{\mathrm{R}}} M^{\intercal} S_{\mathrm{L}} - \tfrac{1}{2}\overline{S^{\mathrm{c}}_{\mathrm{L}}}\, \mu\, S_{\mathrm{L}} + \mathrm{h.c.} \\ &\equiv -\tfrac{1}{2}\overline{n^{\mathrm{c}}_{\mathrm{L}}}\, \mathcal{M}\, n_{\mathrm{L}} + \mathrm{h.c.}\ , \end{aligned} \tag{2.40}$$

where we have defined the Majorana basis as $n_{\mathrm{L}} = (\nu_{\mathrm{L}},\, N^{\mathrm{c}}_{\mathrm{R}},\, S_{\mathrm{L}})^{\intercal}$. According to the above equation the neutrino mass matrix reads

$$\mathcal{M} = \begin{pmatrix} 0 & m_{\mathrm{D}}^{\intercal} & 0 \\ m_{\mathrm{D}} & 0 & M^{\intercal} \\ 0 & M & \mu \end{pmatrix}\,. \tag{2.41}$$

If we assume a hierarchy $M \gg m_{\mathrm{D}},\, \mu$ between the mass scales, the light neutrino masses are given by the inverse seesaw formula

$$m_\nu \approx m_{\mathrm{D}}^{\intercal}\, (M^{\intercal})^{-1}\, \mu\, M^{-1}\, m_{\mathrm{D}}\,. \tag{2.42}$$

In order to obtain sub-eV neutrino masses one typically chooses M of the order of a few TeV and μ in the keV range. Then again, it is apparent from Eq. (2.42) that the neutrino mass is only sensitive to the ratio m_{D}/M. Hence, there is no problem in having M in the GeV range if the Yukawa couplings in the Dirac mass term m_{D} are sufficiently small. The remaining eigenvalues of the neutrino mass matrix are heavy pseudo-Dirac masses of the order of $\pm M + \mu$. The main difference between the type-I and the inverse seesaw is that, in the former, a huge Majorana mass is required for the successful suppression of the neutrino masses. On the contrary, in the inverse seesaw, suppressed masses can be obtained with a small LNV Majorana mass μ and GeV to TeV-scale Dirac mass terms in the heavy neutrino sector.

2.2.3 Baryon and lepton number violation

Baryon and lepton numbers B and L are accidental global symmetries of the SM Lagrangian. Consequently, these quantum numbers are conserved in all perturbative SM particle reactions.[3] Conversely, in our Universe we observe a striking asymmetry between the amount of matter and anti-matter present. The baryon asymmetry of the Universe (BAU) is given by [124]

$$\eta_B = \frac{n_B}{n_\gamma} = 6.2 \times 10^{-10}\,, \tag{2.43}$$

where n_B and n_γ denote the number density of baryons and photons, respectively. A theory that successfully explains the generation of the BAU is called baryogenesis. Standard scenarios of baryogenesis satisfy the three Sakharov conditions [125]: The interactions responsible for baryogenesis must violate baryon number; they have to violate C and CP conjugation; and they need to be out of equilibrium. It is also possible to generate the BAU via LNV, which is dubbed leptogenesis [126]. The idea of this mechanism goes as follows. If LNV effects generate a lepton asymmetry in the Universe (with accordingly adapted Sakharov conditions for lepton number), this asymmetry can be converted into a BAU by a suitable interaction violating a linear combination of baryon and lepton number. A prominent example are the non-perturbative sphalerons [122], which are efficient only at high temperatures and violate the combination $B + L$. Also the combination $B - L$ is typically spontaneously broken in leptogenesis. Discussing the opportunities of leptogenesis lies beyond the scope of this work. We will, however, investigate a model, in which a gauged $\mathrm{U}(1)_{B-L}$ symmetry is spontaneously broken in Chapter 4.

Apart from cosmology, LNV effects also can show up in low-energy and high-energy physics. In the following we will discuss one representative of the former class. Later, in Chapter 4, we will also examine LNV collider signatures.

[3] The non-perturbative sphalerons [122] or, respectively, instantons [123], however, violate $B + L$ while at the same time conserving the difference $B - L$.

Neutrinoless double beta decay

Neutrinoless double beta decay ($0\nu\beta\beta$) is the simultaneous decay of two neutrons in a nucleus of an isotope (A, Z) into two protons and two electrons without the emission of neutrinos according to

$$0\nu\beta\beta : (A,\, Z) \to (A,\, Z+2) + 2e^- \,. \tag{2.44}$$

The non-observation of $0\nu\beta\beta$ can be interpreted as a lower limit on the half-life of the isotope under investigation. Besides a claim of a positive signal of $0\nu\beta\beta$ in the isotope ^{76}Ge by a fraction of the Heidelberg-Moscow collaboration [127, 128], which, however, has received quite some criticism [129], no observation of the decay has been reported to the present day. Recent data collected by the GERDA collaboration strongly disfavors the claim of [127, 128] and sets the currently best lower limit on the half-life of ^{76}Ge as $T^{0\nu}_{1/2} > 3 \times 10^{25}$ y at 90% confidence level [130]. Note that the double beta decay mode *with* the emission of neutrinos

$$2\nu\beta\beta : (A,\, Z) \to (A,\, Z+2) + 2e^- + 2\overline{\nu}_e \tag{2.45}$$

has already been observed in several isotopes (see [131] for a calculation of the values of the half-lives). From a particle physicist's point of view the observation of $0\nu\beta\beta$ would prove the existence of an (effective) operator that violates lepton number by two units. The interpretation of the observation in terms of the Schechter-Valle theorem [132], which states that an observation of the decay would imply that the electron neutrino is massive, is correct but a rather academic one [133].

Theoretically, the half-life of an isotope (A, Z) that might undergo $0\nu\beta\beta$ can be expressed in terms of a phase-space factor $G^{0\nu}(Q,\, Z)$, a nuclear matrix element $M^{0\nu}_{(A,\,Z)}$ and a dimensionless effective parameter η_{eff} according to

$$\left(T^{0\nu}_{1/2}\right)^{-1}_{(A,\,Z)} = G^{0\nu}(Q,\, Z) \left| M^{0\nu}_{(A,\,Z)}\, \eta_{\text{eff}} \right|^2 \,. \tag{2.46}$$

The phase-space factor is responsible for the kinematics of the decay and typically scales with the fifth power of the endpoint energy Q or Q-value of the double-beta spectrum. Accordingly, isotopes with a high Q-value (typically of $\mathcal{O}\,(1)$ MeV) are particularly suitable in order to search for $0\nu\beta\beta$. We have plotted the spectrum for the two decay modes given in Eqs. (2.44) and (2.45) in Figure 2.3. It schematically illustrates the distinct characteristics of the two spectra. Note, however, that the $0\nu\beta\beta$ spectrum is strongly exaggerated in this figure. The nuclear matrix element (NME) in Eq. (2.46) implements the transition of the nucleus into its daughter nucleus. Since it describes a multi-particle process, the NME represents the largest source of uncertainties in deriving particle physics constraints from the experimental bounds on the half-life. Finally, the effective parameter η_{eff} contains the particle physics of the transition $2d \to 2u + 2e^-$ inside of the involved nucleons. Note that an effective Majorana mass of $0\nu\beta\beta$ can be defined by converting the dimensionless effective parameter into a mass according to

$$m^{0\nu}_{\text{eff}} \equiv m_e \eta_{\text{eff}} \,, \tag{2.47}$$

Figure 2.3: Schematic energy spectrum of the two electrons emitted in double beta decay with ($2\nu\beta\beta$, black line) and without neutrinos ($0\nu\beta\beta$, red line). Note that the peak of the $0\nu\beta\beta$ curve at the endpoint energy Q is plotted strongly exaggerated to make it visible in the graph.

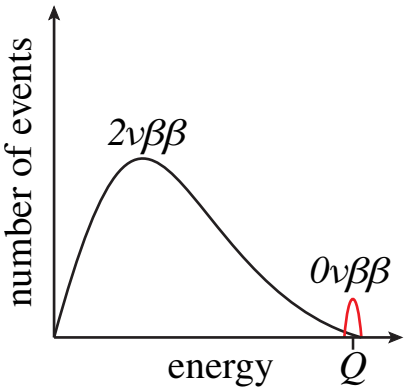

Figure 2.4: Neutrinoless double beta decay (at the constituent-quark level) mediated by neutrino exchange and charged-current interactions. The internal neutrino line implies a sum over all mass eigenstates ν_i with mixing to the electron neutrino given by the mixing matrix elements U_{ei}.

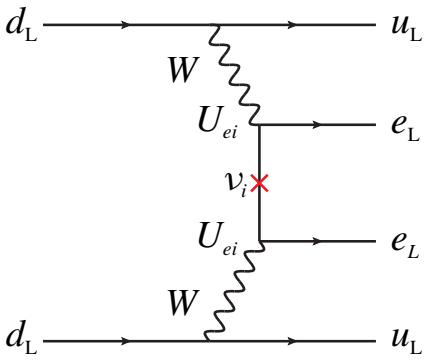

where m_e denotes the electron mass. The effective Majorana mass is conveniently used to transfer the half-life of $0\nu\beta\beta$ into particle physics parameters.

The simplest theoretical explanation for $0\nu\beta\beta$ is referred to as *mass mechanism* (see e.g. [134]), which was first considered in [135, 136]. It assumes that the neutrinos we observe in oscillation experiments mediate the decay as illustrated in Figure 2.4. For the mass mechanism the effective parameter introduced in Eq. (2.46) is given by

$$\begin{aligned} \eta^{\nu}_{\text{eff}} \equiv \frac{m_{ee}}{m_e} &= \frac{1}{m_e}\left(\sum_{i=1}^{3} U_{ei}^2\, m_i\right) \\ &= \frac{1}{m_e}\left(c_{12}^2\, c_{13}^2\, m_1 + s_{12}^2\, c_{13}^2\, \mathrm{e}^{2\mathrm{i}\alpha} m_2 + s_{13}^2\, \mathrm{e}^{2\mathrm{i}\beta} m_3\right) , \end{aligned} \tag{2.48}$$

where the effective light Majorana mass m_{ee} is normalized to the electron mass m_e, and U_{ei} denotes the elements of the neutrino mixing matrix. In the last step we

have assumed the parametrization of the mixing matrix as presented in Eq. (2.39). If the only contribution to $0\nu\beta\beta$ comes from the above equation, the effective Majorana mass defined in Eq. (2.47) is simply given by $m_{\text{eff}}^{0\nu} = m_e \eta_{\text{eff}}^{\nu} \equiv m_{ee}$. To understand the origin of Eq. (2.48) we can evaluate the leptonic fermion line of the diagram in Figure 2.4 according to

$$\mathcal{A}_{0\nu\beta\beta} \sim \sum_{i=1}^{n} P_{\text{L}} U_{ei} \frac{\not{p} + m_i}{p^2 - m_i^2} U_{ei} P_{\text{L}} = P_{\text{L}} \sum_{i=1}^{n} U_{ei}^2 \frac{m_i}{p^2 - m_i^2} \,, \tag{2.49}$$

where we have used the properties of the projection operators $P_{\text{L}}^2 = P_{\text{L}}$, $P_{\text{L}} P_{\text{R}} = 0$ and $P_{\text{L}} \gamma^{\mu} = \gamma^{\mu} P_{\text{R}}$. The summation is performed over all neutrino states that mediate the decay. The typical momentum transfer in $0\nu\beta\beta$ is given by $p^2 = -|p|^2 = -(100 \text{ MeV})^2$.[4] If we approximate Eq. (2.49) for light neutrinos, i.e. for $m_i \ll |p|$, we obtain an expression proportional to Eq. (2.48). If, however, the internal neutrinos are heavy particles meaning $m_i \gg |p|$, we can approximate Eq. (2.49) to obtain the effective parameter for heavy neutrino exchange, which is defined as

$$\eta_{\text{eff}}^{N} \equiv m_p \left(\sum_{i \in \text{heavy}} U_{ei}^2 \frac{1}{m_i} \right) . \tag{2.50}$$

The effective parameter in the above equation is normalized to the proton mass m_p by convention, which is extracted from the NME.

Finally, we remark that massive Majorana neutrinos are not the only way to realize $0\nu\beta\beta$. In principle any new physics that violates lepton number (effectively) by two units can lead to $0\nu\beta\beta$ (see [137] and [138] for a thorough categorization and analysis of the long-range and short-range interactions in $0\nu\beta\beta$.). Additionally, it is possible that not only one but several mechanisms give significant contributions to the amplitude of $0\nu\beta\beta$, which can lead to constructive or destructive interference effects (see e.g. [139–144]).

2.2.4 Dark matter

Evidence for DM has been found in the velocity dispersion of galaxies (first noted in the Coma cluster [145]), in rotation curves of galaxies [146, 147], and in gravitational lensing effects (see e.g. [148] and in particular the evidences from bullet clusters [149, 150]). The measurements of the CMB spectrum [108] and of large-scale structures [151] have shown that ordinary (visible baryonic) matter makes up only about 5 % of the energy budget of the universe. The larger fraction of matter in the Universe's of about 27 % consists of a yet unknown form of stable matter, which is called DM. Finally, the bulk of about 68 % of the energy in the universe exists in yet another unknown form called dark energy.

[4] The momentum transfer is estimated from the typical distances between nucleons in a nucleus of $r^2 \sim \mathcal{O}\left(1 \text{ fm}^2\right)$.

For a long time, now, it has been suggested that DM is made of weakly interacting massive particles (WIMPs) (see [152] for an overview of particle DM candidates). The freeze-out density of a thermal relic X can generally be estimated as [153]

$$\Omega_X \propto \frac{1}{\langle \sigma_{\text{ann.}}\, v \rangle} \sim \frac{m_X^2}{g_X^4} \tag{2.51}$$

where $\langle \sigma_{\text{ann.}}\, v \rangle$ denotes the thermally averaged annihilation cross section. If the particle's mass m_X is chosen at the electroweak scale (at about 100 GeV) and the coupling g_X is associated with the typical weak coupling strength of $g_{\text{weak}} \approx 0.65$, the WIMP happens to be abundant in exactly the right amount in order to match the experimentally observed DM relic density. This natural concurrence of just the right parameters is known as the WIMP miracle. With the latest results from the DM searches of the XENON100 experiment [154] and the LUX experiment [155] a large area of the available parameter region has been excluded for the spin-independent WIMP-nucleon cross section down to the order of $\sigma_{\text{SI}} \sim 10^{-45}$ cm^2, thus, disfavoring WIMP masses between the orders of 10 GeV to 1 TeV. In the next two years the XENON1T DM search will reach its ultimate sensitivity of $\sigma_{\text{SI}} \sim 2 \times 10^{-47}$ cm^2 [156]. If no DM signal is found by XENON1T, the WIMP miracle's appeal of naturally generating the right DM abundance will probably fade away.

A viable alternative to DM constituted by WIMPs is found in warm DM, which is usually characterised by a mass scale in the keV range [157]. A particularly suitable candidate for warm DM is represented by a neutrino, which does not possess SM charges [158]. In Chapter 3 we will present a model that features such a warm DM candidate. There we will explore how the right DM abundance can be obtained in the context of the model.

2.2.5 The Coleman-Weinberg mechanism

In this section we will discuss spontaneous symmetry breaking in conformal theories within the Coleman-Weinberg (CW) mechanism [36]. As already anticipated in the introduction, the concept of the CW mechanism lies in the spontaneous breaking of the scale invariance by higher-order processes: Quantum effects lead to the development of a non-trivial minimum in the effective scalar potential which, in turn, induces spontaneous conformal symmetry breaking. In order to study spontaneous conformal symmetry breaking, we will work in the Gildener-Weinberg (GW) formalism presented in [159], which is especially suitable for scalar sectors with many particles, as it systematizes the minimization of the CW potential. We will present the details of the GW formalism in the following.

Let us assume that the scalar particle spectrum of the theory consists of the real degrees of freedom ϕ_i. Then the most general conformal tree-level potential can be written as

$$V(\mathbf{\Phi}) = \frac{f_{ijk\ell}}{24}\, \phi_i \phi_j \phi_k \phi_\ell \,, \tag{2.52}$$

where $\mathbf{\Phi} = (\phi_1, \phi_2, \ldots)^\intercal$ denotes the vector containing all scalar degrees of freedom. The dimensionless coupling constants $f = f(\Lambda)$ depend on the renormalization scale Λ. The tree-level potential is assumed to possess a flat direction denoted by $\mathbf{\Phi}_{\text{flat}}$, along which it vanishes. Now, quantum corrections, while normally being sub-leading effects, give a relevant contribution to the potential along the flat direction. Accordingly, it is assumed that at a certain energy scale Λ_{GW}, called Gildener-Weinberg scale, the quantum effects induce a bent in the flat direction. In consequence, a non-trivial minimum is generated in the potential, which spontaneously breaks the conformal symmetry.

A necessary condition in order for the potential to develop a minimum is that its first derivative with respect to each real scalar degree of freedom vanishes at the minimum,

$$\left.\frac{\partial V}{\partial \phi_i}\right|_{\text{min}} = 0 \quad \text{for all } i\,. \tag{2.53}$$

If we assume a regular potential, in which all real scalar degrees of freedom appear at least squared, the above equation is trivially satisfied for all components ϕ_i that do not develop a finite vev. Consequently, the minimum condition imposes as many conditions on the scalar couplings as there are non-vanishing vevs in the scalar spectrum. A further condition is that the scalar tree-level potential vanishes at the minimum. These conditions, referred to as Gildener-Weinberg conditions, can be collectively denoted as

$$R(f)|_{\Lambda=\Lambda_{\text{GW}}} = 0 \tag{2.54}$$

and are required to hold at the scale of symmetry breaking Λ_{GW}. It turns out that one of the mentioned conditions is always redundant. Next we will discuss how we can determine the ground state of a conformal theory.

Suppose that the potential vanishes along a ray in scalar space, which is identified as the flat direction $\mathbf{\Phi}_{\text{flat}}$. Then we can characterize the flat direction by a unit vector $\boldsymbol{n}$ pointing in the direction along the ray and the position φ on the ray according to

$$\mathbf{\Phi}_{\text{flat}} = \boldsymbol{n}\,\varphi\,. \tag{2.55}$$

At tree level the flat direction represents a continuous spectrum of degenerate vacua. As already mention, quantum effects, however, lead to a bent of the flat direction thereby singling out the true vacuum at $\langle \mathbf{\Phi}_{\text{flat}} \rangle = \boldsymbol{n}\langle\varphi\rangle$. At one-loop level the effective potential along the flat direction is given by

$$V_{\text{eff}}^{\text{1-loop}}(\mathbf{\Phi}_{\text{flat}}) = A\varphi^4 + B\varphi^4 \log\left(\frac{\varphi^2}{\Lambda_{\text{GW}}^2}\right)\,, \tag{2.56}$$

where Λ_{GW} has been chosen as the renormalization scale, and A and B denote

the loop functions

$$A = \frac{1}{64\pi^2\langle\varphi\rangle^4}\sum_i (-1)^{2s_i} d_i \cdot m_i^4\left(\boldsymbol{n}\langle\varphi\rangle\right)\left(\log\frac{m_i^2(\boldsymbol{n}\langle\varphi\rangle)}{\langle\varphi\rangle^2} - c_i\right), \tag{2.57}$$

$$B = \frac{1}{64\pi^2\langle\varphi\rangle^4}\sum_i (-1)^{2s_i} d_i \cdot m_i^4\left(\boldsymbol{n}\langle\varphi\rangle\right). \tag{2.58}$$

The sums in Eqs. (2.57) and (2.58) run over all particles in the theory, where s_i, d_i and m_i denote the spin, the real degrees of freedom and the tree-level mass of the particle, respectively. The coefficients c_i depend on the renormalization scheme. In the $\overline{\text{MS}}$ scheme (applied here) they are given by $c_i = \frac{5}{6}$ for gauge bosons and $c_i = \frac{3}{2}$ for scalars and fermions. Note that the particle's masses in the loop functions are understood to be evaluated at the minimum of the potential and implicitly depend on the renormalization scale Λ_{GW} through the couplings. At this point it is important to notice that it is reasonable to take Λ_{GW} as the renormalization scale because, due to dimensional transmutation, all dimensional quantities will be proportional to the scale of symmetry breaking.

The minimum of the one-loop effective potential defined in Eq. (2.56) is given by

$$\langle\varphi\rangle = \Lambda_{\text{GW}} \cdot \exp\left(\frac{1}{4} - \frac{A}{2B}\right), \tag{2.59}$$

which finally yields the true vacuum of the theory. This equation shows that the GW scale Λ_{GW} and the scale of the vacuum $\langle\varphi\rangle$ are of the same order of magnitude unless B is anomalously small. This is a necessity to guarantee the validity of the loop expansion as perturbative series in the logarithm $\log\left(\frac{\langle\varphi\rangle}{\Lambda_{\text{GW}}}\right)$.

The vacuum breaks the anomalous scale invariance also spontaneously. As consequence, the theory contains a pseudo-Goldstone boson (PGB), which is massless at tree level, but obtains a mass through loop corrections. In particular, the PGB is the scalar excitation along the flat direction and its mass-squared at one-loop level is given by the curvature of the effective potential Eq. (2.56) according to

$$m_{\text{PGB}}^2 = \left.\frac{\partial^2 V_{\text{eff}}^{\text{1-loop}}}{\partial\varphi^2}\right|_{\varphi=\langle\varphi\rangle} = 8B\langle\varphi\rangle^2. \tag{2.60}$$

As the above equation is the second derivative of the one-loop effective potential, the extremum of the potential is a minimum only if the PGB mass-squared turns out to be positive. In the SM, the loop function B is negative since it is dominated by the top-quark contribution. To render B positive it is necessary to introduce new bosonic degrees of freedom that can counteract the top-quark mass. In the following Chapters 3 and 4 we will study two different conformal theories, which realize this possibility.

Chapter 3

Conformal inverse seesaw mechanism

As laid out in the introduction, the hierarchy problem of the electroweak theory demands for a modification of EWSB. We have also mentioned that the SM needs to be extended in order to allow for neutrino masses. Following the argument of Bardeen, we have discussed that in conformally invariant theories the hierarchy problem is solved naturally by the absence of a physically meaningful cutoff scale. Furthermore, we have seen how the seesaw mechanism can account for naturally small neutrino masses in Section 2.2.1. The general picture of EWSB and neutrino masses in the context of conformal invariance was discussed in much detail in [60]. In that work it was pointed out that in a conformal theory the inverse seesaw mechanism can have an interesting phenomenology, including electroweak precision observables, collider signatures and dark matter. Motivated by this prospect we will study the model of the conformal inverse seesaw (CISS) mechanism in this chapter. The research presented in this chapter is based on the published work [1].

In the CISS the SM gauge group is extended by a local $\mathrm{U}(1)_X$ gauge symmetry, under which the SM particles transform as singlets. The scalar sector of the SM also needs to be extended in order to enable spontaneous symmetry breaking of the conformal scalar potential as was pointed out in Section 2.2.5. We discuss the consequences of the new bosons associated with these extensions, which lead to new collider signatures potentially detectable at the LHC. Furthermore, the model features non-SM neutrinos with masses at the keV scale, which represent excellent warm dark matter (DM) candidates. We show that the model's parameter space allows for stable dark matter with masses and mixings to the SM neutrinos that evade the Tremaine-Gunn bound as well as X-rays limits. Additionally, we discuss the dark matter production mechanism in the CISS that yields the correct relic abundance.

The outline of this chapter is as follows. First, we will introduce the model of the CISS in Section 3.1. Afterwards, we will discuss the diagonalization of the neutrino mass matrix in Section 3.2. In Section 3.3 the electroweak symmetry breaking pattern is explained. Section 3.4 deals with the phenomenology in the

CISS including low-energy particle physics, collider signatures and dark matter production.

3.1 The model

The model of the CISS is based on the SM gauge group with an additional local $\mathrm{U}(1)_X$ symmetry,

$$G_{\mathrm{CISS}} = G_{\mathrm{SM}} \times \mathrm{U}(1)_X \,. \tag{3.1}$$

The SM particles are not charged under the new symmetry group and, hence, do not participate in the interactions with the associated gauge boson X_μ. Therefore, we will refer to the new sector as *hidden* sector and to the vector particle X_μ as *hidden* gauge boson. The fermion sector of the SM is extended by a complete gauge singlet field ν_{R}, and two chiral fields N_{L} and N_{R} each carrying one unit of the hidden charge. Note that introducing pairs of chiral fermions automatically cancels the gauge anomaly associated with $\mathrm{U}(1)_X$. The scalar sector is extended by two SM-singlet representations, namely ϕ_1 and ϕ_2, with $\mathrm{U}(1)_X$ charges one and two, respectively. In Table 3.1 we summarize the charges of the particles relevant for the model. The relevant part of the CISS Lagrangian for one generation is given by

$$\begin{aligned}\mathcal{L}_{\mathrm{CISS}} \supset -\Big\{ & y_{\mathrm{D}} \overline{L_{\mathrm{L}}} \nu_{\mathrm{R}} \widetilde{H} + y_1 \overline{N_{\mathrm{L}}} \nu_{\mathrm{R}} \phi_1 + \tilde{y}_1 \overline{N_{\mathrm{R}}^{\mathrm{c}}} \nu_{\mathrm{R}} \phi_1^* + \tfrac{y_2}{2} \overline{N_{\mathrm{L}}} N_{\mathrm{L}}^{\mathrm{c}} \phi_2 + \tfrac{\tilde{y}_2}{2} \overline{N_{\mathrm{R}}^{\mathrm{c}}} N_{\mathrm{R}} \phi_2^* + \mathrm{h.c.} \Big\} \\ & - \tfrac{\xi}{4} X^{\mu\nu} F_{\mu\nu} - V(H,\, \phi_1,\, \phi_2) \,.\end{aligned} \tag{3.2}$$

The left-handed lepton doublet $L_{\mathrm{L}} = (\nu_{\mathrm{L}},\, \ell_{\mathrm{L}})^\intercal$ was introduced in Table 2.1 and the SM Higgs boson is given by $H = (H^+,\, H^0)^\intercal = \frac{1}{\sqrt{2}}(h_1 + \mathrm{i}\ h_2,\, h_3 + \mathrm{i}\ h_4)^\intercal$ as defined in Eq. (2.3). The complex SM singlets ϕ_1 and ϕ_2 are normalized in a similar way as the Higgs. In the first line of the above equation the fermions' Yukawa couplings are given, where y_{D}, y_1 and $\tilde{y}_1$ are of Dirac type and y_2 and $\tilde{y}_2$ of Majorana type. Note that with the lepton number assignments given in Table 3.1 the Yukawa couplings y_1 and $\tilde{y}_1$ explicitly violate lepton number. Hence, lepton number is not a symmetry of the Lagrangian in the CISS. In the first term in the second line of Eq. (3.2) the expression $X^{\mu\nu} = \partial^\mu X^\nu - \partial^\nu X^\mu$ denotes the field strength tensor of $\mathrm{U}(1)_X$, where ξ parametrizes the kinetic mixing between the gauge bosons of the hidden sector and of the SM hypercharge $\mathrm{U}(1)_{\mathrm{Y}}$. The scalar potential given by

$$\begin{aligned}V(H,\, \phi_1,\, \phi_2) = {} & \frac{\lambda_H}{2}(H^\dagger H)^2 + \frac{\lambda_1}{2}|\phi_1|^4 + \frac{\lambda_2}{2}|\phi_2|^4 \\ & + \kappa_{H1} H^\dagger H |\phi_1|^2 + \kappa_{H2} H^\dagger H |\phi_2|^2 + \kappa_{12} |\phi_1|^2 |\phi_2|^2 \,.\end{aligned} \tag{3.3}$$

We remark that all couplings of the theory are dimensionless. In particular, there are no masses in the model. Hence, the underlying model at tree level describes a conformal theory as discussed in Section 2.2.5.

Table 3.1: Charges under $\mathrm{U}(1)_X$ and $\mathrm{U}(1)_\mathrm{Y}$, and dimension of the $\mathrm{SU}(2)_\mathrm{L}$ representation for the relevant particles in the model. We have included the SM Higgs and lepton doublet here since they possess interactions with the new particles. Note that lepton number is not a symmetry of the model's Lagrangian. Still, we have listed the would-be quantum numbers in the last line of the table.

field	L_L	ν_R	N_L	N_R	H	ϕ_1	ϕ_2
$\mathrm{U}(1)_X$	0	0	1	1	0	1	2
$\mathrm{U}(1)_\mathrm{Y}$	$-1/2$	0	0	0	$1/2$	0	0
$\mathrm{SU}(2)_\mathrm{L}$	**2**	**1**	**1**	**1**	**2**	**1**	**1**
lepton number	1	1	0	0	0	0	0

The particle spectrum of the CISS contains three scalar fields. We will assume that a scalar field develops a non-vanishing vev if it is electrically neutral and CP-even, i.e. invariant under $\mathrm{U}(1)_\mathrm{em}$ and CP transformations, respectively. Accordingly, h_3 and the real parts of ϕ_1 and ϕ_2 are assumed to develop vevs in the model. We will denote the non-vanishing vevs by $\langle h_3\rangle$, $\langle\phi_1\rangle$ and $\langle\phi_2\rangle$, where $\langle\phi_i\rangle$ is a short-hand notation for $\langle\mathrm{Re}\,(\phi_i)\rangle$. In particular, we will assume the following hierarchy among the scalar condensates

$$\langle\phi_1\rangle \gg \langle h_3\rangle > \langle\phi_2\rangle\,. \tag{3.4}$$

The vevs spontaneously break the symmetries of the scalar potential (except for $\mathrm{U}(1)_\mathrm{em}$) as will be described in Section 3.3. There, we will also explain how the mentioned vev hierarchy is obtained. From the kinetic terms for ϕ_1 and ϕ_2 it is then straightforward to derive the mass of the hidden gauge boson in the broken phase,

$$m_X = g_X\left(\langle\phi_1\rangle^2 + 4\langle\phi_2\rangle^2\right)^{1/2} \approx g_X\langle\phi_1\rangle\,, \tag{3.5}$$

where in the approximation we have taken into account the assumed hierarchy of the vevs.

3.2 Neutrino masses and leptonic mixing

In this section we will discuss the neutrino masses and mixing induced by the symmetry breaking pattern in the CISS. In the Majorana basis defined as $n_\mathrm{L} = (\nu_\mathrm{L},\, \nu_\mathrm{R}^\mathrm{c},\, N_\mathrm{L},\, N_\mathrm{R}^\mathrm{c})^\intercal$ the neutrino mass matrix is given by

$$\mathcal{M} = \frac{1}{\sqrt{2}}\begin{pmatrix} 0 & y_\mathrm{D}\langle h_3\rangle & 0 & 0 \\ y_\mathrm{D}\langle h_3\rangle & 0 & y_1\langle\phi_1\rangle & \tilde{y}_1\langle\phi_1\rangle \\ 0 & y_1\langle\phi_1\rangle & y_2\langle\phi_2\rangle & 0 \\ 0 & \tilde{y}_1\langle\phi_1\rangle & 0 & \tilde{y}_2\langle\phi_2\rangle \end{pmatrix} = \begin{pmatrix} 0 & m_\mathrm{D} & 0 & 0 \\ m_\mathrm{D} & 0 & M_1 & M_2 \\ 0 & M_1 & \mu_1 & 0 \\ 0 & M_2 & 0 & \mu_2 \end{pmatrix}\,. \tag{3.6}$$

Note that in writing the above equation we have considered the one-flavor case for simplicity. It is, however, straightforward to extend the matrix to include

Figure 3.1: Schematic illustration of the allowed and forbidden neutrino mass terms, which yield the form of the neutrino mass matrix in the CISS. Solid lines indicate a gauge-invariant Yukawa coupling of the fields connected by that line and mediated by the scalar particle assigned to the line. The terms corresponding to dashed lines are gauge-invariant, too. However, they are not admissible in a conformal theory due to the lack of an adequate scalar degree of freedom that could induce the necessary Yukawa coupling.

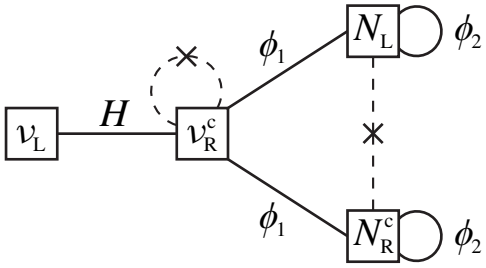

more neutrinos in each sector.[1] In Figure 3.1 we illustrate which neutrino mass terms can be generated in the underlying conformal model. There, we see that the interplay between the spectra of scalar particles on the one hand and neutral leptons on the other leads to the particular pattern of the mass matrix in the CISS. Note that the possible mass terms for ν_{L} with neutrinos other than ν_{R} – including ν_{L} itself – are not present in the Lagrangian given in Eq. (3.2) because such terms would break SM gauge invariance. The hierarchy for the vevs in Eq. (3.4) leads to a mass scale hierarchy according to $M_i > m_{\mathrm{D}} > \mu_i$. Note that we assume an approximate N_{L}-$N_{\mathrm{R}}^{\mathrm{c}}$ exchange symmetry in the neutrino sector, which is softly violated by higher-order interactions. Accordingly, the symmetry fixes $y_i \approx \tilde{y}_i$ or equivalently $M_1 \approx M_2$ and $\mu_1 \approx \mu_2$.

The diagonalization of the mass matrix is presented in Appendix A. The procedure yields two light mass eigenvalues, which to leading order are given by Eqs. (A.22) and (A.23) as

$$m_- \approx \mu_+ \frac{m_{\mathrm{D}}^2}{M^2}\,, \tag{3.7}$$

$$m_+ \approx \mu_+\,, \tag{3.8}$$

where $\mu_\pm \equiv \frac{1}{2}(\mu_1 \pm \mu_2)$ and $M^2 \equiv M_1^2 + M_2^2$. The eigenvalues in the heavy sector given in Eq. (A.24) in the limit $M_{\mathrm{R}} \to 0$ become

$$M_\pm = \frac{1}{2}\left(\mu_+ \pm \sqrt{\mu_+^2 + 4M^2}\right) = \pm M + \frac{\mu_+}{2} \pm \mathcal{O}\left(\frac{\mu_+^2}{M}\right)\,, \tag{3.9}$$

where in the last step we have expanded the heavy eigenvalues in powers of M^{-1}. Finally, for the mixing matrix U, which diagonalizes the mass matrix as

[1] In our phenomenological analysis of the CISS, which will be presented in Section 3.4, we consider a realistic scenario, in which y_{D} is a 3×2 matrix and the remaining Yukawa couplings are 2×2 matrices.

$\mathcal{M}^{\text{diag}} = U^{\intercal}\mathcal{M}U$, the order of magnitude of its elements has been estimated in Eq. (A.21) according to

$$U^{\dagger} \sim \mathcal{O}\begin{pmatrix} 1 & \Theta\eta_+ & \Theta & \Theta \\ \tilde{\Theta} & \eta_- & \frac{1}{\sqrt{2}} & \frac{1}{\sqrt{2}} \\ \Theta & \frac{1}{\sqrt{2}} & \frac{1}{\sqrt{2}} & \frac{1}{\sqrt{2}} \\ \Theta & \frac{1}{\sqrt{2}} & \frac{1}{\sqrt{2}} & \frac{1}{\sqrt{2}} \end{pmatrix} \tag{3.10}$$

with the entries defined as

$$\Theta = \frac{m_{\text{D}}}{M}\,, \qquad \tilde{\Theta} = \Theta\,\frac{\mu_+}{\mu_-} \qquad \text{and} \qquad \eta_\pm = \frac{\mu_\pm}{M}\,. \tag{3.11}$$

In the following we will discuss the implications of Eqs. (3.7) - (3.10) for the neutrinos in the CISS.

The lightest of the eigenvalues, m_-, given by the inverse seesaw formula is to be identified with the mass scale of the SM neutrinos. Note that in a realistic scenario, which will be discussed in Section 3.4, Eqs. (3.7) - (3.9) denote matrices and m_- is equal to the SM neutrino mass matrix m_ν. The eigenvalues $M_\pm$ correspond to a pseudo-Dirac neutrino with Dirac mass proportional to M and Majorana-type corrections of the order of μ_+. Finally, the intermediate mass eigenstate, m_+, can be an excellent warm dark matter candidate if μ_+ is chosen in the keV range. We will quantify this statement in our analysis in Section 3.4. According to the mass spectrum we will denote the neutrino mass eigenstates by

$$\tilde{n} = (\nu_{\text{SM}},\, n_{\text{DM}},\, N_1,\, N_2)^{\intercal} \equiv U^{\dagger} n_{\text{L}}\,. \tag{3.12}$$

With the help of the above equation together with Eq. (3.10) we will now briefly discuss the mixing for the neutrinos to be expected in our model.

As it is common, we will refer to the SM neutrinos as *active* neutrinos, while we will refer to the heavy pseudo-Dirac states as *sterile* neutrinos. Putting this terminology into practice, the active-sterile mixing is given by $\Theta = m_{\text{D}}/M$ [see Eq. (3.10)]. From Eq. (3.7) we see that the leading-order contribution to the active neutrino masses is given by $m_\nu = \Theta^2\mu_+$. Then with $\mu_+ \sim \mathcal{O}\,(1-10)$ keV, we obtain active neutrino masses of m_ν smaller than 1 eV for active-sterile mixing of the order of 10^{-2} or smaller. It is important to notice that the active-sterile mixing in the CISS can be sizable compared to type-I seesaw mixing $\Theta_{\text{type-I}} \sim v_{\text{ew}}/\Lambda_{\text{GUT}} \ll 10^{-2}$ since the neutrino masses of our model are not subject to large scale separation.

The mixing between the dark matter candidates and the active neutrinos is given by $\tilde{\Theta}^2 = (m_{\text{D}}/M)^2\ (\mu_-/\mu_+)^2$. Remember that we assumed an N_{L}-N_{R}^{c} exchange symmetry, which is softly broken by loop corrections. In order to maintain this approximate symmetry we require the quantity μ_-/μ_+, which incorporates the violation of the symmetry, to be smaller than about 10^{-3}. Thus, we can estimate that the mixing $\tilde{\Theta}^2$ is of the order of $10^{-10} - 10^{-12}$. In Section 3.4 we will apply cosmological and astronomical constraints to the mixing $\tilde{\Theta}$ in order to reduce the parameter space of the CISS.

After we have seen how neutrino masses and their mixings arise from the assumed vev hierarchy we will now study the electroweak symmetry breaking in the CISS.

3.3 Electroweak symmetry breaking

In the following we will discuss how the vacuum expectation values of the scalars of the theory spontaneously break the symmetry of the potential introduced in Eq. (3.3). First, we will parametrize the relevant scalar fields and their vevs and derive the minimum conditions for the potential (i.e. the Gildener-Weinberg conditions). Afterwards, we will determine the expressions for all non-vanishing scalar masses. The mass of the PGB of broken scale invariance, which is identical to the potential's curvature at the extremum, will be of particular interest. We will conclude the section with a parameter scan for the PGB mass with respect to the masses of the other particles of the model to identify the mass ranges, for which consistent electroweak symmetry breaking can take place.

In order to locate the minimum of the scalar potential within the Coleman-Weinberg (CW) mechanism [36] we apply the Gildener-Weinberg (GW) formalism [159] as described in Section 2.2.5. Accordingly, we parametrize the electrically neutral, CP-even scalars as

$$\begin{aligned} \mathrm{Re}\,(\phi_1) &= r \cdot n_1 = r\cos\theta\,, \\ \mathrm{Re}\,(\phi_2) &= r \cdot n_2 = r\sin\theta\sin\omega\,, \\ h_3 &= r \cdot n_3 = r\sin\theta\cos\omega\,, \end{aligned} \tag{3.13}$$

where the n_i's are normalized to $\sum_i n_i^2 = 1$, and $r \neq 0$ denotes the radial coordinate along the flat direction $\mathbf{\Phi}_{\text{flat}} = (\mathrm{Re}\,(\phi_1), \mathrm{Re}\,(\phi_2), h_3)^\intercal$ in scalar field space. Remember that for the sake of brevity we write $\mathrm{Re}\,(\phi_i) = \phi_i$. Using the scalar mixing angles we define the parameters $\varepsilon = \tan^2\theta$ and $\delta = \tan^2\omega$. In terms of ε and δ the vevs of the components of the flat direction can be expressed as

$$\begin{aligned} \langle\phi_1\rangle &= \langle r\rangle\sqrt{\frac{1}{1+\varepsilon}} \equiv v\,, \\ \langle\phi_2\rangle &= v\sqrt{\frac{\epsilon\,\delta}{1+\delta}}\,, \\ \langle h_3\rangle &= v\sqrt{\frac{\epsilon}{1+\delta}}\,, \end{aligned} \tag{3.14}$$

where we have extracted the common factor $v \equiv \langle\phi_1\rangle = \langle r\rangle(1+\varepsilon)^{-1/2}$ from the individual vevs. The quantity v represents the scale of spontaneous conformal symmetry breaking and in a conformal theory all physical masses must be proportional to this unique scale. Note that in the present scenario the electroweak vev is given by the Higgs vev as in the SM since both ϕ_1 and ϕ_2 are SM gauge singlets and thus have no influence on the electroweak vev. Accordingly, the scale of

spontaneous conformal symmetry breaking can be connected to the electroweak vev in the SM by the simple relation $v_{\rm ew} \equiv \langle h_3 \rangle = v\,\varepsilon^{1/2}(1+\delta)^{-1/2}$, where we have used Eq. (3.14).

After applying the parametrization in Eq. (3.13) and assuming the vev structure in Eq. (3.14), we can derive the following GW conditions on the couplings and vevs from the first derivatives of the potential in Eq. (3.3) with respect to ϕ_1, ϕ_2 and h_3

$$\left.\frac{\partial V}{\partial \phi_1}\right|_{\rm min} \propto (1+\delta)\lambda_1 + \varepsilon\kappa_{H1} + \varepsilon\delta\kappa_{12} \stackrel{!}{=} 0\,, \tag{3.15}$$

$$\left.\frac{\partial V}{\partial \phi_2}\right|_{\rm min} \propto \sqrt{\varepsilon\delta}(\varepsilon\delta\lambda_2 + \varepsilon\kappa_{H2} + (1+\delta)\kappa_{12}) \stackrel{!}{=} 0\,, \tag{3.16}$$

$$\left.\frac{\partial V}{\partial h_3}\right|_{\rm min} \propto \sqrt{\varepsilon}(\varepsilon\lambda_H + (1+\delta)\kappa_{H1} + \varepsilon\delta\kappa_{H2}) \stackrel{!}{=} 0\,, \tag{3.17}$$

and from the vanishing of the tree-level potential

$$\begin{aligned} V|_{\rm min} \propto\ & \varepsilon^2\lambda_H + (1+\delta)^2\lambda_1 + \varepsilon^2\delta^2\lambda_2 \\ & + 2\varepsilon(1+\delta)\kappa_{H1} + 2\varepsilon^2\delta\kappa_{H2} + 2\varepsilon\delta(1+\delta)\kappa_{12} \stackrel{!}{=} 0\,. \end{aligned} \tag{3.18}$$

The above equation as well as Eqs. (3.15) - (3.17) have to be satisfied simultaneously at the renormalization point $\Lambda_{\rm GW}$. As remarked below Eq. (2.54), one of these conditions is always redundant.

In the following we will discuss the scalar spectrum in the broken phase. To reduce the available parameter space we apply GW conditions in order to eliminate three couplings from the equations of the theory. Then we assume the hierarchy $\langle\phi_1\rangle \gg \langle h_3\rangle > \langle\phi_2\rangle$ among the vevs, which is obtained for small ε and δ. After spontaneous symmetry breaking, we expect three physical, electrically neutral, CP-even scalars that are in general superpositions of h_3 and of the real parts of ϕ_1 and ϕ_2. Note, however, that the mixing in the scalar sector is relatively small so that the physical scalars are predominantly given by one of the fields mentioned. The physical scalar mainly given by h_3 will be denoted as h. In the following it is identified with the scalar observed at the LHC, which couples to the SM fermions. The second scalar mainly consisting of ϕ_2 is labelled $\mathcal{H}$. Finally, the PGB of broken scale invariance is dominantly given by ϕ_1 and will be called $\phi_{\rm PGB}$. Diagonalizing the mass-squared matrix of the CP-even excitations yields the non-zero scalar boson masses for h and $\mathcal{H}$, which are given by

$$\frac{M_h^2}{v^2} = \frac{\lambda_2\lambda_H - \kappa_{H2}^2}{\lambda_H}\,\delta\epsilon\,, \tag{3.19}$$

$$\frac{M_{\mathcal{H}}^2}{v^2} = \left(\lambda_H - \frac{\lambda_H^2 - \kappa_{H2}^2}{\lambda_H}\,\delta\right)\epsilon = \left[\lambda_H - (\lambda_H - \lambda_2)\,\delta\right]\epsilon - \frac{M_h^2}{v^2}\,. \tag{3.20}$$

Note that in a reasonable model the mass defined in Eq. (3.19) must be congruent to the Higgs mass. In agreement with our discussion in Section 2.2.5, the PGB's mass vanishes at tree level and can be computed at one-loop level by means of

Eq. (2.60) according to

$$m_{\mathrm{PGB}}^2 = \frac{1}{8\pi^2\langle r\rangle^2}\left(M_h^4 + M_{\mathcal{H}}^4 + 6m_W^4 + 3m_Z^4 + 3m_X^4 - 12m_t^4 - \sum_{i\,\in\,\mathrm{heavy}} d_i \cdot m_{N_i}^4\right), \tag{3.21}$$

where the sum runs over the heavy neutrino masses and d_i denotes the corresponding neutrino's real degrees of freedom. From the above equation we see that the PGB mass is determined by the masses of the scalars h and $\mathcal{H}$ (the remaining scalar degrees of freedom are massless due to the GW conditions), by the masses of the gauge bosons in the theory, i.e. of the W, Z and X bosons, and finally by the fermion masses, which give a negative contribution to m_{PGB}^2. In this context it is important to remember that $m_{\mathrm{PGB}}^2 > 0$ is a necessary consistency condition since only in this case the extremum of the potential is a minimum. Note that the contributions from the SM fermions apart from the top quark as well as from the light neutrinos are relatively small and, accordingly, have been neglected in Eq. (3.21).

As mentioned at the end of Section 2.2.5, the large top-quark mass always leads to a negative PGB mass-squared in the SM so no conformal symmetry breaking can occur in the electroweak model without additional bosons. In the CISS the PGB mass-squared obtains relevant contributions beyond the SM ones from the second scalar $\mathcal{H}$, the hidden gauge bosons X and the pseudo-Dirac neutrinos, which must compensate the top-quark contribution when summed up. For a constant value of $M_{\mathcal{H}} = 2$ TeV and a Higgs mass of $M_h = 125$ GeV (in agreement with experimental data [10]) the contours of the PGB mass are plotted in Figure 3.2 in the plane of the hidden gauge boson mass m_X and the pseudo-Dirac mass average $m_N \equiv \frac{1}{4}\sum_{i=6}^{9}|m_i|$. The area, in which conformal symmetry breaking is consistent, corresponds to parameter configurations that yield a positive PGB mass-squared, perturbative couplings and a Higgs portal mixing in agreement with the limit of $\sin\beta < 0.44$ [61].[2] To assure that the scalar couplings do not run into Landau poles or that the scalar potential does not develop instabilities before the Planck scale requires a detailed study of the renormalization group (RG) equations in the CISS, which lies beyond the scope of this work. The effects of RG running in quite generic conformal extensions of the SM have been thoroughly investigated in [69]. That study particularly showed that a minimum of parameters must be available in order to enable stable RG running up to the Planck scale. Since the CISS contains more degrees of freedom in all sectors than the minimal stable conformal extension of the SM presented in [69], the parameter space of the underlying model is expected to admit the evolution of the couplings without encountering Landau poles or instabilities below the Planck scale. The plot in the figure nicely illustrates the negative impact of the pseudo-Dirac neutrinos as the PGB mass tends to zero for increasing

[2] Note that the reported limit of $\sin\beta < 0.37$ [56] quoted in [1] meanwhile has been updated by [61]. Since the updated bound is weaker than the original one, naturally, our analysis is not affected by this change.

Figure 3.2: Contour plot of the pseudo-Goldstone boson mass m_{PGB} as function of the hidden gauge boson mass m_X and the averaged heavy pseudo-Dirac neutrino mass m_N. The plot shows the phenomenologically allowed region with a Higgs mass of $M_h = 125$ GeV, second scalar mass $M_{\mathcal{H}} = 2$ TeV, and with consistent radiative conformal symmetry breaking, i.e. positive pseudo-Goldstone mass-squared, perturbative couplings and Higgs portal mixings compatible with the bound $\sin\beta < 0.44$ [61]. Note that for higher values of $M_{\mathcal{H}}$ the region of allowed PGB masses grows towards higher values of m_N.

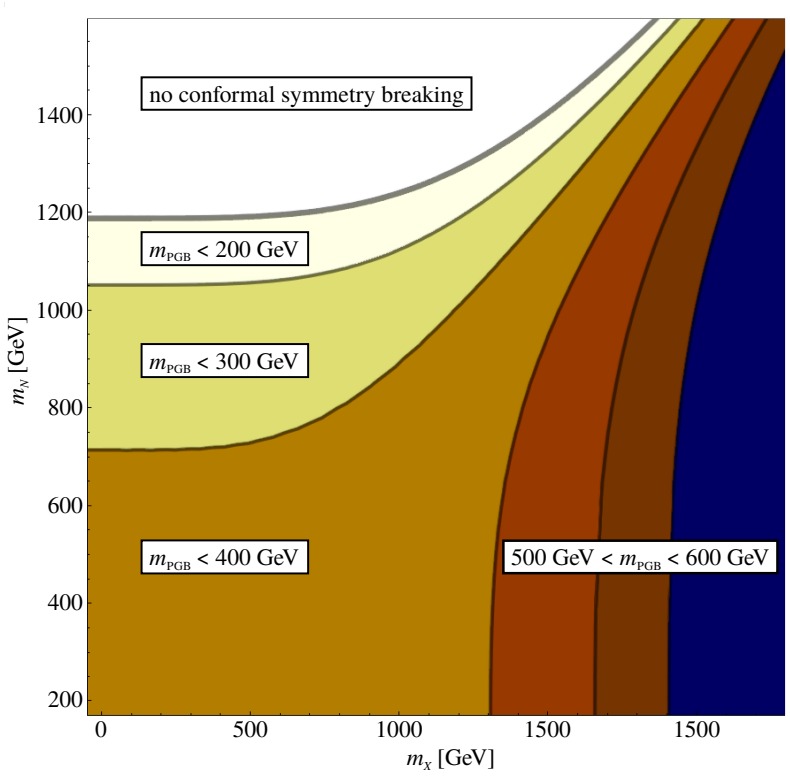

sterile masses and eventually becomes negative. For hidden gauge boson masses below 1 TeV we can even observe a limit of $m_N \lesssim 1.2$ TeV. At the same time, this particular region does not admit PGB masses above 400 GeV. Note that if the mass $M_{\mathcal{H}}$ is increased, the region of viable PGB masses is extended, according to Eq. (3.21), in the direction of higher heavy neutrino masses m_N.

To conclude the discussion of the electroweak symmetry breaking in the CISS we present two benchmark points in the scalar sector:

$$1.\quad \langle\phi_1\rangle = 1380\ \mathrm{GeV}\,,\quad \langle\phi_2\rangle = 38\ \mathrm{GeV}\,,\quad \langle h_3\rangle = 246\ \mathrm{GeV}\,,\quad M_{\mathcal{H}} = 2170\ \mathrm{GeV}\,,\quad M_h = 125.5\ \mathrm{GeV}\,;$$

$$2.\quad \langle\phi_1\rangle = 1250\ \mathrm{GeV}\,,\quad \langle\phi_2\rangle = 181\ \mathrm{GeV}\,,\quad \langle h_3\rangle = 246\ \mathrm{GeV}\,,\quad M_{\mathcal{H}} = 3060\ \mathrm{GeV}\,,\quad M_h = 124.9\ \mathrm{GeV}\,.$$

Both of the above points lie within the uncertainty of the value for the Higgs

mass $m_{\text{Higgs}} = [125.09 \pm 0.21(\text{stat.}) \pm 0.11(\text{syst.})]$ GeV [10] and reproduce the correct value for the SM vev $v_{\text{ew}} \equiv \langle h_3 \rangle$ [see Eq. (2.13) and also the discussion after Eq. (3.14)]. Furthermore, we see that the scale of spontaneous conformal symmetry breaking, $v \equiv \langle \phi_1 \rangle$, is typically in the TeV range as well as the mass of the second scalar, $M_{\mathcal{H}}$. Finally, we can observe the hierarchical pattern between the vevs as anticipated at the beginning of Section 3.2. Note that for the first benchmark point the hierarchy between $\langle \phi_2 \rangle$ and $\langle h_3 \rangle$ is more pronounced than for the second.

It is of particular interest to examine the ratios of the vevs for both benchmark points. We find that the small parameters introduced in the parametrization in Eq. (3.14) are given as $\epsilon \sim \mathcal{O}(10^{-2})$ and $\delta \sim \mathcal{O}(10^{-2} - 10^{-1})$. This confirms that the hierarchy among the vevs assumed in the CISS can be obtained for a quite natural choice of parameters. Furthermore, it reflects the characteristic of conformal theories that there exists only one scale v to which every dimensional quantity must be proportional. In consequence, the scales of the vevs cannot lie too far apart from the common scale of spontaneous symmetry breaking.

3.4 Phenomenology

After we have introduced our model in Section 3.1 and derived the model's mass spectrum and symmetry breaking in Sections 3.2 and 3.3, it is now time to examine the phenomenology of the model. This section is divided into three parts. The first part (Section 3.4.1) deals with the phenomenology of low-energy particle physics, the second (Section 3.4.2) with the collider phenomenology of the underlying model and the third part (Section 3.4.3) with the possibilities for dark matter production in the CISS.

3.4.1 Low-energy particle physics

In this part we will discuss the phenomenology of our model in the low-energy regime. The aim of this discussion is to derive constraints on the parameter space of the CISS. Eventually, these constraints are applied to find viable points in parameter space, which yield keV-scale masses for the dark matter candidates. The results of our analysis are plotted in Figures 3.3 and 3.4. The impact of low-energy phenomenology on these plots is discussed in the following.

Active neutrino masses and oscillations

In Section 3.2 we have considered the neutral lepton mass matrix in the simple one-flavor case. Here we will set up a realistic scenario containing three SM neutrino fields ν_{L}. For each additional neutrino species ν_{R}, N_{L} and N_{R}, we assume two generations consistent with the minimal inverse seesaw model in [160]. According to this set-up, the mass matrix defined in Eq. (3.6) is a 9×9 symmetric matrix, whose elements are matrices. Equally, the mixing matrix is

a 9×9 matrix. Following our discussion in Section 3.2 we expect an eigenvalue spectrum with three active neutrino masses given by Eq. (3.7), two keV masses given by Eq. (3.8) and two pairs of pseudo-Dirac neutrinos with masses as in Eq. (3.9). Note that the leading-order contribution to the active neutrino masses in the matrix form is governed by the inverse seesaw formula as

$$m_- \equiv m_\nu = m_{\mathrm{D}}^{\intercal}(M\mu_+^{-1}M^{\intercal})^{-1}m_{\mathrm{D}}\,. \tag{3.22}$$

Accordingly, we will use the above equation instead of Eq. (3.7) in the following.

For our analysis we consider both neutrino mass orderings, i.e. we carry out our analysis for both possible signs of Δm^2_{31}. To ensure a consistent reproduction of standard neutrino oscillations as described in Section 2.2.1 it is sufficient to have only two non-vanishing SM neutrino masses. Hence, we set the lightest neutrino mass equal to zero, $m_{\text{lightest}} \equiv 0$.[3] Furthermore, we require for the mixing matrix U_{PMNS}, which is given by the upper-left 3×3 block of U, that its elements should be in agreement with their best-fit values.[4] To this end, we employ a parametrization of the Dirac mass matrix m_{D} due to Casas and Ibarra [161]. Note that in their work a generic supersymmetric version of the seesaw mechanism was considered while our model for neutrino masses is based on the inverse seesaw. Hence, we need to adequately derive the formula for the parametrization of m_{D} in terms of the oscillation parameters in the context of the neutral lepton mass matrix in the CISS. Notice that it is valid to only consider the active-neutrino subspace belonging to the massive neutrinos and to neglect the part belonging to the massless eigenstate. Accordingly, we take U_{PMNS} in the following parametrization as 3×2 matrix without any loss of information. Let us collect the two non-vanishing active neutrino masses in a diagonal 2×2 matrix $m_{\text{light}} = \mathrm{diag}(m_2, m_3)$. For appropriate field redefinitions we can assume that the 2×2 matrix μ_+ is also diagonal. Since $m_2 > 0$ and $m_3 > 0$, we can unambiguously define the square-root of the diagonal active neutrino mass matrix as $m_{\text{light}}^{1/2} = \mathrm{diag}(m_2^{1/2}, m_3^{1/2})$ as well as the inverse of the square-root matrix $m_{\text{light}}^{-1/2} = \mathrm{diag}(m_2^{-1/2}, m_3^{-1/2})$. Similar definitions of the (inverse) square-root apply to the Majorana mass matrix μ_+. Then using Eq. (3.22) we can write the following equation

$$\mathbb{1} = \left(m_{\text{light}}^{-1/2} U_{\text{PMNS}}^{\intercal}\, m_{\mathrm{D}}^{\intercal}\, (M^{\intercal})^{-1}\, \mu_+^{1/2}\right)\left(\mu_+^{1/2} U_{\text{PMNS}}\, M^{-1}\, m_{\mathrm{D}}\, m_{\text{light}}^{-1/2}\right)\,. \tag{3.23}$$

Note that the two expressions in parentheses are the transpose of each other. Accordingly, we can define the orthogonal, in general complex 2×2 matrix $O(\alpha)$ parametrized by some mixing angle α as

$$O(\alpha) \equiv \mu_+^{1/2} U_{\text{PMNS}}\, M^{-1}\, m_{\mathrm{D}}\, m_{\text{light}}^{-1/2}\,. \tag{3.24}$$

[3] Note that the rank of the active neutrino mass matrix in Eq. (3.22) obeys $\mathrm{rk}(m_\nu) \leq 2$ as can be easily shown using Eqs. (B.1) and (B.2), which analytically forces us to set the lightest neutrino mass to zero at leading order.

[4] We use the best-fit values for mixing angles and mass-squared differences without errors as given in [115], where a global analysis of three-neutrino oscillations was performed taking into account all current constraints on the mixing parameters.

Solving the above equation for m_{D} yields

$$m_{\mathrm{D}} = M\mu_{+}^{-1/2} O(\alpha) m_{\mathrm{light}}^{1/2} U_{\mathrm{PMNS}}^{\dagger} \,. \tag{3.25}$$

As mentioned before we take U_{PMNS} to be a 3×2 matrix in the above equations. We will use Eq. (3.25) to parametrize m_{D} in our numerical analysis. As a final remark on Eq. (3.25), let us highlight the fact that m_{D} linearly depends on M. As a consequence, a possible hierarchy in the Yukawa couplings of m_{D} and M can cancel in Eq. (3.22) so that the light neutrinos experience only a reduced hierarchy between their masses.

After having taken care of SM neutrino masses and oscillations, we will discuss further low-energy constraints on our model in the following.

Non-unitarity of the PMNS matrix

With the additional neutrinos in our model the lepton mixing matrix U_{PMNS} introduced in the charged-current interactions in the mass basis [see Eq. (2.27)] is no longer necessarily unitary since it is only *part* of the larger unitary mixing matrix U. However, the deviation of the mixing matrix U_{PMNS} from unitarity can be constrained by electroweak data. Indeed, as U_{PMNS} enters the leptonic charged-current interactions, the effects of its non-unitarity manifest themselves in leptonic and semileptonic processes such as leptonic W boson and pion decays and rare lepton decays like $\mu^{\pm} \to e^{\pm}\gamma$. Furthermore, a non-unitary active neutrino mixing matrix even remains present in the leptonic neutral-current interactions, thus, altering the invisible decay width of the Z boson. Likewise, since Fermi's constant G_{F} is determined in muon decays, this physical quantity will also be effected by the non-unitarity of U_{PMNS}. For a detailed discussion of lepton non-unitarity and its implications we refer to [162–164].

For our analysis we define the flavor dependent observables

$$\varepsilon_{\alpha} = \sum_{i>3} |U_{\alpha i}|^2 \quad \text{with} \quad \alpha \in \{e,\, \mu,\, \tau\} \,. \tag{3.26}$$

Taking into account that the mixing between the active neutrinos and the dark matter candidates is suppressed we see from Eq. (3.26) that the non-unitarity parameters are dominated by the active-sterile mixing. As shown in Section 3.2, the strength of this mixing is determined by the ratio m_{D}^2/M^2. Remember that $M \sim \langle \phi_1 \rangle = v$, i.e. the sterile neutrino mass is proportional to the conformal symmetry breaking scale. Then again, m_{D} is generated at the electroweak scale, which cannot be too far away from v. Hence, it is possible to obtain sizable active-sterile mixing in our model. In this context it is of particular interest that a sizable active-sterile mixing paired with heavy sterile masses can improve the fit to electroweak precision observables as shown in [163]. Measurable phenomenological consequences of a large mixing can be expected for non-unitarity parameters ε_{α} above the order of 10^{-6}. The most sensitive observables to the non-unitarity are the already mentioned invisible decay width of the Z boson Γ_Z^{inv} and

Fermi's constant derived from the muon decay constant G_μ. They depend on the non-unitarity parameters of Eq. (3.26) as [163]

$$\frac{\Gamma_Z^{\text{inv}}}{(\Gamma_Z^{\text{inv}})_{\text{SM}}} = \frac{1}{3}\sum_{\alpha=e,\,\mu,\,\tau}(1-\varepsilon_\alpha)^2\,, \tag{3.27}$$

$$G_\mu = G_{\text{F}}(1-\varepsilon_e)(1-\varepsilon_\mu)\,. \tag{3.28}$$

The above equations enable us to constrain our parameter space.

Lepton universality

A further constraint on the parameter space comes from lepton universality. In the SM leptons are coupled to the electroweak gauge bosons with the same strength, regardless of their flavor. One can, however, assume that there exist individual coupling constants for each flavor. The coupling constants can be constrained by various experiments as discussed in [165]. Related to the elements of the mixing matrix this yields the limits

$$\begin{aligned}\varepsilon_e - \varepsilon_\mu &= 0.0022 \pm 0.0025\,,\\ \varepsilon_\mu - \varepsilon_\tau &= 0.0017 \pm 0.0038\,,\\ \varepsilon_e - \varepsilon_\tau &= 0.0039 \pm 0.0040\,.\end{aligned} \tag{3.29}$$

The above limits have been taken into account in order to further narrow down the available parameter space.

Lepton number violation

As mentioned in Section 3.1, in the CISS lepton number is not a symmetry of the tree-level Lagrangian in contrast to the SM tree-level Lagrangian, which conserves baryon and lepton number separately at the perturbative level. In particular, lepton number is violated by one unit in the Yukawa interactions involving ϕ_1. Hence, $0\nu\beta\beta$ is in principle possible in the CISS. Note, however, that the LNV Majorana masses are always proportional to the Yukawa coupling y_2 (or, respectively, $\tilde{y}_2$), which is naturally small for $\mu \sim \mathcal{O}(1)$ keV and $\langle\phi_2\rangle \sim \mathcal{O}(10-100)$ GeV. In the following we will investigate the contributions to $0\nu\beta\beta$ from the different types of neutrinos in the CISS. We will show that because the heavy neutrinos in the model are pseudo-Dirac particles, no $0\nu\beta\beta$ rate above the one expected from light neutrino exchange is predicted. For the basics of $0\nu\beta\beta$ we refer to Section 2.2.3.

With masses in the sub-eV and keV region the active neutrinos and, respectively, the dark matter candidates fall in the category of light neutrinos. Their contribution to the decay rate of $0\nu\beta\beta$ can be described by the effective parameter η_{eff}^{ν} defined in Eq. (2.48) once the dark matter candidates are included into the sum. Note, however, that the dark matter mixing to the active neutrinos is

negligible and we can approximate

$$\eta^{\nu}_{\text{eff}} = \frac{1}{m_e}\left(\sum_{i=1}^{3} U_{ei}^2 m_i + \sum_{i=4}^{5} \tilde{\Theta}^2 m_i\right) \approx \frac{1}{m_e}\left(\sum_{i=1}^{3} U_{ei}^2 m_i\right) = \frac{m_{ee}}{m_e}\,. \tag{3.30}$$

If we insert the eigenvalue for the active neutrinos given in Eq. (3.7), we find from the above equation that the effective light Majorana mass m_{ee} is proportional to $\Theta^2\mu_+$. We can even put an upper limit on the active neutrino contribution if we remember that in the CISS the lightest neutrino is massless. Hence, we can evaluate the sum in Eq. (3.30) with $m_{\text{lightest}} = 0$, which yields the upper bound

$$\begin{aligned} m_{ee} &\equiv \sum_{1}^{3} U_{ei}^2 m_i \\ &\leq \cos\theta_{12}^2 \cos\theta_{13}^2 \sqrt{|\Delta m_{31}^2|} + \sin\theta_{12}^2 \cos\theta_{13}^2 \sqrt{|\Delta m_{31}^2| + \Delta m_{21}^2} \\ &\approx 0.049 \text{ eV}\,, \end{aligned} \tag{3.31}$$

where we have used Eqs. (2.38) and (2.39) and have assumed an inverted ordering (IO) for the SM neutrino masses, which in general yields a larger effective Majorana mass than the normal ordering (NO). Note that in deriving the above limit we have neglected possible phases in the mixing matrix as including them could only lead to even smaller values for m_{ee}. For the numerical estimate we have used the best-fit values for IO given in [115]. The limit for the light neutrino contribution in Eq. (3.31) is well below the reach of current $0\nu\beta\beta$ experiments (see Table 4.2 of the next chapter). Next we consider the pseudo-Dirac neutrino contributions.

In the underlying model the mass eigenvalues m_6 and m_7, and m_8 and m_9 respectively form pseudo Dirac mass pairs. From Eq. (3.9) it follows that the mass sum of a pseudo-Dirac pair is given by

$$m_6 + m_7 \approx m_8 + m_9 \approx \mu_+\,. \tag{3.32}$$

The pseudo-Dirac neutrino masses in the CISS have a wide spectrum and can range from some MeV up to TeV. Hence, they can be lighter or heavier than the typical momentum transfer $|p| = 100$ MeV in $0\nu\beta\beta$ or of about the same size. If the pseudo-Dirac neutrinos are lighter than about 100 MeV, their contribution can be approximated by Eq. (2.48). Note that for pseudo-Dirac masses below 100 MeV the Yukawa couplings y_{D} need to be sufficiently small in order to maintain $\Theta < 1$. Taking into account the active-sterile mixing given by Θ, we obtain for the light pseudo-Dirac neutrino contribution

$$m^{\text{pD}}_{\text{eff}} = \sum_{i=6}^{9} U_{ei}^2 m_i \sim \Theta^2 \mu_+\,, \tag{3.33}$$

where we have used Eq. (3.32). The above equation shows that from light pseudo-Dirac neutrinos we expect a similar contribution to the rate of $0\nu\beta\beta$ as from the active neutrinos, which is limited by Eq. (3.31).

In the case that the pseudo-Dirac neutrinos are heavier than some 100 MeV, we can approximate their contribution with Eq. (2.50), according to which the effective parameter is given by

$$\eta_{\text{eff}}^{\text{pD}} = m_p \left(\sum_{i=6}^{9} U_{ei}^2 \frac{1}{m_i} \right) \sim m_p \frac{\Theta^2 \mu_+}{M^2} \,, \tag{3.34}$$

where the estimate in the last step can be obtained from direct computation. To compare the quantity in the above equation with the light neutrino contribution we need to multiply Eq. (3.34) by the electron mass. Accordingly, the heavy pseudo-Dirac contribution is suppressed with respect to the light neutrino contribution by a factor $m_e m_p / M^2$. For pseudo-Dirac masses above 1 GeV the suppression factor is smaller than 5×10^{-4}, where we have used $m_e = 0.511$ MeV and $m_p = 938.272$ MeV [87]. Note that a more accurate comparison of the light and heavy neutrino contributions to $0\nu\beta\beta$ would actually require to account for the different nuclear matrix elements. The above estimate, however, is sufficient to determine that the contribution of the heavy neutrinos is suppressed.

Finally, when the pseudo-Dirac mass is of the same size as the momentum transfer we put $|p| \approx M$. Then from Eq. (2.49) we can deduce that the effective parameter in this case can be expressed as

$$\eta_{\text{eff}}^{\text{pD}} = m_p \left(\sum_{i=6}^{9} U_{ei}^2 \frac{m_i}{|p|^2 + m_i^2} \right) \sim m_p \frac{\mu_+^2}{M^2} \frac{\Theta^2 \mu_+}{M^2} \,, \tag{3.35}$$

which is even more suppressed than the contribution in Eq. (3.34).

In conclusion we have shown that the neutral leptons and in particular pseudo-Dirac neutrinos in the CISS only give negligible contributions to the rate of $0\nu\beta\beta$. In agreement with this conclusion we did not find any additional constraints on the parameter space from $0\nu\beta\beta$ in our numerical analysis.

Lepton flavor violation

Even though lepton *number* violation is suppressed in our model, it is still possible to have considerable lepton *flavor* violation (LFV). The currently most stringent bound on LFV comes from the MEG collaboration, which has searched for the decay of an anti-muon into a positron and a photon. The collaboration limits the branching ratio for this process to $\text{BR}(\mu^+ \to e^+\gamma) < 5.7 \times 10^{-13}$ at 90% confidence level [166]. The branching ratio can be calculated [167] (see also [168–171]) according to

$$\text{BR}(\mu \to e\gamma) \equiv \frac{\Gamma(\mu \to e\gamma)}{\Gamma(\mu \to e\nu\overline{\nu})} = \frac{3\alpha_{\text{em}}}{32\pi} 2 \left| \sum_{i=1}^{9} U_{ei}^* U_{\mu i} \, g\left(\frac{m_i^2}{m_W^2} \right) \right|^2 \,, \tag{3.36}$$

where α_{em} denotes the electromagnetic fine-structure constant and $g(x)$ is a loop function given by

$$g(x) = \int_0^1 \text{d}a \, \frac{2(1-a)(2-a) + a(1+a)x}{1 - a + ax} (1-a) \,. \tag{3.37}$$

Note that for small neutrino masses the above loop function is simply given by $g(m_i^2/m_W^2) \approx g(0) = 5/3$. We use Eq. (3.36) to calculate the branching ratio obtained in our model and apply the MEG limit to exclude points in parameter space that give too large $\mathrm{BR}(\mu^+ \to e^+\gamma)$. We also consider the potential of the proposed MEG upgrade with a designated sensitivity to branching rations of $\mathrm{BR}(\mu^+ \to e^+\gamma) \approx 6 \times 10^{-14}$ [172].

Another constraint on LFV physics can be obtained from the decay channel $\mu^+ \to e^+e^+e^-$ (abbreviated as $\mu \to 3e$). The current limit on this process is given by $\mathrm{BR}(\mu^+ \to e^+e^+e^-) < 1.0 \times 10^{-12}$ at 90% confidence level [173]. In the meantime, a new experiment, called "Mu3e", has been proposed in order to search for this process and is aiming for a sensitivity to reach $\mathrm{BR}(\mu^+ \to e^+e^+e^-) \approx 1.0 \times 10^{-16}$ [174]. Even though this limit looks supposedly stronger than the one from $\mu \to e\gamma$, note that in our model there is no interaction that leads to $\mu \to 3e$ directly. Hence, the decay $\mu \to 3e$ is suppressed by a factor of α_{em} with respect to $\mu \to e\gamma$ since it can only take place via the decay $\mu \to e\gamma$ with subsequent pair creation $\gamma \to e^+e^-$.

Combined limits

In order to find viable points in the parameter space of the CISS we combine the limits that we have discussed in the preceding subsections. Accordingly, in our analysis we only include points that correctly reproduce the neutrino mass-squared differences and standard oscillations. Furthermore, we apply the non-unitarity and lepton universality limits as well as the constraint from $\mathrm{BR}(\mu \to e\gamma)$.[5] The results of our analysis are presented in Figures 3.3 and 3.4, which we will discuss in the following. Note that both figures show a scenario with inverted neutrino mass ordering. The results for normal ordering are comparable to those of inverted ordering, but with a little weaker limits on $\mathrm{BR}(\mu^+ \to e^+\gamma)$.

The plot in Figure 3.3 shows points in the parameter plane of the sterile neutrino mass average $m_N \equiv \frac{1}{4}\sum_{i=6}^{9} |m_i|$ and the dark matter candidate's mass average $m_{\mathrm{DM}} \equiv \frac{1}{2}\sum_{i=4}^{5} |m_i|$. Each blue dot corresponds to a complete set of model parameters in consistence with the previously discussed low-energy phenomenology. The lower red band shows the lepton universality exclusion limit. Note that the blue dots inside of the excluded region are the result of numerical uncertainties of the analysis. The upper red band shows the exclusion limit from dark matter stability considerations. As the dark matter particles are produced in the early universe, it is necessary that they are sufficiently stable in order to still be abundant today. In our study we require as a criterion for dark matter stability that the particle's lifetime exceeds the age of the universe by a factor of a hundred according to $\tau_{\mathrm{DM}} > 100\,\tau_{\mathrm{Universe}}$. For the age of the universe we use $\tau_{\mathrm{Universe}} = H_0^{-1} = 14.54 \times 10^9 \left(\frac{h_0}{0.673}\right)^{-1}$ y with today's Hubble rate given by $H_0 = 100\,h_0$ km s^{-1} Mpc^{-1} $= (67.3 \pm 1.2)$ km s^{-1} Mpc^{-1} at 68% confidence level

[5] As already mentioned the constraints from $0\nu\beta\beta$ on the parameter space are weaker than limits from the other sources since contributions to the decay are suppressed in the CISS.

Figure 3.3: Parameter subspace of the averaged sterile neutrino pseudo-Dirac mass m_N and averaged dark matter candidate mass m_{DM}. The blue dots correspond to complete sets of model parameters allowed by low-energy phenomenology constraints. The lower red band shows the exclusion limit obtained from lepton universality. The upper red band excludes dark matter masses that yield too short lifetimes. The gray areas show the constraints from the decay $\mu \to e\gamma$, where the solid (dashed) line corresponds to the current (future) limit on the branching ratio of the process. The green area highlights the dark matter mass region favored by relic abundance. Note that the blue dots in Figure 3.4 are the same as the ones shown here, but in the parameter space of dark matter candidate mass against mixing angle.

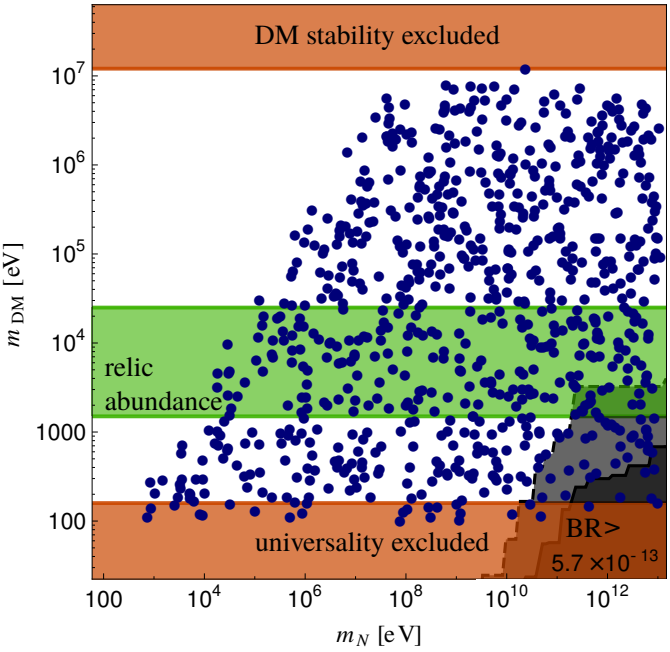

[108]. The lifetime of the dark matter candidate, which mainly decays into the three active neutrinos, can be estimated according to [175]:

$$\tau_{\mathrm{DM}} = 5 \times 10^{26}\ \mathrm{s} \left(\frac{m_{\mathrm{DM}}}{\mathrm{keV}}\right)^{-5} \left(\frac{10^8}{\sin^2(2\tilde{\Theta})}\right) . \tag{3.38}$$

With active-DM mixing in the range of $10^{-10} - 10^{-12}$ (cf. Section 3.2) we obtain from the above equation the rough stability limit of $m_{\mathrm{DM}} \leq 10^4$ keV. The gray areas in the lower-right corner of Figure 3.3 display the LFV limits. The solid line marks the border of the current MEG limit of $\mathrm{BR}(\mu^+ \to e^+\gamma) < 5.7 \times 10^{-13}$. The dashed line cutting into the area of allowed parameter points corresponds to the projected limit of $\mathrm{BR}(\mu^+ \to e^+\gamma) < 6.0 \times 10^{-14}$, which could serve to falsify the CISS in the future. Finally, the green band highlights the mass range for DM candidates, in which the correct DM relic abundance can be produced (we postpone the discussion of the relic abundance until Section 3.4.3).

In Figure 3.4 we show the same points as in Figure 3.3, but this time in the parameter subspace of DM masses versus the DM mixing angle. As before, the

green band shows the region favored by DM relic abundance. The red band on the left takes into account the exclusion limit from the neutrinos' phase-space-density bound (Tremaine-Gunn bound) [176], which can be relaxed down to the keV range by a more conservative treatment of the phase space density [177]. The red area in the top-right half of Figure 3.4 is excluded by X-ray bounds [178]. The blue star indicates a benchmark point with DM mass of about 7 keV motivated by the weak mono-energetic X-ray line at (3.52 ± 0.02) keV that was reported in [179]. At the benchmark point the masses of the pseudo-Dirac pairs are given by $m_{6/7} = 9.25$ GeV with a mass splitting of 9 keV, and $m_{8/9} = 638$ GeV with a mass splitting of 10 keV. For the DM candidate masses we obtain $m_4 = 7.013$ keV and $m_5 = 7.006$ keV with mixing to the active neutrinos of $\sin^2(2\tilde{\Theta}_4) \approx 7 \times 10^{-11}$ and $\sin^2(2\tilde{\Theta}_5) \approx 3.2 \times 10^{-13}$. It is an interesting observation that the mass region, in which the correct amount of DM could be produced, falls just into the small window of dark matter masses with the largest allowed mixing angle. Note that the viable parameter region overlaps with the region, in which the Dodelson-Widrow mechanism [180] does not produce hot dark matter as discussed in [181].

3.4.2 Particle colliders

In this part we will discuss the most promising collider signatures of the new particles of our model. Therefore, we will investigate the different particle sectors of the CISS and identify the reactions that could give a significant contribution above SM backgrounds. For the evaluation of cross sections and decay rates we use the narrow width approximation [182, 183].

Hidden sector fermions

The DM candidates are coupled too weakly to SM particles to give considerable signals at particle colliders. Thus, in the fermion sector we focus on leptonic signals over the SM background from the heavy sterile neutrinos in the CISS. In a generic model with heavy Majorana neutrinos the same-sign di-lepton channel with signature $pp \to W^\pm \to \ell^\pm N \to \ell^\pm \ell^\pm W^\mp$ could lead to a visible signal at particle colliders. In this channel a primary W boson is produced in a quark-anti-quark collision, which then decays into a charged lepton and a heavy Majorana neutrino via the active-sterile mixing. Since it is a Majorana particle, the heavy neutrino, afterwards, can decay into a lepton with the same electric charge as the first one and a secondary W boson. If the secondary W boson further decays into jets, one obtains the Feynman diagram presented in Figure 3.5. Note that this diagram is a tilted $0\nu\beta\beta$ diagram (cf. Figure 2.4). Accordingly, the amplitude for this process is governed by the quantity $|\sum_{i\in\text{heavy}} U_{ei}^2 m_i^{-1}|$, which is proportional to the familiar heavy neutrino contribution to the $0\nu\beta\beta$ rate [see Eq. (3.34)]. In neutrino models with strong LNV an excess in the same-sign di-lepton signal is commonly expected. Models with suppressed LNV such as standard inverse seesaw models (cf. Section 2.2.2) do not generate such an excess. Note, however,

Figure 3.4: Parameter subspace of the averaged dark matter candidate mass $m_{\rm DM}$ and mixing angle $\sin^2(2\tilde{\Theta})$ between dark matter candidates and active neutrinos. The blue dots correspond to complete sets of model parameters allowed by low-energy phenomenology constraints. The red band on the left marks the Tremaine-Gunn bound on the mass of the dark matter candidates. The red area covering the upper-right half corresponds to the bound obtained from X-rays measurements. The green band shows the dark matter mass range favored by relic abundance. The blue star indicates a benchmark point with dark matter mass at 7 keV motivated by the claimed observation of a mono-energetic X-ray line at (3.52 ± 0.02) keV reported in [179]. Note that the blue dots in Figure 3.3 are the same as the ones shown here, but in the parameter space of sterile neutrino mass against dark matter candidate mass.

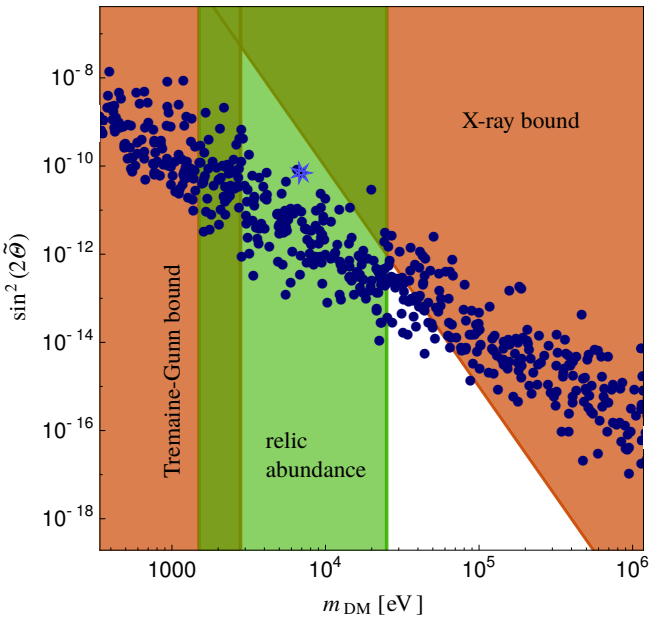

that the inverse seesaw can be modified in order to allow for strong LNV as we will discuss in detail in Chapter 4.

In [184] the efficiency for the detection of a generic Majorana neutrino in the same-sign di-lepton channel at the LHC was investigated. In that work it was estimated that for an upper bound of $|U_{ei}|^2 = 0.0052$ on the mixing and for Majorana masses above 800 GeV the cross section for the di-lepton channel drops below 10^{-2} fb. As discussed in Section 3.4.1 LNV is suppressed in our model and, therefore, we expect a negligible signal in the same-sign di-lepton channel. Let us briefly estimate the contributions from the heavy neutrinos in the CISS. We have two pairs of pseudo-Dirac neutrinos, for which the sum of the heavy

Figure 3.5: Same-sign di-lepton signal with two hadronic jets induced by the decay of a heavy Majorana neutrino n_i. Note that this lepton number violating signature is suppressed in the CISS.

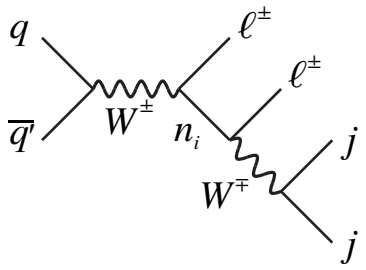

neutrino contributions simplifies to

$$\begin{aligned}\left|\sum_{i\in\text{heavy}} U_{ei}^2 m_i^{-1}\right| &\approx \left|\sum_{\text{pD pairs}} U_{ei}^2 \left(\frac{1}{M+\mu/2}-\frac{1}{M-\mu/2}\right)\right| \\ &\approx \left|U_{e1}^2\frac{\mu}{M^2}+U_{e2}^2\frac{\mu}{M^2}\right| \approx 2\,\Theta^2\frac{\mu}{M^2}\,.\end{aligned} \tag{3.39}$$

From the above equation we see that, compared to the generic Majorana neutrino scenario, the pseudo-Dirac masses in the CISS cause a cancellation that leads to a suppression factor of $\frac{\mu}{M} \leq 10^{-8}$ for the amplitude. In turn, the cross section for the same-sign di-lepton channel is suppressed by a factor of at least 10^{-16} and, thus, is rendered irrelevant for detection. Our result for the cancellation effect agrees with the conclusion in [185].

In [186, 187] it was argued that the best channel involving sterile neutrinos in the case of suppressed LNV is the tri-lepton channel with missing energy, since it has a significantly lower SM background. The Feynman diagram for this process is presented in Figure 3.6. Due to the internal sterile neutrino, the amplitude is proportional to the square of active-sterile mixing and, thus, to the non-unitarity parameter $\varepsilon_\alpha \sim \Theta^2 = m_{\text{D}}^2/M^2$, which has been defined in Eq. (3.26). It was pointed out at the end of Section 3.2 that the neutrino masses in the CISS are not subject to large scale separation and so sizable active-sterile mixings of up to $\varepsilon_\alpha \sim \mathcal{O}(1\%)$ are possible. As we will see in the next subsection (on the hidden scalar sector) the active-sterile mixing can account for the observed excess in the opposite-sign di-lepton channel of $\mathcal{O}(100)$ events at 2.4σ "local" significance published by the CMS collaboration [188] (a *global* significance was not reported). A similar excess should show up in the tri-lepton channel. Note, however, that we expect a suppressed signal of $\mathcal{O}(10)$ events due to the (secondary) off-shell W boson involved.

Another signal was reported in the channel with two electrons plus two jets with a number of $29 \pm 1 \pm 3$ events above SM backgrounds at a center-of-mass energy of $\sqrt{s} = 8$ TeV [189], where the first (second) uncertainty corresponds to the total experimental uncertainty (the particle distribution function cross section uncertainty). Note that in the analysis presented in [189] no charge requirements were imposed on the final state charged leptons. A local significance of 2.8σ at

Figure 3.6: Lepton number conserving tri-lepton collider signature in the CISS mediated by the sterile neutrino n_i. The final-state neutrino ν_{L} escapes the detector as missing transverse energy.

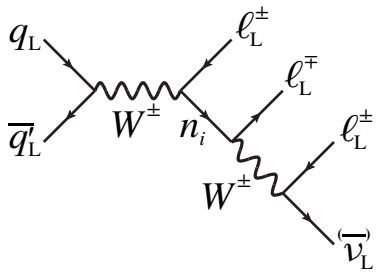

approximately 2 TeV in the di-electron channel was stated (a *global* significance was not reported). If the secondary W boson in Figure 3.6 decays into jets instead of leptons, the diagram corresponds to the signature $pp \to \ell^{\pm}\ell^{\mp} + 2$ jets. Since the amplitude for this channel and for the tri-lepton channel differ only by the branching ratios of the W boson decays into hadrons and into leptons, we expect both signals to be of the same order of magnitude. Thus, the pseudo-Dirac neutrinos in the CISS could give rise to the signal reported in [189].

Note that there exists an alternative production mechanism for sterile neutrinos at hadron colliders that involves t-channel photons and becomes dominant for relatively heavy neutrinos as discussed in [190]. In the future this new mechanism could test mixings down to $\varepsilon_\alpha \approx 10^{-4}$ for neutrino masses of the order of $(100 - 300)$ GeV.

Hidden sector scalars

In this subsection we will discuss the possible decays for the new scalars in the CISS. We will see that the decays of ϕ_{PGB} can lead to interesting collider signatures that could serve in order to test the model in future LHC runs.

The PGB is coupled to SM particles via its mixing to the Higgs boson parametrized by $\sin\beta$ and could manifest itself as a second Higgs-like particle at the LHC. The mixing arises from the diagonalization of the mass-squared matrix in the scalar sector (see Section 3.3) and is proportional to $\langle h_3\rangle/\langle\phi_1\rangle \sim \mathcal{O}(0.1)$. Hence, we expect a general suppression by a factor of a hundred for the cross section of the PGB compared to the one of the Higgs boson. Due to the relatively heavy mass of ϕ_{PGB} around 500 GeV and the large top Yukawa coupling $y_t \sim \mathcal{O}(1)$, the scalar's dominant decay channel into SM particles will be the decay into a $t\bar{t}$ pair. In the hidden sector ϕ_{PGB} can decay into two sterile neutrinos through the Yukawa interaction term proportional y_1.[6] The sterile neutrinos in turn can decay via charged-current or neutral-current interactions, or escape the detector as dark matter. The diagram in Figure 3.7 as an example shows the decay of the PGB into two neutrinos, one of which leaves the detector undetected (n_{DM}),

[6] In the following discussion we will not consider $\tilde{y}_1$ or, respectively, $\tilde{y}_2$ individually, for they bear the same phenomenology as y_1 or, respectively, y_2.

Figure 3.7: Decay of the pseudo-Goldstone boson of broken scale invariance into two sterile neutrinos. One neutrino ($n_{\rm DM}$) escapes the detector as dark matter, while the other further decays via a charged-current interaction yielding the signature $\phi_{\rm PGB} \to \ell^\pm \ell^\mp +$ missing energy. Note that initial-state radiation could possibly add hadronic jets to the signature shown in this figure.

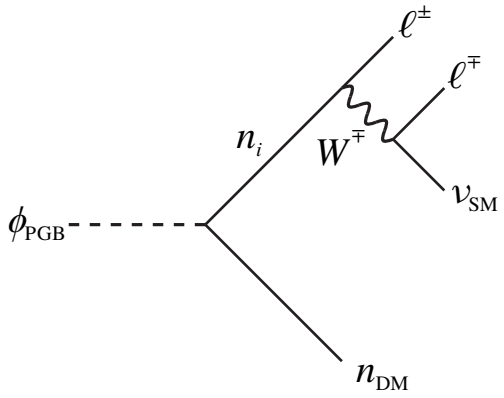

while the other decays through a charged-current interaction according to $\nu_{\rm i} \to \ell^\pm W^\mp \to \ell^\pm \ell^\mp \nu_{\rm SM}$. Note that the channel $\phi_{\rm PGB} \to n_{\rm DM} n_{\rm DM}$, as it involves only one interaction, will give the largest contribution to the total decay width. As already mentioned in the preceding subsection (on pseudo-Dirac neutrinos), an excess in the $\ell^\pm \ell^\mp +$ jets channel without missing transverse energy of 126 ± 41 events at $\sqrt{s} = 8$ TeV at 2.4σ "local" significance has been observed in a data sample collected by the CMS detector corresponding to an integrated luminosity of $\mathcal{L} = 19.4$ fb^{-1} [188].[7] This excess can be explained in the CISS as we will lay out in the following.

The possible hidden decay channels for the PGB can be summarized as

$$\phi_{\rm PGB} \to n_i\, n_j \to a\ell^\pm + \text{jet(s)} + \not{E}_{\rm T} \tag{3.40}$$

with $a \in \{0, \ldots, 4\}$ specifying the number of charged leptons in the final state and $\not{E}_{\rm T}$ denotes the missing transverse energy (carried away by final-state neutrinos). Two comments are in order. First, the jet multiplicity of the decays is not certain due to initial-state radiation. Hence, for our analysis we summed over decay rates whose signatures differed from each other only in the number of jets. Second, there exists one channel without missing energy, namely, the decay $\phi_{\rm PGB} \to 2\ell^\pm + 2(q\overline{q})^\mp$, in which no final-state neutrinos are produced. For the PGB's decay rate into sterile neutrinos we can estimate at tree level

$$\Gamma_{AB} \approx \frac{y_1^2 m_{\rm PGB}}{16\pi} s_{AB}\, |f_{AB}|^2\, k_{AB}\,, \tag{3.41}$$

where the subscripts A, B label the branches of the Feynman diagram that belong to the corresponding primary sterile neutrino. The coefficients s_{AB} and k_{AB}

[7] For completeness, we remark again that no value for the global significance was reported.

denote the symmetry and kinematic factor for the respective rates, while f_{AB} takes into account the relative strengths of the different decay branches. The decay rate for the top-pair production at tree level is given by (see e.g. [191])

$$\Gamma_{\text{top}} = \frac{3\, y_t^2\, m_{\text{PGB}} \sin^2\beta}{16\pi} \left(1 - \frac{4m_t^2}{m_{\text{PGB}}^2}\right)^{3/2} , \tag{3.42}$$

where we have used $y_t^2 = 2\sqrt{2}\, m_t^2 G_{\text{F}}$ [cf. Eqs. (2.13) and (2.21)]. With the equations for the decay rates we are ready to begin our numerical study.

Let us assume that the production cross section for the PGB is given by the corresponding Higgs production cross section suppressed by the portal coupling as κ_{p}^2. For a PGB mass of $m_{\text{PGB}} \approx 500$ GeV we find that, in order to explain the excess, a portal coupling of $\kappa_{\text{p}}^2 \approx 0.25$ is required, which yields a production cross section of $\sigma(pp \to \phi_{\text{PGB}}) \approx 0.25$ pb if we take the Higgs production cross section as in [192]. For the active-sterile mixing we use $\varepsilon \sim \mathcal{O}(0.01)$ as discussed in the previous subsection. For the mixing of the heavy sterile states to non-active neutrinos numerical values of $|U_{Ni}|^2 = 0.8 - 1.0$ are needed. Note that this range is in agreement with DM phenomenology. To give an example we consider the benchmark point with $\varepsilon = 0.017$ and $|U_{Ni}|^2 = 0.97$. For the scalar mixing we choose $\sin\beta = 0.35$ in accordance with the vev hierarchy in the CISS and the limit $\sin\beta < 0.44$ [61]. For these values we find branching ratios of $\text{Br}(\phi_{\text{PGB}} \to \ell^\pm\ell^\mp + \text{jet(s)} + \not{E}_{\text{T}}) \approx 1.6\%$ and $\text{Br}(\phi_{\text{PGB}} \to t\bar{t}) \approx 2.0\%$ corresponding to a signal of approximately 75 events in the di-lepton channel and, respectively, 100 events in the $t\bar{t}$ channel in the energy region of 500 GeV to 600 GeV in agreement with the uncertainties in [193, 194]. For the future LHC run the designated integrated luminosity is reported as 300 fb^{-1} by the year 2021 [195]. For this luminosity the CISS predicts 1170 events in the di-lepton channel and 1530 events in the $t\bar{t}$ channel, which should be sufficiently strong signals to test the hypothesis of our model.

Now that we have analyzed the decays of ϕ_{PGB}, let us briefly discuss the phenomenology of $\mathcal{H}$. The study of the scalar sector in Section 3.3 has shown that the second scalar's vev is of the order of $10 - 100$ GeV. As pointed out in the discussion on LNV in Section 3.4.1, DM masses in the keV range require tiny Yukawa couplings $y_2 \sim \mathcal{O}(10^{-7})$. Consequently $\mathcal{H}$ will mainly decay via the Higgs portal. However, we do not expect many events caused by $\mathcal{H}$, due to its large mass $M_{\mathcal{H}} \sim \mathcal{O}(1)$ TeV, which substantially reduces the production cross section.

Hidden sector gauge boson

Finally, let us investigate the decays in the hidden gauge sector. The mass of the new gauge boson is given by Eq. (3.5). Taking the hierarchy between the scalar vevs into account, we find $m_X \approx g_X\langle\phi_1\rangle \sim \mathcal{O}(1)$ TeV. If we consult Figure 3.2, we see that a PGB mass of $m_{\text{PGB}} \approx 500$ GeV with $M_{\mathcal{H}} \lesssim 2$ TeV can be obtained for a sterile neutrino mass average of $m_N \lesssim m_{\text{PGB}}$ and hidden

gauge boson masses in the range 1 TeV $\lesssim m_X \lesssim$ 2 TeV. As an example we take $m_X = 1.5$ TeV in this subsection. With a mass in the TeV range the hidden gauge boson is well within the reach of the LHC. It can be produced in a proton-proton collision due to its coupling to the Z boson via the kinetic mixing proportional to ξ, which was introduced in Eq. (3.2). Because ξ actually parametrizes the kinetic mixing between X and the gauge boson of $\mathrm{U}(1)_\mathrm{Y}$, B, we need to include an extra factor of $\sin^2\theta_W$ in the suppression of the production cross section [cf. Eq. (2.6)]. Furthermore, since the hidden gauge boson is much heavier than the Z boson, the production is also kinematically suppressed. If we take all the mentioned effects into account, we find that the total suppression factor for the cross section is given by $\xi^2 \sin^2\theta_\mathrm{W}(m_Z^2/m_X^2)$. With the inclusive production cross section for the Z boson of $\sigma(pp \to Z + \text{anything}) \times \mathrm{Br}(Z \to \ell^+\ell^-) = 1.12 \pm 0.01(\text{stat.}) \pm 0.02(\text{syst.}) \pm 0.05(\text{lumi.})$ nb at $\sqrt{s} = 8$ TeV [196] and the branching ratio $\mathrm{Br}(Z \to \ell^+\ell^-) = (3.3658 \pm 0.0023)\%$ [87] we can calculate the production cross section for the hidden gauge boson according to

$$\sigma(pp \to X) = \sigma(pp \to Z + \text{anything})\, \xi^2 \sin^2\theta_\mathrm{W}\, \frac{m_Z^2}{m_X^2}\,. \tag{3.43}$$

where we take $m_Z = 91.1876$ GeV [87] and $\sin^2\theta_W \approx 0.231$ (cf. Section 2.1.1).

The X boson can decay into sterile neutrinos in the same way as ϕ_PGB. The most clearly visible signals of X decays are those with one and two charged leptons in the final state. For the parameters that were used in the previous subsection to explain the signal of [188] we find an upper limit for the kinetic mixing of $|\xi| \lesssim 0.02$ in order to be consistent with [197].

We have studied the collider phenomenology of the hidden sector particles in the CISS and pointed out which deviations from the SM are to be expected. In the next section we will examine the possibilities to produce dark matter in the CISS.

3.4.3 Dark matter relic abundance

The dark matter (DM) candidates in the CISS, which are labelled by n_DM, are the eigenstates of the neutrino mass matrix with eigenvalues proportional to the intermediate scale μ_+ [see Eq. (3.8)]. In the following we will discuss how DM is produced in the CISS and how the correct relic abundance of DM in the Universe is obtained. In particular, we will elaborate on which mechanisms might be responsible for a consistent DM production.

One of the simplest DM production mechanisms, which is generically present in models with sterile right-handed neutrinos, is the Dodelson-Widrow mechanism [180]. In this mechanism the sterile neutrinos represent the DM candidate, which is produced in active-sterile neutrino oscillations. However, the possibility of sterile neutrinos as warm DM produced in oscillations is already severely constrained by structure formation observations [198–200] even though it is not completely ruled out, yet (see for instance the νMSM [175]). In any case, it is

required to adjust the model's parameters to very specific values in order to obtain the correct amount of DM energy density from sterile neutrinos, which is, of course, a valid solution, but might not be satisfying from a theoretical point of view. Even though the Dodelson-Widrow mechanism is active in the CISS, it only produces a fraction of the relic abundance insufficient to explain the total DM energy density for natural model parameters.

Another possibility could be that DM neutrinos are thermalized by the massive hidden gauge boson. However, if the gauge boson is too light, the neutrinos are always overproduced [201]. The so-called over-closure of the Universe still can be avoided if a heavy, relic particle dominates the energy density of the early Universe, which upon decay produces a large amount of entropy (in form of radiation) [202]. In the CISS, such an entropy injection could be obtained from the decay of the heavy pseudo-Dirac neutrinos. However, this scenario suffers the same fate as the Dodelson-Widrow mechanism as making this production scheme work requires a conspiracy between model parameters as discussed in [181, 203, 204].

None of the production mechanisms mentioned so far seems to be suitable for the CISS. Thus, we will discuss yet another possibility for DM production that is naturally realized in our model, namely, the non-thermal freeze-in mechanism [205–208]. The idea of non-thermal freeze-in consists of two synergetic processes. In one process, which is efficient at earlier times in the evolution of the Universe, the abundance of a feebly interacting massive particle (FIMP) is produced via freeze-in from the thermal plasma. In the CISS this FIMP is represented by the scalar $\mathcal{H}$ mainly given by ϕ_2. As we will see $\mathcal{H}$, due to its 'feeble' interactions, never enters thermal equilibrium as opposed to freeze-out scenarios. In the other process the DM particle n_{DM} is produced via the decay $\mathcal{H} \to n_{\text{DM}} n_{\text{DM}}$, which becomes efficient at temperatures $T \sim M_{\mathcal{H}}$. Note that the Boltzmann equation for the evolution of the number density of the DM candidate is always dominated by the production through the decay of the scalar [209]. One important requirement for the freeze-in mechanism to be at work is that the DM candidate n_{DM} is also a FIMP so that the particle is not thermalized. Since the intermediate-scale neutrinos have masses in the keV range, while the vev generating their mass term, $\langle\phi_2\rangle$, is of the order of 1 GeV up to the electroweak scale $v_{\text{ew}} \sim \mathcal{O}(100)$ GeV, we can expect the interaction strength to be $y_{\text{DM}} \approx y_2 \sim 10^{-6} - 10^{-8}$, which is indeed feeble. Another consequence of keV masses is that the effective number of relativistic degrees of freedom N_{eff} is unaffected. Furthermore, the DM particle must not be thermalized by the hidden gauge boson. Accordingly, the ratio of the hidden gauge coupling over the gauge boson mass $g_X/m_X \approx \langle\phi_1\rangle^{-1}$ [cf. Eq. (3.5)] needs to be sufficiently tiny. Since $\langle\phi_1\rangle \sim \mathcal{O}(1)$ TeV, this is the case in the CISS.

In the underlying freeze-in mechanism the yield of DM particles can be calculated via the formula [210]

$$Y_{\text{DM}}(\infty) \approx \frac{2.38\, g_{\phi_2}}{\pi^3 g_*^S \sqrt{g_*^\rho}} \frac{M_{\text{Planck}}}{M_{\mathcal{H}}^2} \Gamma\left(\mathcal{H} \to n_{\text{DM}} n_{\text{DM}}\right) , \tag{3.44}$$

where g_*^S and g_*^ρ denote the effective number of degrees of freedom for the entropy and energy density, respectively, at $T \approx M_{\mathcal{H}}$, and g_{ϕ_2} is given by the internal

degrees of freedom of $\mathcal{H}$. The factor $\Gamma\left(\mathcal{H} \to n_{\rm DM} n_{\rm DM}\right)$ denotes the rate of the scalar's decay into two DM particles. With the yield given in Eq. (3.44) we obtain for the DM relic abundance [210]

$$\Omega_{\rm DM} h^2 = 0.11 \times \left(\frac{m_{\rm DM}}{10 \text{ keV}}\right)^3 \left(\frac{\text{TeV}}{\langle\phi_2\rangle}\right)^2 \left(\frac{100 \text{ GeV}}{M_{\mathcal{H}}}\right) \left(\frac{10^3}{g_*^S \sqrt{g_*^\rho}}\right) . \tag{3.45}$$

Let us investigate which DM mass is needed in the CISS in order to align the above equation with the reported value of $\Omega_{\rm DM} h^2 = 0.1199 \pm 0.0027$ at 68% confidence level [108] for the relic DM energy density. The vev of the second scalar $\langle\phi_2\rangle$ can vary between tens and hundreds of GeV, while the mass $M_{\mathcal{H}}$ is in the TeV range. The additional degrees of freedom in the CISS compared to the SM add up to 16 and practically do not make any difference at $T \approx M_{\mathcal{H}}$. At such high temperatures we roughly have $g_*^S \approx g_*^\rho \approx 100$ [211], so that $10^3/(g_*^S \sqrt{g_*^\rho}) \approx 1$. Hence, a DM mass between 1 keV and 10 keV is favored in the freeze-in mechanism within the CISS as indicated by the green bands in Figures 3.3 and 3.4. Note that, in contrast to the model discussed in [210], a DM mass at this scale comes natural in the CISS so that we do not have to rely on cancellations for the mass terms.

Before we conclude the discussion of the relic abundance we remark a final subtlety of the model. In the CISS there are in total two DM neutrinos with a small mass splitting of the order of μ_-. Due to the much smaller mixing with the active neutrinos, the heavier of these neutrino is not produced in the Dodelson-Widrow mechanism and, thus, is less abundant than the lighter DM candidate by at least $20\% - 30\%$. This leads to a slightly asymmetric double X-ray line with an energy splitting of μ_- in the sub-keV range, which should give a very characteristic signal in future astrophysical observations.

Chapter 4

Extended conformal inverse seesaw mechanism

In the preceding chapter we have discussed the model of the conformal inverse seesaw (CISS) mechanism and its phenomenological implications in full detail. There, we have seen that in the set-up of the CISS lepton number violation (LNV) is systematically suppressed due to cancellations in contributions from the sum of pseudo-Dirac masses. In this chapter we will extend the CISS in order to allow for ample LNV effects. The model of the extended conformal inverse seesaw (ECISS) mechanism, which will be presented in the following, is based on the published work [2]. In the discussion we will put special emphasis on the differences between the CISS and its extension. The model of the ECISS will be introduced in Section 4.1. Afterwards, in Section 4.2, we will derive the neutrino mass spectrum and mixing pattern followed by the discussion of electroweak symmetry breaking in the ECISS in Section 4.3. In Section 4.4 we will analyze the impact of the new LNV physics on neutrinoless double beta decay and on signatures at particle colliders.

4.1 The model

The main ingredient of the ECISS, which will allow for considerable LNV, is a large Majorana mass term for the right-handed neutrinos ν_{R}. Such a term can be obtained if the CISS is extended by a suitable scalar degree of freedom that can induce the desired Yukawa coupling. If this scalar upon spontaneous symmetry breaking develops a large vev, the right-handed neutrinos can acquire an equally large Majorana mass term. Another interesting aspect of the model is that in the ECISS the additional gauge group $\mathrm{U}(1)_X$ can be identified with $\mathrm{U}(1)_{B-L}$, where B and L denote baryon and lepton number, respectively. In the CISS this identification was not possible since there did not exist any way to consistently assign a $B-L$ quantum number to ϕ_1, the scalar responsible for the Dirac-type Yukawa couplings between ν_{R} on one hand and N_{L} and N_{R} on the other hand [cf. Eq. (3.2)]. In the ECISS this issue is overcome by providing the scalar sector

Table 4.1: Charges under $\mathrm{U}(1)_{B-L}$, $\mathrm{U}(1)_\mathrm{Y}$ and dimension of the $\mathrm{SU}(2)_\mathrm{L}$ representation for the fermions and scalars in the extended conformal inverse seesaw model.

field	Q_L	u_R	d_R	L_L	e_R	ν_R	N_L	N_R	H	χ_2	χ_4	χ_6
$\mathrm{U}(1)_{B-L}$	1/3	1/3	1/3	−1	−1	−1	3	3	0	2	4	6
$\mathrm{U}(1)_\mathrm{Y}$	1/6	2/3	−1/3	−1/2	−1	0	0	0	1/2	0	0	0
$\mathrm{SU}(2)_\mathrm{L}$	**2**	**1**	**1**	**2**	**1**	**1**	**1**	**1**	**2**	**1**	**1**	**1**

with two different scalars, which jointly share the role of ϕ_1 in the symmetry breaking, but are separately responsible for the Yukawa coupling for N_L and ν_R, and N_R and ν_R. Additionally, one of the new scalars can also generate the mentioned Majorana mass term for ν_R so it can serve two purposes at the same time.

In Table 4.1 we summarize the fermionic and scalar particle spectrum and the quantum numbers of the ECISS including the new $B-L$ charges. Naturally, the fermions of the SM carry baryon and lepton numbers and, due to the gauging of $\mathrm{U}(1)_{B-L}$, their covariant derivatives therefore need to be altered. When the new gauge boson, which we denote by Z', is included, the derivatives are replaced by

$$D_\mu \to D'_\mu = D_\mu - \mathrm{i} g_{\mathrm{BL}} \left(B-L\right) Z'_\mu \tag{4.1}$$

for each SM fermion, where g_{BL} denotes the $\mathrm{U}(1)_{B-L}$ gauge coupling.

The relevant part of the Lagrangian in the ECISS is given by

$$\begin{aligned}\mathcal{L}_{\mathrm{ECISS}} \supset & -\Big\{ y_\mathrm{D} \overline{L_\mathrm{L}} \nu_\mathrm{R} \widetilde{H} + y \overline{N_\mathrm{L}} \nu_\mathrm{R} \chi_4 + y \overline{N_\mathrm{R}^\mathrm{c}} \nu_\mathrm{R} \chi_2^* \\ & + \tfrac{y_\mathrm{R}}{2} \overline{\nu_\mathrm{R}^\mathrm{c}} \nu_\mathrm{R} \chi_2 + \tfrac{y'}{2} \overline{N_\mathrm{L}} N_\mathrm{L}^\mathrm{c} \chi_6 + \tfrac{y'}{2} \overline{N_\mathrm{R}^\mathrm{c}} N_\mathrm{R} \chi_6^* + \mathrm{h.c.} \Big\} \\ & - \tfrac{\xi_{\mathrm{BL}}}{4} Z'^{\mu\nu} F_{\mu\nu} - V(H,\, \chi_2,\, \chi_4,\, \chi_6)\,.\end{aligned} \tag{4.2}$$

The first two lines in the above equation show the Dirac-type and Majorana-type Yukawa interactions, respectively. Note that, after spontaneous symmetry breaking, we assume a symmetry similar to the one in the CISS with respect to the simultaneous exchanges $N_\mathrm{L} \leftrightarrow N_\mathrm{R}^\mathrm{c}$ and $\langle\chi_2\rangle \leftrightarrow \langle\chi_4\rangle$ in the Yukawa sector. Accordingly, we have introduced the same Yukawa couplings y and y' in a suitable way for the operators involving N_L and N_R. The third line of Eq. (4.2) contains the kinetic mixing between the Abelian gauge bosons, which is parametrized by ξ_{BL} and the potential of the scalar sector. The expression for the scalar potential will be given in Section 4.3. Under the assumption that all electrically neutral, CP-even scalars develop a non-vanishing vev the mass-squared of the new gauge boson is given by

$$m_{Z'}^2 = 4 g_{\mathrm{BL}}^2 (\langle\chi_2\rangle^2 + 4\langle\chi_4\rangle^2 + 9\langle\chi_6\rangle^2)\,. \tag{4.3}$$

As in the CISS we write $\langle\chi_i\rangle$ as abbreviation for $\langle \mathrm{Re}\,(\chi_i)\rangle$. Note that, since the Higgs is not charged under $\mathrm{U}(1)_{B-L}$ and the new scalars are not charged under the SM gauge group, the masses of the electroweak gauge bosons are given by their SM values, which have been presented in Section 2.1.1.

4.2 Neutrino masses and leptonic mixing

In this section we will analyze the neutrino mass spectrum and the mixing matrix in the ECISS. Compared to the mass spectrum of the CISS [given in Eqs. (3.7)-(3.9)] we will see that the inclusion of the heavy Majorana mass term M_{R} only changes the pseudo-Dirac eigenvalues.

We take the Majorana basis as $n_{\mathrm{L}} = (\nu_{\mathrm{L}},\, \nu_{\mathrm{R}}^{\mathrm{c}},\, N_{\mathrm{L}},\, N_{\mathrm{R}}^{\mathrm{c}})^{\intercal}$ as defined in the CISS. Then, after spontaneous symmetry breaking, the neutrino mass matrix is given by

$$\mathcal{M} = \frac{1}{\sqrt{2}} \begin{pmatrix} 0 & y_{\mathrm{D}}\langle h_3\rangle & 0 & 0 \\ y_{\mathrm{D}}\langle h_3\rangle & y_{\mathrm{R}}\langle \chi_2\rangle & y\langle \chi_2\rangle & y\langle \chi_4\rangle \\ 0 & y\langle \chi_2\rangle & y'\langle \chi_6\rangle & 0 \\ 0 & y\langle \chi_4\rangle & 0 & y'\langle \chi_6\rangle \end{pmatrix} = \begin{pmatrix} 0 & m_{\mathrm{D}} & 0 & 0 \\ m_{\mathrm{D}} & M_{\mathrm{R}} & M_1 & M_2 \\ 0 & M_1 & \mu_1 & 0 \\ 0 & M_2 & 0 & \mu_2 \end{pmatrix} . \tag{4.4}$$

As will be explained in Section 4.3 we assume that all electrically neutral, CP-even scalars develop a non-vanishing vev with the hierarchy $\langle \chi_2\rangle = \langle \chi_4\rangle \gg \langle h_3\rangle > \langle \chi_6\rangle$. With this symmetry breaking pattern the mass scales M_1, M_2 and M_{R} are all proportional to the same vev. At the same time, we want M_{R} to be the largest of the mass terms in Eq. (4.4). Accordingly, we assume $y < y_{\mathrm{R}}$ for the Yukawa couplings, which together with the vev hierarchy leads to the desired mass scale hierarchy $M_{\mathrm{R}} > M_i > m_{\mathrm{D}} > \mu_i$.

As in the CISS we refer to Appendix A for the diagonalization of the mass matrix defined in Eq. (4.4). Using the abbreviations $\mu_{\pm} \equiv \frac{1}{2}(\mu_1 \pm \mu_2)$ and $M^2 \equiv M_1^2 + M_2^2$ the light neutrino mass spectrum in the ECISS is given by Eqs. (A.22) and (A.23) as

$$\begin{aligned} m_- &\approx \mu_+ \frac{m_{\mathrm{D}}^2}{M^2} \,, \\ m_+ &\approx \mu_+ \,, \end{aligned} \tag{4.5}$$

which remains unchanged with respect to the CISS. However, for $M_{\mathrm{R}} \neq 0$ the heavy eigenvalues given by Eq. (A.24) take on a different form. Since $M_{\mathrm{R}} > M$, they can be expanded yielding

$$\begin{aligned} M_- &\approx -\frac{M^2}{M_{\mathrm{R}}} \,, \\ M_+ &\approx M_{\mathrm{R}} \,, \end{aligned} \tag{4.6}$$

where we have neglected contributions proportional to $\mu_+ \ll M$.[1] The mixing matrix U diagonalizes the mass matrix given in Eq. (4.4) and connects the mass and flavor bases according to

$$\mathcal{M}^{\mathrm{diag}} = U^{\intercal} \mathcal{M} U \,, \tag{4.7}$$

$$\tilde{n} \equiv (\nu_{\mathrm{SM}},\, n_{\mathrm{DM}},\, N_1,\, N_2)^{\intercal} = U^{\dagger} n_{\mathrm{L}} \,. \tag{4.8}$$

[1] Note that the resemblance of the heavy eigenvalues in Eq. (4.6) to the type-I seesaw formula is no coincidence but follows from the definition of $\mathcal{M}_{\mathrm{R}}$ in Eq. (A.10) for $M_{\mathrm{R}} > M \gg \mu_s$.

The order of magnitude of the mixing matrix's elements can be estimated as in the CISS by Eq. (A.21) as

$$U^\dagger \sim \mathcal{O}\begin{pmatrix} 1 & \Theta\eta_+ & \Theta & \Theta \\ \tilde{\Theta} & \eta_- & \frac{1}{\sqrt{2}} & \frac{1}{\sqrt{2}} \\ \Theta & \frac{1}{\sqrt{2}} & \frac{1}{\sqrt{2}} & \frac{1}{\sqrt{2}} \\ \Theta & \frac{1}{\sqrt{2}} & \frac{1}{\sqrt{2}} & \frac{1}{\sqrt{2}} \end{pmatrix}, \tag{4.9}$$

where the abbreviations $\Theta = m_{\mathrm{D}}/M$, $\tilde{\Theta} = \Theta\mu_-/\mu_+$ and $\eta_\pm = \mu_\pm/M$ have been used. Let us discuss the neutrino mass spectrum and mixing of the ECISS.

The light eigenvalues given in Eq. (4.5) correspond to the active neutrino masses and to the mass of the dark matter candidate, respectively, as was the case in the CISS. Thus, maintaining dark matter masses of $\mu_+ \sim \mathcal{O}(1-10)$ keV and active-sterile mixing angles of $\Theta \lesssim 10^{-2}$ leads to active neutrino masses of $m_\nu \lesssim 1$ eV within the phenomenological limits. Furthermore, from Eqs. (4.8) and (4.9) it can be seen that the mixing between the dark matter candidates n_{DM} and the active neutrinos is, again, proportional to $\tilde{\Theta}^2 = \Theta^2(\mu_-/\mu_+)^2 \approx 10^{-10} - 10^{-12}$ for the small parameter $\mu_-/\mu_+ \lesssim 10^{-3}$, which violates the $N_{\mathrm{L}} \leftrightarrow N_{\mathrm{R}}^{\mathrm{c}}$ exchange symmetry in the neutrino sector (cf. Section 3.2). Accordingly, the dark matter candidates are quasi-stable [for the dark matter lifetime formula see Eq. (3.38)]. Moreover, the dark matter particles can be produced in the same freeze-in mechanism as in the CISS.

The major difference between the neutrino mass spectrum in the CISS and in its extension is due to the heavy masses given in Eq. (4.6). While in the CISS these masses corresponded to a pair of pseudo-Dirac neutrinos, we obtain in the ECISS one heavy Majorana neutrino denoted by N_2 with mass given by the large LNV scale $M_+ = M_{\mathrm{R}}$ and another Majorana state N_1 with suppressed Majorana mass $M_- = M^2/M_{\mathrm{R}}$, which is still relatively large compared to the light neutrino masses. Therefore, large LNV phenomena are expected to occur in the ECISS. It is, however, important to notice that besides LNV the low-energy phenomenology of the CISS discussed in Section 3.4.1 is unaffected by the presence of M_{R}. This is due to the fact that in the ECISS the light neutrino mass spectrum as well as the neutrino mixing is the same as in the CISS.

4.3 Electroweak symmetry breaking

In the ECISS the general, conformally invariant tree-level potential, which was introduced in Eq. (4.2), is given by

$$\begin{aligned} V(H,\,\chi_2,\,\chi_4,\,\chi_6) = {} & \frac{\lambda_H}{2}(H^\dagger H)^2 + \frac{\lambda_2}{2}|\chi_2|^4 + \frac{\lambda_4}{2}|\chi_4|^4 + \frac{\lambda_6}{2}|\chi_6|^4 \\ & + \kappa_{H2}H^\dagger H|\chi_2|^2 + \kappa_{H4}H^\dagger H|\chi_4|^2 + \kappa_{H6}H^\dagger H|\chi_6|^2 \\ & + \kappa_{24}|\chi_2|^2|\chi_4|^2 + \kappa_{46}|\chi_4|^2|\chi_6|^2 + \kappa_{26}|\chi_2|^2|\chi_6|^2 \\ & + \left(\tilde{\kappa}_1\chi_2^3\chi_6^* + \tilde{\kappa}_2\chi_2^*\chi_4^2\chi_6^* + \text{h.c.}\right). \end{aligned} \tag{4.10}$$

Note that in particular the terms in the last row of the above equation are gauge invariant and, thus, have to be included in a general theory. We will, however, assume that the scalar potential is symmetric with respect to the exchange $\chi_2 \leftrightarrow \chi_4$, which constrains the couplings as $\lambda_2 = \lambda_4$, $\kappa_{H2} = \kappa_{H4}$, $\kappa_{26} = \kappa_{46}$, and especially $\tilde{\kappa}_1 = \tilde{\kappa}_2 = 0$. Accordingly, the potential in Eq. (4.10) can be rewritten as

$$\begin{aligned} V(H, \chi_2, \chi_4, \chi_6) = \frac{\lambda_H}{2}(H^\dagger H)^2 + \frac{\lambda_2}{2}\left(|\chi_2|^4 + |\chi_4|^4\right) + \frac{\lambda_6}{2}|\chi_6|^4 \\ + \kappa_{H2} H^\dagger H \left(|\chi_2|^2 + |\chi_4|^2\right) + \kappa_{H6} H^\dagger H |\chi_6|^2 \\ + \kappa_{24}|\chi_2|^2|\chi_4|^2 + \kappa_{26}\left(|\chi_2|^2 + |\chi_4|^2\right)|\chi_6|^2 \,. \end{aligned} \tag{4.11}$$

Aside from forcing the couplings $\tilde{\kappa}_1$ and $\tilde{\kappa}_2$ to vanish, the assumed exchange symmetry possesses another important feature, namely, that the symmetry breaking of the four-scalar potential of the ECISS can effectively be performed in a similar way as it was done for the three-scalar potential of the CISS in Section 3.3. For EWSB we assume the following vev hierarchy

$$\begin{aligned} \langle \chi_2 \rangle \equiv \langle \chi_4 \rangle &= \frac{\langle r \rangle}{\sqrt{2}} \sqrt{\frac{1}{1+\epsilon}} \equiv \frac{v}{\sqrt{2}} \,, \\ \langle \chi_6 \rangle &= v \sqrt{\frac{\epsilon\,\delta}{1+\delta}} \,, \\ \langle h_3 \rangle &= v \sqrt{\frac{\epsilon}{1+\delta}} \,, \end{aligned} \tag{4.12}$$

where r denotes the radial coordinate along the flat direction $\mathbf{\Phi}_{\text{flat}} = (\chi_2, \chi_4, \chi_6, h_3)^\intercal$, and ϵ and δ are small parameters [cf. Eqs. (3.13) and (3.14)]. Note that the scalar exchange symmetry is respected by $\langle \chi_2 \rangle \equiv \langle \chi_4 \rangle$. The largest of the vevs, v, is the unique scale of the underlying model, which is induced by conformal symmetry breaking. Note that the parametrization as given above suggests the hierarchy $\langle \chi_2 \rangle = \langle \chi_4 \rangle \gg \langle h_3 \rangle > \langle \chi_6 \rangle$ if ε and δ are chosen small.

After spontaneous symmetry breaking, we obtain three massive scalars in addition to the PGB of broken scale invariance. As in the CISS we have a physical scalar mainly composed of h_3, which is denoted by h, and another scalar $\mathcal{H}$ mainly consisting of χ_6. The mass-squares of h and $\mathcal{H}$ in the ECISS are – mutatis mutandis – given by Eqs. (3.19) and (3.20), respectively. The PGB and the remaining massive scalar (apart from h and $\mathcal{H}$) are connected to the subsystem of χ_2 and χ_4. In spontaneous conformal symmetry breaking the PGB of broken scale invariance is always associated with the scalar degree of freedom that develops the largest vev. Since in the ECISS both χ_2 and χ_4 are assumed to develop the same vev v, the scalar spectrum does not only contain the PGB, which possesses a vanishing tree-level mass, but also another scalar with suppressed mass. We will denote this scalar by S (and the PGB by ϕ_{PGB} as before). The additional mass-squared at tree level is given by

$$\frac{M_S^2}{v^2} = \left[\frac{\lambda_H}{2} - (\lambda_H - \kappa_{H6})\delta\right]\epsilon^2 \,. \tag{4.13}$$

From the above equation we see that compared to M_h^2 and $M_{\mathcal{H}}^2$ the new scalar mass-squared is suppressed by an extra factor of ϵ. But we should not jump to conclusions: Noting the parallelism between ϕ_{PGB} and S due to the assumed exchange symmetry between $\langle\chi_2\rangle$ and $\langle\chi_4\rangle$ it is possible that the mass of S obtains sizable contributions from loop-corrections similar to the PGB. A quantitative study of whether such contributions are present or not would require a thorough analysis of the one-loop effective potential and lies beyond the scope of this work. We will, however, see that our results are not particularly sensitive to M_S. If we neglect M_S^2 for the time being, the one-loop PGB mass-squared in the ECISS is of the form of Eq. (3.21) and comprises the scalar masses $M_h \equiv m_{\text{Higgs}}$ and $M_{\mathcal{H}}$, the masses of the electroweak gauge bosons and of the additional Z' boson, which all give positive contributions, as well as the fermion masses, which contribute with a minus sign. The dominant contributions in the fermion sector are the top mass and the heavy neutrino masses as in the CISS. It is important to notice that including a sizable mass M_S in the formula for the PGB mass will even stabilize the RG running of the theory.

4.4 Lepton number violation

In this section we will investigate the phenomenology of LNV in the ECISS. First we discuss neutrinoless double beta decay followed by an analysis of same-sign di-lepton signals at particle colliders. Both of the mentioned processes involve charged-current interactions, which have been formulated for the flavor and for the mass bases in Eqs. (2.22) and (2.27), respectively. Note that the lepton mixing matrix U_{PMNS} introduced there, in the ECISS denotes a 3×9 matrix. Accordingly, all massive neutrino species defined in Eq. (4.8) enter the CC interactions. In the following we will discuss the impact of this alteration on $0\nu\beta\beta$.

4.4.1 Phenomenology of neutrinoless double beta decay

In this subsection we will analyze the potential signal for $0\nu\beta\beta$ in the ECISS. We will calculate the half-life $T_{1/2}^{0\nu}$ defined in Eq. (2.46) and determine the corresponding effective Majorana mass $m_{\text{eff}}^{0\nu}$, which has been introduced in Eq. (2.47).

In the ECISS the decay rate for $0\nu\beta\beta$ obtains contributions both from light and from heavy neutrino exchange. In particular, the active neutrinos and the dark matter candidates are relatively light, while the Majorana states N_1 and N_2 are relatively heavy compared to the typical momentum transfer in $0\nu\beta\beta$ of $|p|^2 = (100\text{ MeV})^2$. Note that the phenomenology in the light neutrino sector in the ECISS is the same as in the CISS. Accordingly, the effective parameter for light neutrino exchange is given by Eq. (3.30) and the effective light Majorana mass cannot be larger than $m_{ee} \approx 0.049$ eV [see Eq. (3.31)].

With Eq. (2.50) the effective parameter in the heavy sector can be expressed

as

$$\eta_{\text{eff}}^{N} \equiv m_p \left(\sum_{i=6}^{7} U_{ei}^2 \frac{1}{m_i} + \sum_{i=8}^{9} U_{ei}^2 \frac{1}{m_i} \right) \equiv \frac{m_p}{m_N} \,, \tag{4.14}$$

Note that due to the presence of M_R as largest mass scale in the neutrino mass matrix, the heavy neutrinos in the ECISS are Majorana particles as opposed to the pseudo-Dirac neutrinos in the CISS. Accordingly, the contribution in Eq. (4.14) is not subject to cancellations in the present model.

The light and heavy neutrino exchange in general have different nuclear matrix elements (NMEs). We will denote them by M_ν and M_N, respectively.[2] Then, from Eq. (2.46) we can derive the expression for the inverse half-life in the ECISS according to

$$\left(T_{1/2}^{0\nu}\right)^{-1} = G^{0\nu} \left| M_\nu \eta_{\text{eff}}^{\nu} + M_N \eta_{\text{eff}}^{N} \right|^2 \approx G^{0\nu} \left| \frac{M_\nu}{m_e} \right|^2 \left| m_{ee} + m_e m_p \frac{M_N}{M_\nu} m_N^{-1} \right|^2 \,, \tag{4.15}$$

where in the last step we have used $m_{ee} = m_e \eta_{\text{eff}}^{\nu}$ and Eq. (4.14). From the previous equation together with Eq. (2.47) it follows that the effective Majorana mass in the ECISS is given by

$$m_{\text{eff}}^{0\nu} = m_{ee} + m_e m_p \frac{M_N}{M_\nu} m_N^{-1} \,. \tag{4.16}$$

For the analysis of the effective Majorana mass in the ECISS we assume that the contribution from the light neutrinos is negligible. This is a reasonable assumption due to the upper bound on m_{ee}. But if one contribution is dominant compared to the other, the interference between them can be neglected without loss of generality. Note, however, that in general the above equation implies interference effects between the light and heavy neutrino contributions.

The current limits for the half-life of $0\nu\beta\beta$ and the effective Majorana mass derived thereof for the two isotopes under investigation, namely, ^{76}Ge and ^{136}Xe are listed in Table 4.2.[3] In order to study whether the quantities defined in Eqs. (4.15) and (4.16) can saturate the experimental limits, we need knowledge of the phase space factor and the NMEs. In Table 4.3 we show the numerical values, which were used in the present analysis, for the phase space factor and the NMEs of the two isotopes. With the ranges for the NMEs and neglecting the light neutrino contribution we can conservatively estimate the effective Majorana mass as

$$m_{\text{eff}}^{0\nu} \approx m_e m_p \frac{M_N}{M_\nu} m_N^{-1} \gtrsim \sum_{i=6}^{9} \left(\frac{U_{ei}^2}{10^{-4}} \right) \left(\frac{10 \text{ GeV}}{m_i} \right) \text{eV} \,, \tag{4.17}$$

[2] Note that we suppress the specification of the isotope (A, Z) here and in the following.

[3] We chose the isotopes ^{76}Ge and ^{136}Xe for our analysis, because they yield the currently strongest limits on the half-life of $0\nu\beta\beta$.

Table 4.2: The current lower limits on the half-life $T^{0\nu}_{1/2}$ and upper limits on the effective mass parameter $m^{0\nu}_{\text{eff}}$ of neutrinoless double beta decay for the isotopes ^{76}Ge and ^{136}Xe. The range for the effective mass parameter is due to the different methods of calculating the nuclear matrix elements.

Isotope	$T^{0\nu}_{1/2}$ [10^{25} y]	$m^{0\nu}_{\text{eff}}$ [eV]	Experiment	
^{76}Ge	> 1.9	n/a	HdM	[212]
	> 1.57	$< (0.33 - 1.35)$	IGEX	[213, 214]
	> 2.1	n/a	GERDA	[130]
	> 3.0	$< (0.2 - 0.4)$	HdM+IGEX+GERDA	[130]
^{136}Xe	> 1.6	$< (0.14 - 0.38)$	EXO	[215]
	> 1.9	n/a	KamLAND-Zen	[216]
	> 3.6	$< (0.12 - 0.25)$	EXO+KamLAND-Zen	[216]

Table 4.3: The numerical values of the phase-space factor $G_{0\nu}$ and nuclear matrix elements for the isotopes ^{76}Ge and ^{136}Xe taken from [143]. The nuclear matrix elements M_ν and M_N for light and, respectively, heavy neutrino exchange were obtained in the self-consistent renormalized quasiparticle random phase approximation [143]. Note that the ranges for the nuclear matrix elements correspond to the extremal values given in the reference.

Isotope	$G_{0\nu}$ [10^{-15} y^{-1}]	M_ν	M_N
^{76}Ge	7.98	3.85–5.82	172.2–411.5
^{136}Xe	59.2	2.19–3.36	117.1–172.1

where we have used Eq. (4.14) and have inserted the electron and proton mass as given below Eq. (3.34). From the above equation we see, that for active-sterile mixings U_{ei} of the order of 1% and heavy neutrino masses of some 100 GeV, we obtain effective Majorana masses of the order of 0.1 eV. Thus, one can saturate the experimental limits given in Table 4.2. Conversely, for increasing neutrino mass or decreasing active-sterile mixing, effective Majorana masses as small as 10^{-4} eV can easily be obtained as well.

In Figure 4.1 we show the results of our analysis for the effective Majorana mass $m^{0\nu}_{\text{eff}}$ (left panel) and the half-life $T^{0\nu}_{1/2}$ (right panel) of $0\nu\beta\beta$ in the ECISS. The contributions from heavy neutrinos predicted in the model by Eqs. (4.15) and (4.16) are displayed as yellow dots. Note that we only present dots that lie around the current limits even though one can in principle find configurations in the ECISS that fill up the entire parameter space shown in the figure. Lightest neutrino masses within the purple-shaded areas are disfavored by cosmological data: The areas labelled Planck and Planck + BAO show the limits from Planck data [108], where for the latter the effects of baryon acoustic oscillations (BAO) were additionally taken into account; the limit labelled Planck + BAO + Lyα was derived combining Planck + BAO limit with Lyman-α forest data [113, 114] and

Figure 4.1: Heavy neutrino contributions to the effective Majorana mass (left panel) and the corresponding half-life (right panel) of neutrinoless double beta decay versus the lightest neutrino mass displayed as yellow dots. The dots show values that saturate the experimental limits on neutrinoless double beta decay, which are represented by turquoise horizontal lines and the respective shaded areas for the combined limits in ^{76}Ge and in ^{136}Xe (for the numerical values see Table 4.2). Note that the seemingly more stringent constraints in the plot of the effective Majorana mass are a result of the uncertainty in the nuclear matrix elements. The purple-shaded areas labelled Planck, Planck + BAO and Planck + BAO + Lyα correspond to the limit on the sum of light neutrino masses from cosmological data [108, 113, 114]. The vertical red line marks the projected reach of the KATRIN detector [111, 112]. The green and red areas, respectively, show the 3σ allowed ranges in a three-neutrino scheme for oscillations in normal ordering (NO) and for inverted ordering (IO), respectively. The quasi-degenerate regime (QD), where NO and IO merge, is indicated.

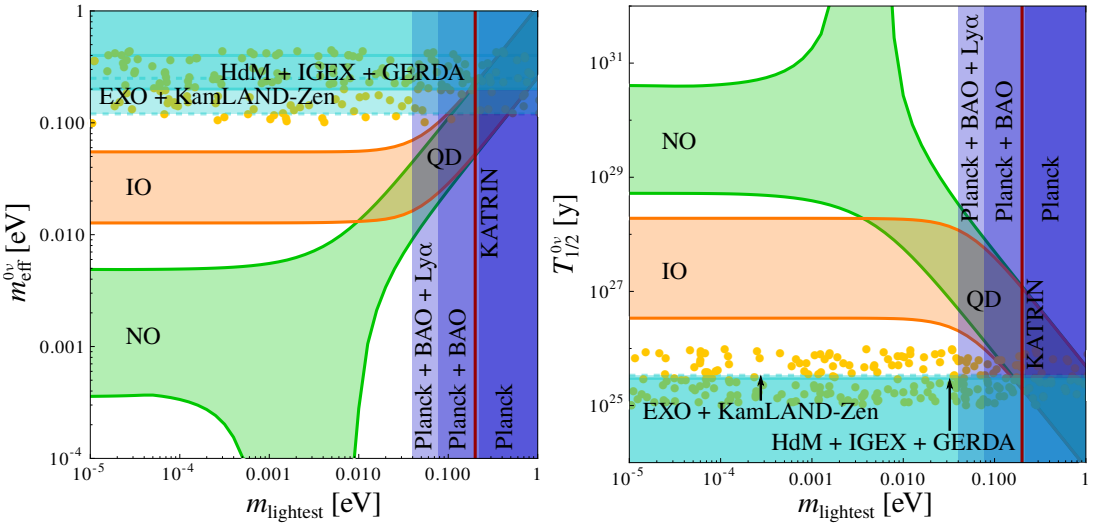

represent the currently strongest limit on the sum of relativistic neutrino masses. The projected reach of the KATRIN detector for electron-neutrino masses down to $m_{\nu_e} \approx 0.2$ eV [111, 112] is marked by the vertical red line. The turquoise areas correspond to the combined limits for the effective Majorana mass and the half-life in ^{76}Ge and ^{136}Xe as given in Table 4.2. Note that the excluded area for $m^{0\nu}_{\rm eff}$ appears larger than the one for $T^{0\nu}_{1/2}$ due to the uncertainty in the NMEs. When comparing the position of the yellow dots and the excluded areas, it becomes apparent that the heavy neutrino contribution in the ECISS can easily saturate current experimental bounds on $0\nu\beta\beta$.

If upcoming experiments observed a signal of $0\nu\beta\beta$, it could be explained by the LNV due to heavy Majorana neutrinos in the ECISS. In particular, a signal outside of the parameter region allowed by the mass mechanism could be interpreted as hint at the ECISS. Note, however, that such a feature is quite common to models adopting the seesaw mechanism. Hence, we will now study the collider phenomenology related to LNV in the ECISS in order to find more indicators to test our model.

Figure 4.2: *Left*: Same-sign di-lepton signal with two hadronic jets in the ECISS induced by the decay of a heavy Majorana neutrino n_i. *Right*: Decay of the Z' in the ECISS. The decay yields a same-sign di-lepton signal with four hadronic jets.

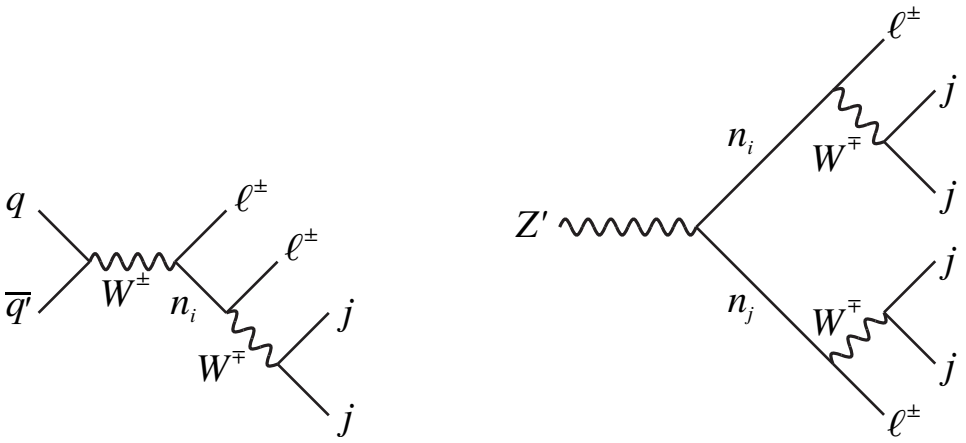

4.4.2 Probing lepton number violation at colliders

In this subsection we will discuss LNV same-sign di-lepton collider signatures. The cleanest channels that could probe LNV in the ECISS are $pp \to N_1\ell^{\pm} \to \ell^{\pm}\ell^{\pm}+2\,\text{jets}$ and $pp \to Z' \to \ell^{\pm}\ell^{\pm}+4\,\text{jets}$, both without missing transverse energy, where N_1 denotes the Majorana neutrino state with mass $m_{N_1} \sim M^2/M_{\text{R}}$ [see M_- given in Eq. (4.6)]. Note that N_2 with typical masses of the order of 10 TeV or larger is too heavy to give relevant contributions to cross sections at the LHC with a center-of-mass energy of 8 TeV. Both reactions are depicted in Figure 4.2. The Feynman diagram shown on the left is typical for theories, in which LNV can be mediated by the presence of Majorana neutrinos, while the one on the right is generic for LNV induced by spontaneous breaking of the $\text{U}(1)_{B-L}$ gauge symmetry. The amplitudes for the processes shown in the figure depend on the active-sterile mixing $U_{\ell N}$ and on the mass m_{N_1} of the heavy neutrinos N_1.

The size of the neutrino mass naturally has significant impact on the particle's half-life. It has been estimated that for N_1 masses of about 1 GeV up to 30 GeV and mixings $U_{\ell N} \sim 10^{-2}$ the neutrino can travel a distance of some $(10^{-3} - 1)$ m in the detector before it decays [217, 218]. The delayed decay leads to a displaced vertex, which could improve the sensitivity on the active-sterile mixing. Another observable that permits insight on the heavy neutrino mass scale is the opening angle between the two charged leptons in the $(\ell^{\pm}\ell^{\pm} + 2\,\text{jets})$ signal. While for $m_{N_1} \approx 100$ GeV the charged leptons leave the vertex within a tight cone, they are emitted mostly back-to-back for $m_{N_1} \approx 800$ GeV [184].

The $(\ell^{\pm}\ell^{\pm} + 4\,\text{jets})$ signal is induced by a Z' decay as shown in Figure 4.2 (right). Note that there exists another s-channel diagram with this signature. To see this remember that in conformal symmetry breaking all scalars that develop a finite vev are mixed among each other. This includes the physical Higgs boson, which in the ECISS is given by a superposition of all scalar degrees of freedom of

the theory.[4] Accordingly, the scalars χ_i couple to the physical Higgs and can be produced in proton-proton collisions via the mixing to the Higgs boson provided the center-of-mass energy is sufficiently high.

Therefore, the signal in Figure 4.2 (right) can be obtained as well by replacing the Z' by a χ_i. Taking into account that the $(\ell^\pm\ell^\pm + 4\,\text{jets})$ signal from a Z' or χ_i decay occurs via the s-channel, one should in principle be able to see the resonances of all mediators in the total invariant mass of the final states. The resonances from the scalars are, however, expected to be suppressed by the small mixing to the Higgs. We remark that aside from the aforementioned s-channel diagrams, the $(\ell^\pm\ell^\pm + 4\,\text{jets})$ signal can also arise in a t-channel topology as described in [190]. For a thorough study of the pair production of two heavy neutrinos in the decay of a Z' we refer to [219].

In [47, 48] it was shown that a gauged $\mathrm{U}(1)_{B-L}$ symmetry in a conformal theory is naturally broken at the scale of spontaneous conformal symmetry breaking, which lies at the order of TeV. Accordingly, the mass of the corresponding gauge boson in the ECISS is expected to be at that scale, too. The searches for a resonance in 20.3 (20.5) fb^{-1} of data in the di-electron (di-muon) channel collected by the ATLAS collaboration and in 20.6 (19.7) fb^{-1} of data in the di-electron (di-muon) channel collected by the CMS collaboration at a center-of-mass energy of 8 TeV exclude Z' masses below $(2-3)$ TeV at 95% confidence level for several models including such, in which the Z' is the gauge boson associated with $\mathrm{U}(1)_{B-L}$ [220, 221]. With more data from Run 2 at the LHC at a higher center-of-mass energy of 13 TeV but with yet a smaller luminosity of presently 3.2 fb^{-1}, the lower bound was improved to 3.40 TeV at 95% confidence level [222]. By means of Eq. (4.3) we can estimate that for a conformal symmetry breaking scale of $\mathcal{O}(1)$ TeV and natural gauge couplings g_{B-L} of the order of 0.1 to 1 the Z' mass in the ECISS is expected to be slightly above that limit. As more data is collected at the LHC, the exclusion limit on the Z' mass is expected to further increase. Hence, the present model is probably going to be tested in the near future. For completeness we note that the limits on the Z' boson's mass given by [220–222] were derived considering specific models. Judging whether these limits directly apply also to our model would require a dedicated analysis of the cross section of the Z' production in the ECISS, which lies beyond the scope of this work.

In the following we will estimate the strength of the LNV $(\ell^\pm\ell^\pm + 2\,\text{jets})$ signal at the LHC to be expected from the Majorana neutrinos in the ECISS. The naturally sizable active-sterile mixing in the model can lead to sufficiently large signals in the same-sign di-lepton channel. Simultaneously, the active neutrinos' sub-eV masses, consistent with oscillation data, are maintained owing to the inverse seesaw formula. The cross section for the diagram shown in Figure 4.2

[4] Of course, h_3, the scalar degree of freedom that couples to the SM fermions, must give the dominant contribution to the physical Higgs.

(left) can be calculated in the narrow width approximation (cf. Section 3.4.2) as

$$\sigma(pp \to N_1 \ell^\pm \to \ell^\pm \ell^\pm + 2\,\text{jets}) = \sigma(pp \to N_1 \ell^\pm) \times \text{Br}(N_1 \to \ell^\pm + 2\,\text{jets})\,. \tag{4.18}$$

Within the present scenario the branching ratio of the heavy neutrino decay can be expressed as

$$\text{Br}(N_1 \to \ell^\pm + 2\,\text{jets}) = \frac{\Gamma(N_1 \to W\ell^\pm)}{\Gamma_N^{\text{total}}} \times \text{Br}(W \to 2\,\text{jets})\,, \tag{4.19}$$

where $\text{Br}(W \to 2\,\text{jets}) = 0.674$ [87]. The total decay rate of the heavy neutrino is constituted by the following individual rates

$$\Gamma(N_1 \to W\ell^\pm) = \frac{g^2|U_{\ell N}|^2}{32\pi}\frac{m_{N_1}^3}{m_W^2}\left(1 - \frac{m_W^2}{m_{N_1}^2}\right)^2\left(1 + 2\frac{m_W^2}{m_{N_1}^2}\right), \tag{4.20a}$$

$$\Gamma(N_1 \to Z\nu,\, Z\overline{\nu}) = \frac{g^2|U_{\ell N}|^2}{64\pi\,\cos^2\theta_{\text{W}}}\frac{m_{N_1}^3}{m_Z^2}\left(1 - \frac{m_Z^2}{m_{N_1}^2}\right)^2\left(1 + 2\frac{m_Z^2}{m_{N_1}^2}\right), \tag{4.20b}$$

$$\Gamma(N_1 \to h\nu,\, h\overline{\nu}) = \frac{g^2|U_{\ell N}|^2}{64\pi}\frac{m_{N_1}^3}{m_W^2}\left(1 - \frac{M_h^2}{m_{N_1}^2}\right)^2, \tag{4.20c}$$

$$\Gamma(N_1 \to S\nu,\, S\overline{\nu}) = \frac{g^2|U_{\ell N}|^2}{64\pi}\frac{m_{N_1}^3}{m_W^2}\left(1 - \frac{M_S^2}{m_{N_1}^2}\right)^2, \tag{4.20d}$$

which were calculated assuming $m_\ell,\, m_\nu \ll m_{N_1}$ and where h denotes the Higgs-like particle observed at the LHC. Obtaining Eqs. (4.20a) and (4.20b) is straightforward, but some comments on computing the rates given in Eqs. (4.20c) and (4.20d) are in order. The decay rate of the heavy neutrino into the Higgs given in Eq. (4.20c) and an active (anti-)neutrino contains a sum over the Yukawa couplings between all three involved particles due to the mixing between mass and flavor eigenstates of the neutrinos on the one hand, and due to the mixing in the scalar sector on the other hand. As already mentioned, h is in general a superposition of all CP-even scalar degrees of freedom which, however, is dominated by h_3, the scalar that couples to the SM fermions. Accordingly, the dominant contribution to $\Gamma(N_1 \to h\nu,\, h\overline{\nu})$ is proportional to y_{D}^2 [cf. Eq. (4.2)], which can be expressed in terms of the $\text{SU}(2)_{\text{L}}$ gauge coupling g, the W boson mass m_W and the heavy neutrino mass $m_{N_1} = M^2/M_{\text{R}}$ as

$$y_{\text{D}}^2 = \frac{2m_{\text{D}}^2}{v_{\text{ew}}^2} = \frac{2m_{N_1}^2}{v_{\text{ew}}^2}\frac{m_{\text{D}}^2}{M^2}\frac{M_{\text{R}}^2}{M^2} \approx \frac{g^2 m_{N_1}^2}{2m_W^2}\,, \tag{4.21}$$

where in the last step we have used Eq. (2.13) and approximated $\frac{m_{\text{D}}^2}{M^2}\frac{M_{\text{R}}^2}{M^2} = \Theta^2\frac{M_{\text{R}}^2}{M^2} \approx 1$. The decay rate in Eq. (4.20d) can be estimated in a similar way. Since S mainly consists of χ_2 and χ_4, it couples to the neutrinos with strength y. This coupling can be expressed according to

$$y^2 = \frac{2M^2}{v_{\text{ew}}^2}\,\varepsilon = \frac{2m_{N_1}^2}{v_{\text{ew}}^2}\,\varepsilon\,\frac{M_{\text{R}}^2}{M^2} \approx \frac{g^2 m_{N_1}^2}{2m_W^2}\,, \tag{4.22}$$

Table 4.4: The expected number of events in the same-sign di-lepton channel mediated by heavy neutrino decay with two jets and no missing transverse energy. The values for production cross section (second column) are taken from [223]. Note that for the values shown in the table an extra factor of 10^{-1} has been included to compensate for the different mixing used in our model. The third and fourth columns give the approximate number of events expected in the current and upcoming LHC run. Note that the center-of-mass energy for the upcoming run is given by $\sqrt{s} = 14$ TeV.

m_{N_1} [GeV]	$\sigma(pp \to N_1\ell^\pm)$ [pb]	# at $\mathcal{L} = 19.4$ [fb^{-1}]	# at $\mathcal{L} = 300$ [fb^{-1}]
200	0.100	556	8600
500	0.005	25	390

where $\varepsilon = v_{\text{ew}}^2/v^2$ and in the last step we have approximated $\varepsilon \frac{M_{\text{R}}^2}{M^2} \approx 1$.

With the help of Eq. (4.18) we will investigate how many events in the same-sign di-lepton channel are expected in the ECISS. To this end, we assume a mixing of $|U_{\ell N}|^2 = 10^{-4}$ and consider two different masses for m_{N_1} with the production cross section $\sigma(pp \to N_1\ell^\pm)$ taken from [223]. In that analysis a mixing of $|U_{\ell N}|^2 = 10^{-3}$ was assumed. Accordingly, the numerical values for the production cross section that we use for our calculation are smaller by a factor of 10^{-1} compared to those in [223]. In Table 4.4 we summarize the results of our study, where we compute the number of events for the luminosities of the current and projected performance of the LHC [195]. For the calculation of the numbers in the table we have assumed a mass of $M_S \approx \sqrt{\varepsilon} M_h$ in agreement with Eq. (4.13). Remember that after this equation, we had mentioned the possibility that M_S could obtain sizable loop corrections. Considering larger values for M_S leads to a slight increase of the event numbers by a factor of $\mathcal{O}(1)$, but in conclusion leads to the same qualitative signal.

From Table 4.4 we see that the cross section for a heavy neutrino with $m_{N_1} = 200$ GeV produces too many events in the same-sign di-lepton channel, so this relatively small mass is to be excluded. But the signal from the $m_{N_1} = 500$ GeV neutrino is consistent with current measurements at the LHC, which do not observe any significant excess above the SM background expectation in the same-sign di-lepton channel [189, 224]. In the future the roughly 400 events predicted for the next run should lead to a clear signal at the LHC.

The discussion of the LNV Z' decay as well as the expected number of events in the LNV di-lepton channel with two jets previously presented, show that the ECISS will probably be tested once further LHC data become available.

Finally, we mention a possibility to use gravitational waves in order to probe conformal theories with gauged $\text{U}(1)_{B-L}$ as discussed in [68]. First, it is assumed that some scalar particle with $B-L$ charge spontaneously breaks both the conformal symmetry and $\text{U}(1)_{B-L}$ by developing a finite vev via the Coleman-Weinberg mechanism. After spontaneous symmetry breaking the evolution of the vacuum is determined by an effective potential taking into account finite-temperature effects. It is further assumed that the $\text{U}(1)_{B-L}$ symmetry is restored at the time of

reheating so that the vacuum is trapped in a minimum of the effective potential at the origin of scalar field space. As the Universe cools down, the minimum at the origin becomes a false vacuum at some critical temperature and a true vacuum at finite vevs is developed. Accordingly, the scalar will eventually tunnel from the false into the true vacuum. Note that this is a first-order phases transition. The bubble nucleation associated with the tunnelling hence can lead to strong gravitational waves induced by bubble collisions, turbulences and sound waves. It was pointed out in [68] that in a conformal theory with gauged $B - L$ symmetry the gravitational waves' amplitude is expected to be large and thus detectable by future interferometer experiments. Accordingly, gravitational waves could represent an investigation method complementary to collider searches for the parameter space of conformal theories. This possibility is of particular interest in the context of the recent discovery of gravitational waves by LIGO [225] opening up the observational window into the distant past of the Universe.

Chapter 5

Analysis of the generalized type-I seesaw

In the preceding chapters we have studied two different realizations of the inverse seesaw mechanism in the context of conformal electroweak symmetry breaking. In both cases the neutrino mass matrix played a decisive role in model building as well as in phenomenological predictions. In this chapter we will study the neutrino mass matrix in a formal context. The study is based on original work of the author and has not yet been published. The definitions and calculations used for the results presented in this chapter are summarized in Appendix B.

This chapter is organized as follows. In Section 5.1 we will introduce the set-up for the neutrino mass matrix. There, we will also give some motivation for the venture of analyzing the matrix in a general way. Then, in Section 5.2 we will discuss for which scenarios the mass matrix possesses exactly vanishing neutrino masses. Finally, we will derive the eigenvalue spectrum of the neutrino mass matrix for several scenarios in Section 5.3.

5.1 The set-up

In order to perform the following analysis in the most general way we restrain ourselves to using the least possible number of assumptions regarding the set-up. So let us consider a theory with two different neutrino species ν_{L}^{A} and ν_{R}^{B}, which could for instance represent the active (i.e. interacting with the electroweak gauge bosons) and sterile (i.e. non-interacting) neutrinos with a and b generations, respectively. Furthermore, we assume that the neutrinos of sector A do not have a Majorana mass term. This could for example be due to a gauge symmetry for which the neutrinos of sector A are part of a gauge multiplet (like the neutrinos in the SM), while the neutrinos of sector B are gauge singlets with respect to this symmetry. Then the neutrino mass Lagrangian in the Majorana basis $n_{\mathrm{L}} = (\nu_{\mathrm{L}}^{A},\, \nu_{\mathrm{R}}^{B,\mathrm{c}})^{\intercal}$ is given by

$$\mathcal{L}_{\mathrm{mass}} = -\overline{\nu_{\mathrm{R}}^{B}} M_{\mathrm{D}} \nu_{\mathrm{L}}^{A} - \tfrac{1}{2}\overline{\nu_{\mathrm{R}}^{B,\mathrm{c}}} M_{\mathrm{R}} \nu_{\mathrm{R}}^{B} + \mathrm{h.c.} \;= -\tfrac{1}{2}\overline{n_{\mathrm{L}}^{\mathrm{c}}}\, \mathcal{M}\, n_{\mathrm{L}} + \mathrm{h.c.}\;, \tag{5.1}$$

where $M_{\rm D}$ denotes a $b \times a$ matrix and $M_{\rm R}$ a symmetric $b \times b$ matrix. The complete symmetric neutrino mass matrix in this theory is an $(a+b) \times (a+b)$ block-matrix, which is given by

$$\mathcal{M} = \begin{pmatrix} 0 & M_{\rm D}^{\intercal} \\ M_{\rm D} & M_{\rm R} \end{pmatrix} \quad \in \quad \mathbb{C}^{(a+b)\times(a+b)} \,. \tag{5.2}$$

Note that at this point of the discussion we do not specify how large the elements of $M_{\rm D}$ and $M_{\rm R}$ are relative to each other. Neither do we determine whether $M_{\rm R}$ is singular or not. Also, the numbers of generations a and b are arbitrary at this stage of the discussion (aside from being positive integers, of course). The matrix given in the above equation represents the most general form of the neutrino mass matrix in the type-I seesaw.

Before we present the results, let us briefly review the status quo of the analytical study of the mass matrix's eigenvalue spectrum. In the canonical type-I seesaw, discussed in Section 2.2.1, three assumptions on the mass matrix given in Eq. (5.2) are made. It is assumed that all eigenvalues of $M_{\rm R}$ are non-zero (i.e. $M_{\rm R}$ is non-singular) and much larger than those of $M_{\rm D}$ (usually denoted as "$M_{\rm R} \gg M_{\rm D}$"). Furthermore, it is assumed that there exists an equal number of neutrinos in sector A and sector B (i.e. $a = b$). Under these assumptions the masses of the neutrino species A after the diagonalization can be found order by order by means of the seesaw formula [90], which at leading order yields

$$m_{\nu_A} = -M_{\rm D}^{\intercal}\, M_{\rm R}^{-1}\, M_{\rm D} \,. \tag{5.3}$$

The masses in sector B are given by $M_{\rm R}$ to very good approximation. Note that it is straightforward to prove that the seesaw formula also applies in the case $a < b$. The canonical type-I seesaw in the case $a > b$ was investigated in [226]. There it was shown that the matrix given in Eq. (5.2) with $a > b$ possesses $a - b$ exactly vanishing eigenvalues regardless of the relation between $M_{\rm R}$ and $M_{\rm D}$. In other words, for each Majorana mass in sector B one obtains upon diagonalization exactly one non-vanishing Majorana mass in sector A. This behaviour is tagged "seesaw fair play rule". Note that in the analysis presented in [226] the assumption that $M_{\rm R}$ is non-singular was maintained.

The possibility of a singular seesaw mechanism was first discussed in [96–98]. The singular set-up deserves attention on its own for it is in principle able to successfully explain neutrino mass-squared differences and mixing angles [227, 228]. However, usually only a specific set-up with fixed numbers of sterile neutrinos and vanishing eigenvalues is considered, see e.g. [96, 227–230]. This motivates us to study the possibility of a singular Majorana mass term in a general context. It is important to notice that the appearance of singular matrix structures is not exotic. Imagine that the Majorana masses of the neutrinos from sector B are induced by some flavor-blind interaction, which becomes relevant at some higher scale (as for instance discussed in [231]). If this flavor blindness is exact, the Majorana mass term is necessarily singular. We remark that such universal interactions are nothing special. Indeed, the gauge couplings in the SM are not sensitive to the flavors of the fermions.

To the best of our knowledge the only more general analytical treatment of the eigenvalue spectrum in a seesaw with possibly singular Majorana mass term was performed in [232].[1] Under the assumption that $M_{\rm R}$ is much larger than $M_{\rm D}$ it was shown in that work that the number of small neutrino masses, which are naturally obtained in the type-I seesaw, must be smaller than or equal to $|a-b+t|$, where $t \equiv {\rm rk}(M_{\rm R}) \leq b$ denotes the rank of $M_{\rm R}$. Note that the matrix $M_{\rm R}$ is singular if and only if $t < b$. As a test for the validity of the method used in the analysis we have confirmed that the results are in agreement with the status quo as described in the preceding paragraphs.

In the following we will present our analysis with all technical details given in Appendix B. When we investigate the different possible structures of the mass matrix given in Eq. (5.2), we categorize the scenarios by means of the following three properties:

$$\begin{aligned}
&1.\quad \det(M_{\rm R}): && \begin{cases} \det(M_{\rm R}) \neq 0: & \text{non-singular} \\ \det(M_{\rm R}) = 0: & \text{singular} \end{cases} \\
&2.\quad a \text{ vs. } b: && \begin{cases} a > b: & \text{unsaturated (u)} \\ a = b: & \text{saturated (s)} \\ a < b: & \text{over-saturated (o)} \end{cases} \\
&3.\quad M_{\rm R}: && \begin{cases} M_{\rm R} \gg M_{\rm D}: & \text{Majorana (M)} \\ M_{\rm R} \ll M_{\rm D}: & \text{pseudo-Dirac (PD)} \\ M_{\rm R} = 0: & \text{Dirac (D)} \end{cases}
\end{aligned} \qquad (5.4)$$

Several comments are in order. First, note that in the singular Majorana and pseudo-Dirac cases the relation between $M_{\rm R}$ and $M_{\rm D}$ refers to the non-vanishing eigenvalues of $M_{\rm R}$. Second, we always count the Dirac case among the non-singular category even though $\det(M_{\rm R})$ is zero in that scenario. The reason for this will become apparent in the course of the discussion in Section 5.3. Third, for the second category in Eq. (5.4) we have introduced the notion of 'saturation'. As we will see in the following discussion, the eigenvalues of the neutrino mass matrix in Eq. (5.2), if possible, always form pairs with mass scales characteristic for the relations between $M_{\rm R}$ and $M_{\rm D}$ given in the third category. This matching works perfectly in the *saturated* cases. However, in the *unsaturated* cases there are not enough Majorana masses at hand so that vanishing eigenvalues appear in the eigenvalue spectrum (as will be shown in Section 5.2). Conversely, in the *over-saturated* scenarios the matrix $M_{\rm R}$ possesses an overweight of Majorana masses. In consequence, there are always non-vanishing eigenvalues, which do not participate in the matching. Fourth, we remark that for the Dirac case the unsaturated and the over-saturated versions are analytically identical. Accordingly, we will not discuss the over-saturated Dirac scenario separately as it can

[1] We acknowledge that in [98] a singular scenario, which is contained as a sub-class in the more general discussion presented in [232], was studied.

be obtained from the unsaturated one by exchanging a and b. And fifth, note that the relation $M_{\mathrm{R}} \simeq M_{\mathrm{D}}$ is not listed in the third category in Eq. (5.4). Such a relation between the mass terms would typically correspond to a theory, in which the neutrino masses in both sectors A and B are generated by the same physics at the same scale. But then the distinction between the sectors would not make sense in the first place. Hence, we do not consider the case $M_{\mathrm{R}} \simeq M_{\mathrm{D}}$.

Varying through all scenarios listed in Eq. (5.4) we encounter three qualitatively different structures of the neutrino mass matrix. We define them as

$$\mathcal{M}_1 = \begin{pmatrix} 0 & M_{\mathrm{D}}^{\intercal} \\ M_{\mathrm{D}} & M_{\mathrm{R}} \end{pmatrix} \in \mathbb{C}^{(a+b)\times(a+b)}\,, \tag{5.5}$$

$$\mathcal{M}_2 = \begin{pmatrix} 0 & M_{\mathrm{D}}^{\intercal} \\ M_{\mathrm{D}} & 0 \end{pmatrix} \in \mathbb{C}^{(a+b)\times(a+b)}\,, \tag{5.6}$$

$$\mathcal{M}_3 = \begin{pmatrix} 0 & M_{\mathrm{D}s}^{\intercal} & M_{\mathrm{D}t}^{\intercal} \\ M_{\mathrm{D}s} & 0 & 0 \\ M_{\mathrm{D}t} & 0 & M_{\mathrm{R}t} \end{pmatrix} \in \mathbb{C}^{(a+s+t)\times(a+s+t)}\,, \tag{5.7}$$

where the dimensions a, b, s and t are all positive and $s + t = b$. In the above equations $M_{\mathrm{D}s}$ and $M_{\mathrm{D}t}$ are defined as $s \times a$ and $t \times a$ matrices, respectively. The matrices M_{R} and $M_{\mathrm{R}t}$ are defined as *invertible*, square matrices of dimension b and t, respectively.[2] If not stated otherwise, we will assume that a matrix has maximal rank in the following discussion. The first structure given in Eq. (5.5) corresponds to the canonical seesaw if $M_{\mathrm{R}} \gg M_{\mathrm{D}}$, and to the pseudo-Dirac seesaw if $M_{\mathrm{R}} \ll M_{\mathrm{D}}$, both with non-singular M_{R}. The second structure defined in Eq. (5.6) is easily identified as the typical Dirac-type matrix. Finally, the third structure in Eq. (5.7) is the canonical form encountered in singular seesaw scenarios, where we have the relation $M_{\mathrm{R}t} \gg M_{\mathrm{D}}$ in the singular Majorana case, and $M_{\mathrm{R}t} \ll M_{\mathrm{D}}$ in the singular pseudo-Dirac case. For completeness let us give two examples for our categorization:

1. The "singular uPD (a, s, t)" corresponds to a neutrino mass matrix of type 3 given by Eq. (5.7), because it is a *singular* scenario; the dimensions of the matrix satisfy the relation $a > b = s + t$ since it is an *unsaturated* scenario; and, finally, the relation between the involved mass matrices is $M_{\mathrm{R}t} \ll M_{\mathrm{D}}$ according to the defining property of a *pseudo-Dirac* scenario.

2. The "non-singular sM (3, 3)" corresponds to the canonical type-I seesaw.

In this fashion all possible scenarios for the mass matrix given in Eq. (5.2) can be categorized by the three properties specified in Eq. (5.4). Note that in some cases we will suppress the indication of a structure's dimensions for the sake of brevity. In the following we will present and discuss the results of our analysis derived in Appendix B.

[2] Note that for a square matrix the three following properties are equivalent: i) it is invertible, ii) it has maximal rank, and iii) it is non-singular [cf. Eq. (B.5)].

5.2 Exactly vanishing eigenvalues

When analyzing or constructing a neutrino mass matrix in a given model, it is convenient to know *in advance* how many of the neutrino masses exactly vanish. Such an information is relevant for instance in the context of active neutrino masses as less than two massive active neutrinos are inconsistent with oscillation phenomenology (cf. Section 2.2.1). Another example could be a model, in which a certain number of vanishing eigenvalues is desired in order to generate neutrino masses through higher-order loop corrections. Note, however, that an exactly vanishing eigenvalue can be stable against radiative corrections as was shown in [233] for the minimal seesaw model [234].

In our study we have analyzed how many exactly vanishing eigenvalues are present in all possible scenarios for the matrices given in Eqs. (5.5) - (5.7). Note that the number of vanishing eigenvalues is independent of the relation between $M_{\rm R}$ and $M_{\rm D}$ (including the case $M_{\rm R} \simeq M_{\rm D}$). The results, which are summarized in Table B.1, show that all matrix structures in unsaturated scenarios (i.e. the ones with $a > b$) always possess $a - b$ exactly vanishing eigenvalues. There is another structure with vanishing eigenvalues, which is classified as $\mathcal{M}_3(\mathrm{o}^*)$, i.e. the singular matrix structure given by Eq. (5.7) in an over-saturated scenario with the additional condition that not only $b > a$, but also $s > a$. This structure yields $s - a$ exactly vanishing eigenvalues. The unsaturated and the $\mathcal{M}_3(\mathrm{o}^*)$ structures are the only ones with exactly vanishing eigenvalues. All other scenarios possess solely non-vanishing eigenvalues. As anticipated below Eq. (5.4), this result is no coincidence, but rather we coined the expression 'unsaturated' to reflect this behaviour.

The outcome for the unsaturated scenarios and for the case $\mathcal{M}_3(\mathrm{o}^*)$ are a generalization of the seesaw fair-play rule. As mentioned above, in [226] the singular case was not analyzed. In this respect, the results presented here complete the study of vanishing eigenvalues in the generalized type-I seesaw performed in that work.

5.3 Eigenvalue spectrum of the mass matrix

In Section B.2.2 we perform a systematic study of the eigenvalue spectrum for all scenarios for the mass matrix given in Eq. (5.2). In our survey we have found that the eigenvalue spectra of some matrix structures can be related to those of other matrix structures. We call scenarios of this type *reducible*. Every scenario that is not reducible is called *irreducible*. In the flowchart displayed in Figure 5.1 we show how the cases can be related to each other. The figure will be discussed in the following. More detailed information about the reducible and irreducible structures is listed in Tables B.2 and B.3.

Let us first take a look at the unsaturated (u) scenarios in the upper row of Figure 5.1. There we see that all *unsaturated* scenarios can be reduced to the corresponding *saturated* scenario (following the vertical arrows pointing down). In

Figure 5.1: Flowchart of all possible scenarios in the generalized type-I seesaw. Scenarios with a black frame are reducible. The arrows show to which structure a reducible scenario is related. A label on an arrow indicates an additional condition that needs to be satisfied. The red-framed scenarios are those, for which we could not obtain a form of the characteristic polynomial, from which the eigenvalues could be derived. Conversely, for the scenarios with a green frame we have found the eigenvalue spectrum. The abbreviation "sing." stands for "singular". The categorization of the scenarios is defined in Eq. (5.4).

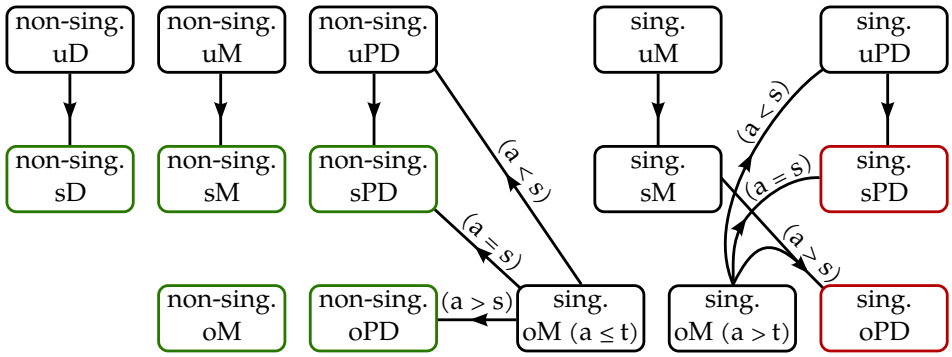

practice, this means that for example the non-singular unsaturated Majorana scenario or in brief non-singular uM (a, b) can be reduced to the saturated Majorana scenario or in brief non-singular sM (b, b). Notice the change in the structure's dimensions in going from the unsaturated to the saturated case. As discussed in the previous section each unsaturated scenario possesses $a - b$ exactly vanishing eigenvalues. Equivalently, it possesses $2b$ non-vanishing eigenvalues, which can be obtained from the non-singular sM (b, b) scenario in the case of the non-singular uM (a, b). As mentioned above a more detailed overview of the correspondences for all unsaturated cases containing additional information on the change in the structure's dimensions is given in Table B.2.

Next we consider the singular scenarios, which are aligned on the right-hand side of the figure. Except for the singular over-saturated Majorana scenario with the additional condition that $a \leq t$, there is no connection from the singular to the non-singular side on the left. Following the arrows on the singular side we see that each singular scenario – save the mentioned exception – eventually ends up in the singular saturated or over-saturated pseudo-Dirac scenarios (the ones with a red frame). We have analyzed these scenarios, but could not obtain a form of the characteristic polynomial, from which the eigenvalues could be derived. Information about the eigenvalues strongly depends on the different relations between a, s and t. Details on the reducible structures in the singular scenarios are given in Table B.3.

Finally, we study the non-singular side on the left of Figure 5.1. Here, all structures end up in green-framed, irreducible scenarios. For these irreducible scenarios we have found a solution to the eigenvalue problem. Our method of analyzing the eigenvalue spectrum of the irreducible structures presented in Section B.2.2 is different from the treatment in the canonical type-I seesaw. As already mentioned,

the seesaw can be applied if $M_{\rm R}$ is non-singular and if the relation $M_{\rm R} \gg M_{\rm D}$ holds. Then the expressions for the eigenvalues are found order by order in matrix form through the seesaw formula. In our analysis we consider the exact characteristic polynomial defined in Eq. (B.42) of the matrix under investigation in order to find the eigenvalue spectrum. This method represents a new ansatz to the eigenvalue problem of the neutrino mass matrix. The results of our analysis for the eigenvalue spectra in the non-singular saturated scenarios are summarized for convenience in Table 5.1. They are obtained from Eqs. (B.49) - (B.51) and for the non-singular over-saturated scenarios by Eqs. (B.54) and (B.55). As already mentioned, the eigenvalue spectra of the non-singular unsaturated scenarios can be derived from the spectra of the corresponding saturated cases. In the following we discuss the results.

In Table 5.1 we have assumed that the eigenvalues of $M_{\rm D}$ are generically proportional to some mass scale $m_{\rm D}$. A similar assumption applies to the eigenvalues of $M_{\rm R}$. Note that in the non-singular over-saturated Majorana case the total number of eigenvalues with mass scale $m_{\rm R}$ is given by b in agreement with the expectation from the type-I seesaw. The most interesting observation that can be made from the table is that the eigenvalues of the mass matrix, if possible, always form pairs. This result analytically confirms the intuitive expectation that the matrix's symmetry should somehow be imprinted in the eigenvalue spectrum. If we take a look at the scales of the eigenvalue pairs in the table we see that they nicely reflect the characteristic mass scales of the Majorana, pseudo-Dirac and Dirac scenarios, respectively. In Figure 5.2 we schematically illustrate the evolution of an eigenvalue pair as a function of the Majorana mass. Note that on the y-axis we show the absolute values of the eigenvalues. In the unsaturated case with $a > b$ the overweight of the zero block in the mass matrix manifests itself in the $a - b$ eigenvalues, which are not paired, as they exactly vanish (in agreement with the results in Section B.2.1). Equally, in the over-saturated scenarios with $a < b$ the overweight in the Majorana mass term $M_{\rm R}$ produces $b - a$ single eigenvalues proportional to $m_{\rm R}$.

Lastly, we show the eigenvalue spectra for the different cases of the singular over-saturated Majorana scenario with the additional condition $a \leq t$ in Table 5.2. The spectra have been derived using the flowchart in Figure 5.1 (or respectively using Table B.3) and Table 5.1. Note that the singular over-saturated Majorana scenario with $a \leq t$ always possesses t eigenvalues proportional to $m_{\rm R}$. The remaining eigenvalues are obtained from a substructure that realizes a *non-singular* pseudo-Dirac scenario of the form

$$\mathcal{M}' = \begin{pmatrix} 0 & M_{{\rm D}s} \\ M_{{\rm D}s}^{\intercal} & M_{\rm X} \end{pmatrix} \quad \in \ \mathbb{C}^{(s+a)\times(s+a)}\,, \tag{5.8}$$

where $M_{\rm X} = -M_{{\rm D}t}^{\intercal} M_{{\rm R}t}^{-1} M_{{\rm D}t}$ [see Eq. (5.7)]. Accordingly, we have $\det(M_{\rm X}) \neq 0$ and the eigenvalues of $M_{\rm X}$ are proportional to $m_{\rm X} \equiv m_{\rm D}^2/m_{\rm R}$. Whether this structure is unsaturated, saturated or over-saturated depends solely on the relation between s and a as can be seen in the table.

Table 5.1: Eigenvalue spectra of the neutrino mass matrix for all different scenarios in the non-singular seesaw with defining properties. The "#" and "$\sim$" signs indicate the number of eigenvalues and the corresponding mass scale, respectively. The "$= 0$" signifies that the eigenvalues exactly vanish. Note that for the Dirac type matrix the cases $a > b$ and $a < b$ are (analytically) equivalent. Note as well that the phase of the negative eigenvalues can always be absorbed by a redefinition of the fields.

non-singular Majorana (M), $M_{\mathrm{R}} \gg M_{\mathrm{D}}$

unsaturated (u) $a > b$	saturated (s) $a = b$	over-saturated (o) $a < b$
$\#b \sim -m_{\mathrm{D}}^2/m_{\mathrm{R}}$	$\#b \sim -m_{\mathrm{D}}^2/m_{\mathrm{R}}$	$\#a \sim -m_{\mathrm{D}}^2/m_{\mathrm{R}}$
$\#b \sim m_{\mathrm{R}}$	$\#b \sim m_{\mathrm{R}}$	$\#a \sim m_{\mathrm{R}}$
$\#(a-b) = 0$		$\#(b-a) \sim m_{\mathrm{R}}$

non-singular pseudo-Dirac (PD), $M_{\mathrm{R}} \ll M_{\mathrm{D}}$

unsaturated (u) $a > b$	saturated (s) $a = b$	over-saturated (o) $a < b$
$\#b \sim +m_{\mathrm{D}} + m_{\mathrm{R}}/2$	$\#b \sim +m_{\mathrm{D}} + m_{\mathrm{R}}/2$	$\#a \sim +m_{\mathrm{D}} + m_{\mathrm{R}}/2$
$\#b \sim -m_{\mathrm{D}} + m_{\mathrm{R}}/2$	$\#b \sim -m_{\mathrm{D}} + m_{\mathrm{R}}/2$	$\#a \sim -m_{\mathrm{D}} + m_{\mathrm{R}}/2$
$\#(a-b) = 0$		$\#(b-a) \sim m_{\mathrm{R}}$

non-singular Dirac (D), $M_{\mathrm{R}} = 0$

unsaturated (u) $a > b$	saturated (s) $a = b$	unsaturated (u) $a < b$
$\#b \sim +m_{\mathrm{D}}$	$\#b \sim +m_{\mathrm{D}}$	$\#a \sim +m_{\mathrm{D}}$
$\#b \sim -m_{\mathrm{D}}$	$\#b \sim -m_{\mathrm{D}}$	$\#a \sim -m_{\mathrm{D}}$
$\#(a-b) = 0$		$\#(b-a) = 0$

Table 5.2: Eigenvalue spectra of the neutrino mass matrix for the singular over-saturated Majorana scenario with dimensions (a, s, t) and the additional condition $a \leq t$. The "#" and "$\sim$" signs indicate the number of eigenvalues and the corresponding mass scale, respectively. The "$= 0$" signifies that the eigenvalues exactly vanish. The mass scale m_{X} is proportional to $m_{\mathrm{D}}^2/m_{\mathrm{R}}$. Note that the phase of the negative eigenvalues can always be absorbed by a redefinition of the fields.

singular over-saturated Majorana (a, s, t), $a \leq t$

$s > a$	$s = a$	$s < a$
$\#a \sim +m_{\mathrm{D}} + m_{\mathrm{X}}/2$	$\#a \sim +m_{\mathrm{D}} + m_{\mathrm{X}}/2$	$\#s \sim +m_{\mathrm{D}} + m_{\mathrm{X}}/2$
$\#a \sim -m_{\mathrm{D}} + m_{\mathrm{X}}/2$	$\#a \sim -m_{\mathrm{D}} + m_{\mathrm{X}}/2$	$\#s \sim -m_{\mathrm{D}} + m_{\mathrm{X}}/2$
$\#(s-a) = 0$		$\#(a-s) \sim m_{\mathrm{X}}$
$\#t \sim m_{\mathrm{R}}$	$\#t \sim m_{\mathrm{R}}$	$\#t \sim m_{\mathrm{R}}$

Figure 5.2: Schematic illustration of the evolution of a pair of eigenvalues with increasing Majorana mass (red lines) on a double-logarithmic plot. At a Majorana mass of about m_{D} the transition between the (pseudo-)Dirac and the seesaw regime takes place (dashed line).

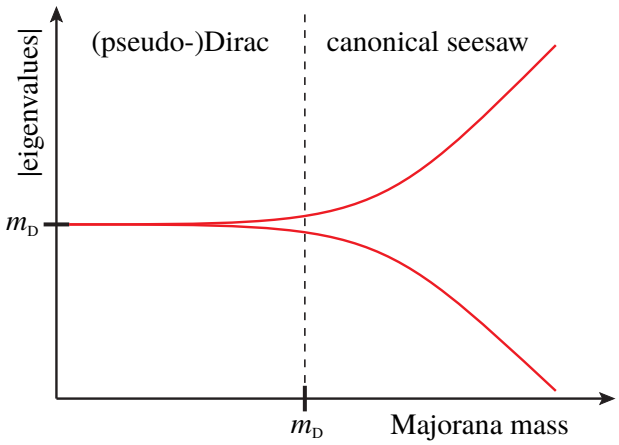

Chapter 6

Conclusion

With the final confirmation of the Standard Model (SM) of particle physics by the discovery of the Higgs boson, but without new physics at the Large Hadron Collider (LHC), the gauge hierarchy problem appears to be unavoidable within electroweak symmetry breaking. Interpreting the appearance of quadratic corrections due to quantum effects as a technical flaw, we have followed the argument of Bardeen, according to which the anomalous symmetry breaking in theories with a scale-invariant Lagrangian can only lead to logarithmic divergences. Theories with this quality (in slight abuse of terminology) have been referred to as conformal theories. It has been argued that spontaneous symmetry breaking in conformal theories by higher-order corrections represents a viable alternative to standard electroweak symmetry breaking. In order to also accommodate small neutrino masses, we have studied the conformal inverse seesaw (CISS) mechanism in two implementations. Furthermore we have analyzed the neutrino mass matrix in the context of a generalized type-I seesaw.

The CISS has been presented in Chapter 3. In the model the scalar and the neutrino sectors of the SM are expanded. Also, the gauge group of the SM is extended by a hidden Abelian gauge group. It has been emphasized that by virtue of the conformal symmetry all fermion mass terms must be induced by Yukawa interactions. Hence, the pattern in the neutrino mass matrix that is required for the inverse seesaw is generated by the adjustment of the particle spectra in the scalar and in the neutrino sectors of the CISS.

We have shown how sub-eV masses for the SM neutrinos in agreement with oscillation data can be obtained from the neutrino mass matrix. The diagonalization of the mass matrix also brings about heavy neutrinos with pseudo-Dirac masses typically of the order of a few TeV. It has been noted that smaller pseudo-Dirac masses, however, are also allowed. Furthermore, we have remarked that the mixing between the active and the sterile neutrinos in the CISS can naturally be of the order of up to 1% as the model is not subject to a large scale separation. Accordingly, processes involving the active-sterile mixing can proceed unsuppressed. The neutrino spectrum in the CISS also contains a long-lived warm dark matter (DM) candidate with masses from about 1 keV to 10 keV and tiny mixing to the active neutrinos of the order of 10^{-10} to 10^{-12}. It has been discussed how the

DM particle can be produced in the early universe via a non-thermal freeze-in mechanism. There, we have provided a computation of the relic abundance expected in the CISS, which for the mass range and mixing angles given above is in agreement with measurements of the large-scale structure and of the spectrum of the cosmic microwave background radiation. We have mentioned that the DM in the CISS can explain the mono-energetic X-ray line at about 3.5 keV reported in [179]. It is remarkable that in the CISS there are in total two DM neutrinos, whose mass splitting lies in the sub-keV range. As it has been pointed out, the mass splitting manifests itself in form of a slightly asymmetric double X-ray line, which, if observed, would constitute a strong hint at the CISS.

In the context of spontaneous conformal symmetry breaking, we have discussed how a particular hierarchy among the scalar vacuum expectation values (vevs) that induces the desired hierarchy among the masses in the neutrino sector can be obtained naturally. The scale of spontaneous conformal symmetry breaking in the CISS is of the order of a TeV. The scalar spectrum in the broken phase contains the Higgs, the pseudo-Goldstone boson (PGB) of broken scale invariance and an additional massive scalar. The PGB mass dominantly depends on the masses of the heaviest particles in the model. The analysis of the parameter space has shown that consistent spontaneous conformal symmetry breaking is obtained for PGB masses of the order of hundreds of GeV, while the masses of the additional scalar, the heavy neutrinos and the gauge boson associated with the hidden gauge group are all at the symmetry breaking scale. In this context consistent means that the PGB mass-squared is positive, the scalar couplings are perturbative, and that the numerical values of the electroweak vev and the Higgs mass fall within the experimental uncertainties. Also, the mixing of the Higgs with other scalar fields is in agreement with current experimental limits. We have mentioned that, in the future, it would be important to assure that the renormalization group evolution of the theory remains stable up to the Planck scale in a study as it was performed in [69]. As we have pointed out, the model of the CISS in principle possesses sufficient leeway in the couplings to make the evolution work. The question is how natural the required values for the couplings turn out to be.

After the discussion of the neutrino and scalar spectrum in the CISS, an analysis of the phenomenology of the model has been carried out. There, it has been shown that the viable parameter space of the CISS passes all electroweak precision test. In particular, we have seen that the future limits of the branching ratio from the lepton flavor violating decay $\mu \to e\gamma$ has the potential to exclude the heaviest sterile neutrino masses of a few TeV. Furthermore, two collider signatures have been identified, namely the ones in the opposite-sign di-lepton and the (also lepton number conserving) tri-lepton channel, which can give rise to signals above SM backgrounds. We have estimated that the excess of about 130 events in the opposite-sign di-lepton plus jets channel observed by the CMS collaboration [188] can be explained in the CISS within the experimental uncertainties by the decays of a PGB with a mass of 500 GeV. We have also computed that the number of expected events in the aforementioned channel for the future luminosity of

300 fb^{-1} amounts to more than a thousand, which should leave a clear signal in the detectors at the LHC.

In Chapter 4 we have studied the extended conformal inverse seesaw (ECISS), which supplements the CISS with large lepton number violation (LNV). In the ECISS the scalar and the neutrino sectors of the CISS are altered in order to allow for a large Majorana mass term for the right-handed neutrinos, which can induce an equally large LNV. Another important difference between the models lies in the hidden Abelian gauge group which, in the ECISS, is identified with U(1)$_{B-L}$. It has been confirmed that the presence of the heavy Majorana mass leaves both electroweak and DM phenomenology of the CISS invariant.

We have analyzed the new LNV phenomenology in the ECISS. It has been shown that the contribution of the heavy sterile neutrinos to the effective Majorana mass of neutrinoless double beta decay ($0\nu\beta\beta$) can saturate current experimental limits on the half-life for masses of the order of 10 GeV and active-sterile mixings of about 1%. We have noted that if future $0\nu\beta\beta$ experiments discover the decay, such a signal can be accounted for by the ECISS. In particular, a signal in a parameter region, which is inaccessible to $0\nu\beta\beta$ mediated by three light Majorana neutrinos (i.e. by the mass mechanism), would represent a point in favor of the model. We have discussed the LNV decays of the sterile neutrinos and the Z' boson associated with U(1)$_{B-L}$. In the same-sign di-lepton plus two jets channel the ECISS predicts a signal of about 390 events at the LHC for a luminosity of 300 fb^{-1} at a center-of-mass energy of 14 TeV from sterile neutrino decays with a mass of 500 GeV. This makes the model testable by future LHC data. We have also discussed that the viable Z' mass region, which lies typically slightly above the order of the spontaneous conformal symmetry breaking scale at a few TeV, is going to be tested by the LHC in the near future. Finally, we have pointed out the possibility to probe conformal theories with a gauged U(1)$_{B-L}$ by gravitational waves. It has been laid out that gravitational waves with amplitudes large enough to be detected by future interferometer experiments can be created in the bubble nucleation by a first-order phase transition of the ground state.

Lastly, in Chapter 5 we have given a systematic analysis of the neutrino mass matrix in a generalized set-up of the type-I seesaw mechanism. The generic neutrino sector that has been considered consists of two different neutrino species with arbitrary numbers of generations, which are connected by a Dirac mass term. One of the species is assumed to have an arbitrary Majorana mass term, which signifies that the Majorana mass term could be much smaller or much larger than the Dirac mass term, it could be singular, or vanish completely. In this set-up we have studied the different available scenarios for the neutrino mass matrix.

We have predicted the number of exactly vanishing eigenvalues of the mass matrix for all scenarios. In the discussion of the eigenvalue spectra obtained in the different scenarios, it has been shown that many of the scenarios can be related to others, thereby simplifying the analysis. We have derived the eigenvalue spectrum of the mass matrix for all scenarios with a non-singular Majorana mass term and also for one singular scenario. The results demonstrate that the mass matrix tends to form eigenvalue pairs with mass scales characteristic for the

corresponding scenario. We have remarked that this observation confirms the intuitive presumption that the symmetry of the neutrino mass matrix should be reflected in the eigenvalues.

In a future study, it will be important to systematically analyze the unitary transformation matrix that diagonalizes the mass matrix. In particular, if the active neutrinos are involved (which will be the usual case), the transformation matrix needs to be consistent with oscillation data. A more profound understanding of the connection between a certain structure of the mass matrix and the transformation matrix could be used to tailor matrix structures that yield a desired neutrino mixing pattern. In the next stage of the systematic discussion, it will be interesting to expand the investigated set-up to include a third neutrino species. In this extended set-up, double seesaw structures can be realized, which many seesaw variants are based on as, for instance, the inverse seesaw. The double seesaw structure, however, would contain substantially more degrees of freedom and the systematic analysis of all possible scenarios might turn out to be difficult.

Finally, we propose a new direction for the study of conformal theories as we will briefly elaborate. As we have seen in the course of this thesis, the symmetry breaking scale in conformal theories, which brings forth consistent electroweak symmetry breaking, is naturally of the order of a few TeV. Accordingly, the new physics associated with the spontaneous symmetry breaking also is located at that scale. Now, suppose that in Run 2 at the LHC no signs of physics beyond the SM would be found. Then, the hypothesis of the SM being a generic conformal theory would be difficult to maintain. In answer to this matter, we propose to study how a larger separation between the conformal symmetry breaking scale and the electroweak scale can consistently be attained. In the discussion of the CISS we have shown how a relatively mild hierarchy among the vevs of the different scalars is obtained. So one ansatz to separate the scale of conformal symmetry breaking from the electroweak scale could be to study whether it is possible to magnify this hierarchy among the vevs. We hope that this new direction may deepen our understanding of the mechanisms of spontaneous electroweak symmetry breaking.

This page is intentionally left blank

Appendices

This page is intentionally left blank

Appendix A

Neutrino mass matrix diagonalization

In this part of the appendix we will derive the neutrino masses and mixing matrix for the neutral lepton mass matrix in the conformal inverse seesaw (CISS) discussed in Chapter 3 and its extensions (ECISS) discussed in Chapter 4.

We define the Majorana basis as $n_{\rm L} = (\nu_{\rm L},\, \nu^{\rm c}_{\rm R},\, N_{\rm L},\, N^{\rm c}_{\rm R})^{\intercal}$. After electroweak symmetry breaking, the mass Lagrangian in the Majorana basis is given by

$$\mathcal{L}^{\nu}_{\rm mass} = -\tfrac{1}{2}\,\overline{n^{\rm c}_{\rm L}}\,\mathcal{M}\,n_{\rm L} + \text{h.c.}\ , \tag{A.1}$$

where the mass matrix in the ECISS reads

$$\mathcal{M} = \begin{pmatrix} 0 & m_{\rm D} & 0 & 0 \\ m_{\rm D} & M_{\rm R} & M_1 & M_2 \\ 0 & M_1 & \mu_1 & 0 \\ 0 & M_2 & 0 & \mu_2 \end{pmatrix} . \tag{A.2}$$

The mass matrix in the CISS is obtained from the above equation by taking the limit $M_{\rm R} \to 0$. In writing Eq. (A.2) we have considered the one-flavor case for simplicity. Note that in both the CISS and the ECISS an approximate exchange symmetry in the $N_{\rm L}$-$N^{\rm c}_{\rm R}$ sector is assumed, which leads to $M_1 \approx M_2$ and $\mu_1 \approx \mu_2$. Accordingly, there are four different mass scales present in Eq. (A.2), which are assumed to obey the hierarchy $M_{\rm R} > M_i > m_{\rm D} > \mu_i$.

A good strategy for finding the diagonal form of the mass matrix is to split up the transformation into a block-diagonalization denoted by $\mathcal{V}$, and a transformation $\mathcal{W}$ that diagonalizes the individual blocks obtained from the transformation with $\mathcal{V}$. The diagonal mass matrix can then be found by the transformation with the unitary mixing matrix $U \equiv \mathcal{V}\cdot\mathcal{W}$ as

$$\mathcal{M}^{\rm diag} = U^{\intercal}\mathcal{M}U = (\mathcal{V}\cdot\mathcal{W})^{\intercal}\,\mathcal{M}\,(\mathcal{V}\cdot\mathcal{W}) \tag{A.3}$$

and, accordingly, the mass basis is defined by

$$\tilde{n}_{\rm L} = U^{\dagger} n_{\rm L}\,. \tag{A.4}$$

As we will see in the following the results derived here are valid for vanishing M_{R} as well as for $M_{\mathrm{R}} \neq 0$ so they equally apply to the CISS as well as to the ECISS.

The block-diagonalization $\mathcal{V}$ consists of three transformations, which will be discussed in the following. As first transformation we perform a rotation in the N_{L}-$N_{\mathrm{R}}^{\mathrm{c}}$-plane with $\tan\theta = \frac{M_1}{M_2}$ in order to eliminate the M_1 entries in the mass matrix. This transformation leaves the ν_{L}-$\nu_{\mathrm{R}}^{\mathrm{c}}$-plane invariant, but mixes N_{L} and $N_{\mathrm{R}}^{\mathrm{c}}$ according to

$$\begin{pmatrix} N_{1\mathrm{L}} \\ N_{2\mathrm{L}} \end{pmatrix} \equiv \begin{pmatrix} \cos\theta & \sin\theta \\ -\sin\theta & \cos\theta \end{pmatrix} \begin{pmatrix} N_{\mathrm{L}} \\ N_{\mathrm{R}}^{\mathrm{c}} \end{pmatrix} . \tag{A.5}$$

After applying the above transformation, we obtain the following structure for the mass matrix

$$\mathcal{M}^{(1)} = \begin{pmatrix} 0 & m_{\mathrm{D}} & 0 & 0 \\ m_{\mathrm{D}} & M_{\mathrm{R}} & 0 & M \\ 0 & 0 & \mu_a & \delta\mu \\ 0 & M & \delta\mu & \mu_s \end{pmatrix} , \tag{A.6}$$

where we have defined the abbreviations

$$\begin{aligned} M &= \sqrt{M_1^2 + M_2^2} \,, & \delta\mu &= \tfrac{M_1 M_2 (\mu_1 - \mu_2)}{M_1^2 + M_2^2} \,, \\ \mu_a &= \tfrac{M_2^2 \mu_1 + M_1^2 \mu_2}{M_1^2 + M_2^2} \,, & \mu_s &= \tfrac{M_1^2 \mu_1 + M_2^2 \mu_2}{M_1^2 + M_2^2} \,. \end{aligned} \tag{A.7}$$

In the second transformation step we simply reorder the Majorana basis according to

$$n_{\mathrm{L}}' = \begin{pmatrix} \nu_{\mathrm{L}} \\ N_{1\mathrm{L}} \\ N_{2\mathrm{L}} \\ \nu_{\mathrm{R}}^{\mathrm{c}} \end{pmatrix} = \begin{pmatrix} 1 & 0 & 0 & 0 \\ 0 & 0 & 1 & 0 \\ 0 & 0 & 0 & 1 \\ 0 & 1 & 0 & 0 \end{pmatrix} \begin{pmatrix} \nu_{\mathrm{L}} \\ \nu_{\mathrm{R}}^{\mathrm{c}} \\ N_{1\mathrm{L}} \\ N_{2\mathrm{L}} \end{pmatrix} . \tag{A.8}$$

After changing to the basis n_{L}', the mass matrix reads

$$\mathcal{M}^{(2)} = \begin{pmatrix} 0 & 0 & 0 & m_{\mathrm{D}} \\ 0 & \mu_a & \delta\mu & 0 \\ 0 & \delta\mu & \mu_s & M \\ m_{\mathrm{D}} & 0 & M & M_{\mathrm{R}} \end{pmatrix} . \tag{A.9}$$

As third step we want to apply the seesaw mechanism. To this end, let us divide the matrix in the above equation into four 2×2 block matrices following

$$\begin{aligned} \mathcal{M}_{\mathrm{L}} &= \begin{pmatrix} 0 & 0 \\ 0 & \mu_a \end{pmatrix} , & \mathcal{M}_{\mathrm{D}} &= \begin{pmatrix} 0 & \delta\mu \\ m_{\mathrm{D}} & 0 \end{pmatrix} , \\ \mathcal{M}_{\mathrm{R}} &= \begin{pmatrix} \mu_s & M \\ M & M_{\mathrm{R}} \end{pmatrix} , & \mathcal{M}_{\mathrm{R}}^{-1} &= \tfrac{1}{\det(\mathcal{M}_{\mathrm{R}})} \begin{pmatrix} M_{\mathrm{R}} & -M \\ -M & \mu_s \end{pmatrix} . \end{aligned} \tag{A.10}$$

Note that $\mathcal{M}_{\mathrm{R}}^{-1}$ exists even in the limit $M_{\mathrm{R}} \to 0$. In order to apply the seesaw mechanism with $\mathcal{M}_{\mathrm{R}}$ as the heavy scale we need to require that the eigenvalues of $\mathcal{M}_{\mathrm{R}}$ are larger than those of $\mathcal{M}_{\mathrm{D}}$. The exact eigenvalues of $\mathcal{M}_{\mathrm{R}}$ can be found by means of Eq. (B.8) as

$$M_{\pm} = \frac{1}{2}\left(\mu_s + M_{\mathrm{R}} \pm \sqrt{(\mu_s - M_{\mathrm{R}})^2 + 4M^2}\right) . \tag{A.11}$$

The eigenvalues of $\mathcal{M}_{\mathrm{D}}$ are similarly found to be $\pm(\delta\mu\, m_{\mathrm{D}})^{1/2}$. Remember that we assumed an approximate symmetry in the N_{L}-$N_{\mathrm{R}}^{\mathrm{c}}$ sector [see the discussion after Eq. (A.2)]. If we take this symmetry into account, we can approximate for the abbreviations defined in Eq. (A.7)

$$\begin{aligned} M &\approx \sqrt{2}M_1 \approx \sqrt{2}M_2\,, & \delta\mu &\approx \tfrac{1}{2}(\mu_1 - \mu_2) \equiv \mu_-\,, \\ \mu_a &=\approx \tfrac{1}{2}(\mu_1 + \mu_2) \equiv \mu_+\,, & \mu_s &\approx \tfrac{1}{2}(\mu_1 + \mu_2) = \mu_+\,. \end{aligned} \tag{A.12}$$

The parameter μ_- can be used to quantify the amount of violation of the exchange symmetry, which is expected to be small. Hence, it is safe to assume that $|M_{\pm}| \gg (\delta\mu\, m_{\mathrm{D}})^{1/2}$ and that we can apply the seesaw mechanism.[1] By means of the block matrices in Eq. (A.10) the seesaw transformation can be found to arbitrary order as shown in [90]. To leading order the transformation is given by

$$S_1 = \begin{pmatrix} \mathbb{1} & B_1 \\ -B_1^{\dagger} & \mathbb{1} \end{pmatrix} \quad \text{with} \quad B_1 = \frac{1}{M^2 - \mu_s M_{\mathrm{R}}} \begin{pmatrix} m_{\mathrm{D}} M & -\mu_s m_{\mathrm{D}} \\ -\delta\mu\, M_{\mathrm{R}} & \delta\mu\, M \end{pmatrix} , \tag{A.13}$$

where the identity matrices are 2×2 matrices. After applying the seesaw to $\mathcal{M}^{(2)}$ given in Eq. (A.9) we obtain

$$\mathcal{M}^{(3)} = \begin{pmatrix} \mathcal{M}_{\text{light}} & 0 \\ 0 & \mathcal{M}_{\text{heavy}} \end{pmatrix} , \tag{A.14}$$

where all entries of $\mathcal{M}^{(3)}$ are 2×2 matrices and the non-vanishing blocks to leading order are given by [90]

$$\begin{aligned} \mathcal{M}_{\text{light}} &= \mathcal{M}_{\mathrm{L}} - \mathcal{M}_{\mathrm{D}}^{\intercal}\, \mathcal{M}_{\mathrm{R}}^{-1} \mathcal{M}_{\mathrm{D}} \\ &= \begin{pmatrix} 0 & 0 \\ 0 & \mu_a \end{pmatrix} + \frac{1}{M^2 - \mu_s M_{\mathrm{R}}} \begin{pmatrix} m_{\mathrm{D}}^2 \mu_s & -\delta\mu\, m_{\mathrm{D}}\, M \\ -\delta\mu\, m_{\mathrm{D}}\, M & \delta\mu^2 M_{\mathrm{R}} \end{pmatrix} , \end{aligned} \tag{A.15}$$

$$\mathcal{M}_{\text{heavy}} = \mathcal{M}_{\mathrm{R}}\,. \tag{A.16}$$

Note that we already have derived the eigenvalues of $\mathcal{M}_{\text{heavy}}$ to leading order in Eq. (A.11). Under the assumption that $M^2 > \mu_s M_{\mathrm{R}}$ the eigenvalues of $\mathcal{M}_{\text{light}}$

[1] For the mass scales considered in Chapters 3 and 4 the relation $|M_{\pm}| \gg (\delta\mu\, m_{\mathrm{D}})^{1/2}$ translates into $M \gg 0.1$ eV, which is easily satisfied by M.

can be expanded in powers of M^{-2}.[2] Using Eq. (B.8) the result of the expansion reads

$$m_- = \mu_+ \frac{m_\mathrm{D}^2}{M^2}\left(1 - \frac{\mu_-^2}{\mu_+^2}\right) + \mathcal{O}\left(M^{-3}\right) \approx \mu_+ \frac{m_\mathrm{D}^2}{M^2}\,, \tag{A.17}$$

$$m_+ = \mu_+ \left(1 + \frac{\mu_-^2}{\mu_+^2}\frac{m_\mathrm{D}^2 + \mu_+ M_\mathrm{R}}{M^2}\right) + \mathcal{O}\left(M^{-3}\right) \approx \mu_+\,. \tag{A.18}$$

From the above equations we see that the approximated eigenvalues of $\mathcal{M}_\mathrm{light}$ do not depend on M_R.

The mass matrix in the form of Eq. (A.14) is now block-diagonal. The transformations that have led to the block-diagonal form constitute the unitary matrix $\mathcal{V}$, which has been introduced in Eq. (A.3). The individual blocks $\mathcal{M}_\mathrm{light}$ and $\mathcal{M}_\mathrm{heavy}$ can further be diagonalized by the unitary 2×2 matrices $\mathcal{W}_\mathrm{light}$ and $\mathcal{W}_\mathrm{heavy}$. Both transformations can be summarized in a single diagonalization matrix according to

$$\mathcal{W} = \begin{pmatrix} \mathcal{W}_\mathrm{light} & 0 \\ 0 & \mathcal{W}_\mathrm{heavy} \end{pmatrix}. \tag{A.19}$$

With the block-diagonalization matrix $\mathcal{V}$ and the individual diagonalizations collected in $\mathcal{W}$ the mixing matrix is determined as $U = \mathcal{V}\cdot\mathcal{W}$. We will refrain from writing down the exact expression for U since it is rather complicated. Instead, we give an estimate for the order of magnitude of the mixing matrix's elements. With the abbreviations

$$\Theta = \frac{m_\mathrm{D}}{M}\,, \qquad \tilde{\Theta} = \Theta\,\frac{\mu_+}{\mu_-} \qquad \text{and} \qquad \eta_\pm = \frac{\mu_\pm}{M} \tag{A.20}$$

the order of magnitude of $U^\dagger$ to leading order is given by

$$U^\dagger \sim \mathcal{O}\begin{pmatrix} 1 & \Theta\eta_+ & \Theta & \Theta \\ \tilde{\Theta} & \eta_- & \frac{1}{\sqrt{2}} & \frac{1}{\sqrt{2}} \\ \Theta & \frac{1}{\sqrt{2}} & \frac{1}{\sqrt{2}} & \frac{1}{\sqrt{2}} \\ \Theta & \frac{1}{\sqrt{2}} & \frac{1}{\sqrt{2}} & \frac{1}{\sqrt{2}} \end{pmatrix}. \tag{A.21}$$

Note that in the above equation we have used $U^\dagger$ (and not U) so the columns correspond to flavors and the rows to mass eigenstates.

Let us summarize the findings in this appendix. We have started with a mass matrix in the form of Eq. (A.2). We derived its block-diagonal form in Eq. (A.14) with the light and heavy mass matrices as defined in Eqs. (A.15) and (A.16). Furthermore, we have found the eigenvalues of the light and heavy mass matrices to leading order in Eqs. (A.17) and (A.18), and in Eq. (A.11), respectively. And we just have given an estimate of the order of magnitude for the mixing matrix in Eq. (A.21). All of the mentioned equations hold for $M_\mathrm{R} \neq 0$ as well as in the

[2] Note that in the limit $M_\mathrm{R} \to 0$ the largest scale is M so the expansion in powers of M^{-2} can be performed trivially in the CISS.

limit $M_{\mathrm{R}} \to 0$. For reference we reprint the eigenvalue spectrum of the neutrino mass matrix, which is given by

$$m_- = \mu_+ \frac{m_{\mathrm{D}}^2}{M^2} \left(1 - \frac{\mu_-^2}{\mu_+^2}\right) + \mathcal{O}\left(M^{-3}\right) \approx \mu_+ \frac{m_{\mathrm{D}}^2}{M^2}\,, \tag{A.22}$$

$$m_+ = \mu_+ \left(1 + \frac{\mu_-^2}{\mu_+^2} \frac{m_{\mathrm{D}}^2 + \mu_+ M_{\mathrm{R}}}{M^2}\right) + \mathcal{O}\left(M^{-3}\right) \approx \mu_+\,. \tag{A.23}$$

$$M_\pm = \frac{1}{2}\left(\mu_+ + M_{\mathrm{R}} \pm \sqrt{\left(\mu_+ - M_{\mathrm{R}}\right)^2 + 4M^2}\right)\,, \tag{A.24}$$

where in the last equation we have inserted $\mu_s \approx \mu_+$ [see Eq. (A.12)].

Appendix B

Matrix calculus

In this part of the appendix we will discuss general and specific properties of matrices used in this work. In Section B.1 we will revive basic concepts of matrix calculus, which will represent a nice catalogue of convenient formulas. In Section B.2 we will perform the calculations in connection with the formal study of the neutrino mass matrix presented in Chapter 5.

B.1 Basics

The basics of matrix calculus introduced in this section can be found in any textbook on linear algebra, see for instance [235].

B.1.1 The rank of a matrix

Consider the matrices A, B and C with dimensions $m \times n$, $n \times k$ and $k \times \ell$, respectively. Then the following inequalities hold

$$\mathrm{rk}(A) \leq \min(m\,,n)\,, \tag{B.1}$$

$$\mathrm{rk}(AB) \leq \min\Big(\mathrm{rk}(A)\,,\mathrm{rk}(B)\Big)\,, \tag{B.2}$$

$$\mathrm{rk}(AB) + \mathrm{rk}(BC) \leq \mathrm{rk}(B) + \mathrm{rk}(ABC)\,. \tag{B.3}$$

From Eq. (B.1) we see that

$$A \text{ has maximal rank} \quad \Leftrightarrow \quad \mathrm{rk}(A) = \min(m\,,n)\,. \tag{B.4}$$

We take Eq. (B.4) as the definition of the matrix property *maximal rank*. In the discussion that follows we will assume that a matrix in principle has maximal rank if there is no particular condition that reduces its rank.

B.1.2 Square matrices

For a square matrix M with dimension m the three following properties are equivalent:

$$\begin{array}{lllll} \text{i)} & M \text{ is invertible} & \Leftrightarrow & \exists M^{-1}\,, \\ \text{ii)} & M \text{ has maximal rank} & \Leftrightarrow & \mathrm{rk}(M) = m\,, \\ \text{iii)} & M \text{ is non-singular} & \Leftrightarrow & \det(M) \neq 0\,. \end{array} \tag{B.5}$$

A general complex-valued square matrix M can always be diagonalized by a bi-unitary transformation according to

$$V^\dagger\, M\, U = M^{\mathrm{diag}} = \mathrm{diag}(\lambda_1,\, \ldots,\, \lambda_m)\,, \tag{B.6}$$

where λ_i denote the eigenvalues of M. Note that U and V can always be chosen in a way that all λ_i are real non-negative numbers. Similar to the general case a symmetric matrix $M = M^\intercal$ is diagonalized by means of an orthogonal transformation

$$R^\intercal M R = M^{\mathrm{diag}} \tag{B.7}$$

with M^{diag} as before in Eq. (B.6). In the simple case that M denotes a symmetric 2×2 matrix a direct computation shows that the eigenvalues $\lambda_\pm$ of M can in general be expressed through the matrix's invariants according to

$$\lambda_\pm = \tfrac{1}{2}\left(\mathrm{tr}(M) \pm \sqrt{\mathrm{tr}(M)^2 - 4\det(M)}\right)\,. \tag{B.8}$$

B.1.3 Block matrices

Consider arbitrary matrices A, B, C and D with dimensions $m \times k$, $m \times \ell$, $n \times k$ and $n \times \ell$, respectively. Then we define that a block-matrix M with dimension $(m+n) \times (k+\ell)$ has the form

$$M = \begin{pmatrix} A & B \\ C & D \end{pmatrix}\,. \tag{B.9}$$

Now let M be an $(m+n) \times (m+n)$-dimensional block-matrix. Then A and D are square matrices. If A is invertible, one can show that the determinant of M can be expressed as

$$\det(M) = \det(A)\det\left(D - CA^{-1}B\right)\,. \tag{B.10}$$

Equally, if D is invertible, we have

$$\det(M) = \det(D)\det\left(A - BD^{-1}C\right)\,. \tag{B.11}$$

When defining a general $(m+n) \times (k+\ell)$ block-matrix M as in Eq. (B.9) we imply that it possesses the alternative representation

$$M = \begin{pmatrix} M_{m\times k} & M_{m\times \ell} \\ M_{n\times k} & M_{n\times \ell} \end{pmatrix} \tag{B.12}$$

or for symmetric M with $m = k$ and $n = \ell$

$$M = \begin{pmatrix} M_{m\times m} & (M_{\ell\times m})^\intercal \\ M_{\ell\times m} & M_{\ell\times\ell} \end{pmatrix} , \tag{B.13}$$

where in both equations the labels specify the dimensions of the matrices.

B.1.4 Kernel

Consider a general $m \times n$ matrix M with $m \leq n$.[1] Then the kernel of M, which is denoted by $\ker(M)$, is defined as the vector space spanned by all n-dimensional vectors $\boldsymbol{v}$ satisfying

$$M\boldsymbol{v} \stackrel{!}{=} \mathbf{0} . \tag{B.14}$$

The rank of M and the dimension of the kernel are related via the number n of columns of M according to

$$n = \mathrm{rk}(M) + \dim(\ker(M)) . \tag{B.15}$$

With Eq. (B.1) it follows that every rectangular matrix with $m < n$ possesses a non-trivial kernel, i.e. $\ker(M) \neq \emptyset$. If M is a square matrix, the condition in Eq. (B.14) is equivalent to the condition for an eigenvector with vanishing eigenvalue. This means that for $m = n$

$$\#(\text{vanishing eigenvalues of } M) = \dim(\ker(M)) . \tag{B.16}$$

B.1.5 Kernel projections

Now we will develop a transformation technique to project out the true rank of a matrix. By the expression 'to project out' we mean a transformation that brings a matrix into a form in which the number of non-zero columns is equal to the rank of the matrix. Let us abbreviate $r \equiv \mathrm{rk}(M)$ and $p \equiv \dim(\ker(M)) = n - r$, where we used Eq. (B.15). We assume that the kernel of M is given by

$$\ker(M) = \left\{ \boldsymbol{v}_1^{\mathrm{k}}, \ldots, \boldsymbol{v}_p^{\mathrm{k}} \right\} \neq \emptyset , \tag{B.17}$$

where $\boldsymbol{v}_i^{\mathrm{k}}$ denotes an n-dimensional unit vector satisfying Eq. (B.14) and we specifically demand $p > 0$, i.e. that the kernel contains at least one vector. Furthermore, we assume $r > 0$, which is equivalent to $M \neq 0$. If we regard all vectors of the kernel as columns and use them to form the matrix

$$U^{\mathrm{k}}_{n\times p} = \left(\boldsymbol{v}_1^{\mathrm{k}} \ \ldots \ \boldsymbol{v}_p^{\mathrm{k}} \right) , \tag{B.18}$$

it follows from Eq. (B.14) that

$$M\, U^{\mathrm{k}}_{n\times p} = 0_{m\times p} , \tag{B.19}$$

[1] If $m > n$, simply exchange M by $M^\intercal$ and m by n in the following discussion.

where $0_{m\times p}$ denotes an $m \times p$ matrix with all elements equal to zero. With the help of $U^{\mathrm{k}}_{n\times p}$ we can define an $n \times n$ unitary matrix

$$U_{\mathrm{ker}} \equiv \begin{pmatrix} U_{n\times r} & U^{\mathrm{k}}_{n\times p} \end{pmatrix} , \tag{B.20}$$

where the matrix $U_{n\times r}$ is built from the $r = n - p$ unit vectors of dimension n orthogonal to $\ker(M)$. The particular form of $U^{\mathrm{k}}_{n\times p}$ and $U_{n\times r}$ is not relevant for our discussion. When we now multiply M by U_{ker} from the right we are led to

$$M' \equiv M\, U_{\mathrm{ker}} = \begin{pmatrix} M\, U_{n\times r} & M\, U^{\mathrm{k}}_{n\times p} \end{pmatrix} = \begin{pmatrix} M'_{m\times r} & 0_{m\times p} \end{pmatrix} . \tag{B.21}$$

Notice that if M is a symmetric square matrix, it follows from Eq. (B.19) that $(U^{\mathrm{ker}}_{n\times p})^{\intercal} M = 0_{p\times m}$. Then, it is easy to derive that

$$U^{\intercal}_{\mathrm{ker}}\, M\, U_{\mathrm{ker}} = \begin{pmatrix} M'_{r\times r} & 0 \\ 0 & 0 \end{pmatrix} = \begin{pmatrix} (U_{n\times r})^{\intercal}\, M\, U_{n\times r} & 0 \\ 0 & 0 \end{pmatrix} \tag{B.22}$$

for symmetric M.

B.1.6 Canonical matrix structures

Consider the symmetric block-matrix

$$M = \begin{pmatrix} A & C^{\intercal} \\ C & B \end{pmatrix} , \tag{B.23}$$

where A and B are symmetric matrices with dimension a and b, respectively. Accordingly, C has dimension $b\times a$. The matrix M has the form of a neutrino mass matrix in the Majorana basis encountered in a generic theory with two neutrino sectors (cf. Chapter 5). In such a theory M is always sandwiched between the neutrino state vector $n_{\mathrm{L}} = \left(\nu^{A}_{\mathrm{L}},\, \nu^{B,\,\mathrm{c}}_{\mathrm{R}}\right)^{\intercal}$ and the vector's charge-conjugate. Since the neutrino fields ν^{A}_{L}, ν^{B}_{R} are – from an analytical point of view – arbitrary, we can absorb a unitary transformation of the form

$$U^{\dagger} n_{\mathrm{L}} = \begin{pmatrix} U^{\dagger}_{A} & 0 \\ 0 & U^{\dagger}_{B} \end{pmatrix} \begin{pmatrix} \nu^{A}_{\mathrm{L}} \\ \nu^{B,\,\mathrm{c}}_{\mathrm{R}} \end{pmatrix} \equiv \begin{pmatrix} \tilde{\nu}^{A}_{\mathrm{L}} \\ \tilde{\nu}^{B,\,\mathrm{c}}_{\mathrm{R}} \end{pmatrix} = \tilde{n}_{\mathrm{L}} \tag{B.24}$$

into the field definitions *without mixing the sectors*. We can exploit these degrees of freedom to bring M into a simpler form. Note, however, that if the ν^{A}_{L} are identified with the neutrinos in the Standard Model, the matrix U_A will enter the charged-current interactions (cf. Section 2.1.3). In the following we will develop two useful canonical forms of M. The first has a simpler diagonal structure and the second a simpler off-diagonal structure. In practise we can assume that M is already in one of the simpler canonical forms without loss of generality.

For the first structure let R_A and R_B denote orthogonal matrices that diagonalize A and B, respectively [see Eq. (B.7)]. Then we can define the orthogonal transformation matrix

$$U_{(\mathrm{i})} = \begin{pmatrix} R_A & 0 \\ 0 & R_B \end{pmatrix} . \tag{B.25}$$

Note that the elements of these transformations are typically of $\mathcal{O}(1)$. In the spirit of Eq. (B.24) we now define the first canonical matrix structure as

$$M_{(\mathrm{i})}^{\mathrm{canonical}} = U_{(\mathrm{i})}^{\intercal} M U_{(\mathrm{i})} = \begin{pmatrix} A' & C'^{\intercal} \\ C' & B' \end{pmatrix} = \begin{pmatrix} A^{\mathrm{diag}} & (R_B^{\intercal} C R_A)^{\intercal} \\ R_B^{\intercal} C R_A & B^{\mathrm{diag}} \end{pmatrix} , \tag{B.26}$$

which, obviously, has a simpler diagonal structure than the original matrix.

Now we turn our attention to the second structure. The derivation here is a little more involved, but no problem with our preparations in Section B.1.5. We go back to the matrix in Eq. (B.23). Let us assume without loss of generality that $b > a$ and put $b = a + \alpha$ with $\alpha > 0$. Then we can split up B and C according to

$$B = B^{\intercal} = \begin{pmatrix} B_{a\times a} & (B_{\alpha\times a})^{\intercal} \\ B_{\alpha\times a} & B_{\alpha\times\alpha} \end{pmatrix} , \qquad C = \begin{pmatrix} C_{a\times a} \\ C_{\alpha\times a} \end{pmatrix} , \tag{B.27}$$

where the labels denote the dimensions of the individual block matrices. With Eq. (B.27) the matrix M can be written as

$$M = \begin{pmatrix} A & (C_{a\times a})^{\intercal} & (C_{\alpha\times a})^{\intercal} \\ C_{a\times a} & B_{a\times a} & (B_{\alpha\times a})^{\intercal} \\ C_{\alpha\times a} & B_{\alpha\times a} & B_{\alpha\times\alpha} \end{pmatrix} . \tag{B.28}$$

Now we know from the discussion in Section B.1.4 that $C^{\intercal}$ has a non-trivial kernel of dimension α.[2] Therefore, we can define a unitary $b \times b$ transformation matrix U_{ker} analogously to Eq. (B.20) from the kernel of $C^{\intercal}$, which obeys

$$C^{\intercal} U_{\mathrm{ker}} \equiv C^{\intercal} \begin{pmatrix} U_{b\times a} & U_{b\times\alpha}^{\mathrm{k}} \end{pmatrix} = \begin{pmatrix} C^{\intercal} U_{b\times a} & 0_{a\times\alpha} \end{pmatrix} . \tag{B.29}$$

With U_{ker}, and with the same R_A as already used in the first structure we build the unitary matrix

$$U_{(\mathrm{ii})} = \begin{pmatrix} R_A & 0 \\ 0 & U_{\mathrm{ker}} \end{pmatrix} . \tag{B.30}$$

With the help of the above matrix we finally define the second canonical matrix structure as

$$\begin{aligned} M_{(\mathrm{ii})}^{\mathrm{canonical}} &= U_{(\mathrm{ii})}^{\intercal} M U_{(\mathrm{ii})} = \begin{pmatrix} A' & C'^{\intercal} \\ C' & B' \end{pmatrix} \\ &= \begin{pmatrix} A^{\mathrm{diag}} & \left(C'_{a\times a}\right)^{\intercal} & \left(C'_{\alpha\times a}\right)^{\intercal} \\ C'_{a\times a} & B'_{a\times a} & \left(B'_{\alpha\times a}\right)^{\intercal} \\ C'_{\alpha\times a} & B'_{\alpha\times a} & B'_{\alpha\times\alpha} \end{pmatrix} \\ &= \begin{pmatrix} A^{\mathrm{diag}} & ((U_{b\times a})^{\intercal} C R_A)^{\intercal} & 0_{a\times\alpha} \\ (U_{b\times a})^{\intercal} C R_A & (U_{b\times a})^{\intercal} B\, U_{b\times a} & \left((U_{b\times\alpha}^{\mathrm{k}})^{\intercal} B\, U_{b\times a})\right)^{\intercal} \\ 0_{\alpha\times a} & (U_{b\times\alpha}^{\mathrm{k}})^{\intercal} B\, U_{b\times a} & (U_{b\times\alpha}^{\mathrm{k}})^{\intercal} B\, U_{b\times\alpha}^{\mathrm{k}} \end{pmatrix} . \end{aligned} \tag{B.31}$$

This second structure may not look too appealing at first sight, but it takes on a very simple and useful form when $B = 0$.

[2] Remember that we assume that matrices in principle have maximal rank.

B.2 Seesaw related matrix calculus

In this section we will derive the eigenvalue spectra of the matrix structures encountered in the generalized type-I seesaw mechanism (see Chapter 5). We will use the categorization introduced in Eq. (5.4) and analyze the matrix structures as defined in Eqs. (5.5) - (5.7). The results of the analysis of the matrix structures are summarized in Tables B.1, B.2, B.3 and 5.1.

B.2.1 Exactly vanishing eigenvalues

As already pointed out in Eq. (B.16) the number of exactly vanishing eigenvalues of a square matrix is equal to the dimension of the kernel. An exactly vanishing eigenvalue in the neutrino mass matrix is especially interesting, since it corresponds to an exactly massless neutrino mass eigenstate at tree level. In an analytical context, vanishing eigenvalues can be quite cumbersome in the diagonalization procedure. Hence, it is advantageous to know the kernel of a matrix in advance and, if necessary, to project out the kernel in order to split the matrix into its singular and non-singular part. In the following we will apply the techniques introduced in Sections B.1.4 and B.1.5 to determine under which circumstances the neutrino mass matrix develops a non-trivial kernel. Let us first reprint the definitions of the three qualitatively different matrix structures introduced in Eqs. (5.5) - (5.7) for convenience. They were defined as

$$\mathcal{M}_1 = \begin{pmatrix} 0 & M_{\mathrm{D}}^{\intercal} \\ M_{\mathrm{D}} & M_{\mathrm{R}} \end{pmatrix} \in \mathbb{C}^{(a+b)\times(a+b)}\,, \tag{B.32}$$

$$\mathcal{M}_2 = \begin{pmatrix} 0 & M_{\mathrm{D}}^{\intercal} \\ M_{\mathrm{D}} & 0 \end{pmatrix} \in \mathbb{C}^{(a+b)\times(a+b)}\,, \tag{B.33}$$

$$\mathcal{M}_3 = \begin{pmatrix} 0 & M_{\mathrm{D}s}^{\intercal} & M_{\mathrm{D}t}^{\intercal} \\ M_{\mathrm{D}s} & 0 & 0 \\ M_{\mathrm{D}t} & 0 & M_{\mathrm{R}t} \end{pmatrix} \in \mathbb{C}^{(a+s+t)\times(a+s+t)}\,, \tag{B.34}$$

where M_{R} and $M_{\mathrm{R}t}$ are invertible symmetric matrices. It is important to notice that for the derivation of the kernels we do not need to fix the relation between the eigenvalues of M_{R} and M_{D}. The kernel is independent of it.

We begin by examining the kernel of the first matrix structure. Applying Eq. (B.14) yields the conditions

$$\mathcal{M}_1\, \boldsymbol{v}_{a+b} = \begin{pmatrix} 0 & M_{\mathrm{D}}^{\intercal} \\ M_D & M_{\mathrm{R}} \end{pmatrix} \begin{pmatrix} \boldsymbol{v}_a \\ \boldsymbol{v}_b \end{pmatrix} \stackrel{!}{=} \begin{pmatrix} \mathbf{0}_a \\ \mathbf{0}_b \end{pmatrix}\,, \tag{B.35}$$

where $\boldsymbol{v}_i$ denotes a generic i-dimensional vector. The above equation corresponds to the following two linear systems of equations

$$M_{\mathrm{D}}^{\intercal}\, \boldsymbol{v}_b \stackrel{!}{=} \mathbf{0}_a\,, \tag{B.36}$$

$$M_{\mathrm{D}}\, \boldsymbol{v}_a + M_{\mathrm{R}}\, \boldsymbol{v}_b \stackrel{!}{=} \mathbf{0}_b\,. \tag{B.37}$$

In our general discussion we need to distinguish the three cases (u): $a > b$ (unsaturated), (s): $a = b$ (saturated), and (o): $a < b$ (over-saturated). In the unsaturated and saturated cases Eq. (B.36) can only be satisfied trivially, i.e. by setting $\boldsymbol{v}_b \equiv \boldsymbol{0}_b$.[3] Then in the *unsaturated* case we have $a > b$ degrees of freedom of $\boldsymbol{v}_a$ to satisfy the b conditions of Eq. (B.37). This can be done non-trivially and leaves us $a - b > 0$ degrees of freedom. We find, accordingly, for the kernel in the case $a > b$ that

$$\dim\left(\ker(\mathcal{M}_1)\right) = a - b\,, \tag{B.38}$$

and for the vectors spanning the kernel

$$\boldsymbol{v}_{\text{ker}} = \begin{pmatrix} \boldsymbol{v}_a \\ \boldsymbol{0}_b \end{pmatrix}, \quad \text{with} \quad M_{\text{D}}\,\boldsymbol{v}_a \overset{!}{=} \boldsymbol{0}_b\,. \tag{B.39}$$

In the *saturated* case, where $a = b$ we can satisfy Eq. (B.37) only by putting $\boldsymbol{v}_a = \boldsymbol{0}_a$ so the kernel is empty in this case.

In the *over-saturated* case, with $a < b$, first let us try to satisfy the conditions of Eq. (B.37).[4] We need all a degrees of freedom of $\boldsymbol{v}_a$ and $b - a$ degrees of freedom of $\boldsymbol{v}_b$ to satisfy the b conditions of the equation. But then we only have a degrees of freedom of $\boldsymbol{v}_b$ left to satisfy Eq. (B.36). This leads to $\boldsymbol{v}_b \overset{!}{=} \boldsymbol{0}_b$ and subsequently to $\boldsymbol{v}_a \overset{!}{=} \boldsymbol{0}_a$ so the kernel is empty as in the saturated case.

Let us briefly summarize our findings for the matrix structure $\mathcal{M}_1$. Under the assumption that M_{R} is invertible, and that M_{D} has maximal rank we have found that for the unsaturated case, $a > b$, the dimension and span of the kernel are given by

$$\dim\left(\ker(\mathcal{M}_1)\right) = a - b\,, \tag{B.40}$$

$$\boldsymbol{v}_{\text{ker}} = \begin{pmatrix} \boldsymbol{v}_a \\ \boldsymbol{0}_b \end{pmatrix}, \quad \text{with} \quad M_{\text{D}}\,\boldsymbol{v}_a \overset{!}{=} \boldsymbol{0}_b\,, \tag{B.41}$$

respectively. For the saturated and over-saturated cases with $a \leq b$ the kernel is empty, i.e. there are no vanishing eigenvalues.

In a similar way we can find the kernels in the different cases for the structures $\mathcal{M}_2$ and $\mathcal{M}_3$, too, where in the latter we use the ansatz $\boldsymbol{v}_{\text{ker}} = (\boldsymbol{v}_a, \boldsymbol{v}_s, \boldsymbol{v}_t)^\intercal$ for a vector of the kernel. In Table B.1 we summarize all the non-trivial kernels and the conditions on their corresponding vector space. All cases not listed in this table have a trivial kernel and do not possess any vanishing eigenvalues.

B.2.2 Reducible and irreducible matrix structures

In this part we will describe our method used to find the eigenvalue spectra of the different scenarios encountered in the generalized type-I seesaw. In general

[3] Remember that we assume that M_{D} has maximal rank.

[4] Naturally, the argument is unaffected if we start satisfying the conditions of Eq. (B.36) first.

Table B.1: Non-trivial kernels for the different structures and cases in the generalized type-I seesaw. The second and third columns show the dimension and span, respectively. The last column is the defining condition for the kernel vector space. Note that in the third row for the Dirac case the relation $a < b$ exceptionally corresponds to an unsaturated scenario. Note as well that the case in the last row, $\mathcal{M}_3$ (o*), is a special version of the over-saturated case with $b > a$, in which additionally $s > a$.

structure (case)	dim(ker)	span	condition
$\mathcal{M}_1$ (u): $a > b$	$a - b$	$\boldsymbol{v}_{\text{ker}} = \begin{pmatrix} \boldsymbol{v}_a \\ \boldsymbol{0}_b \end{pmatrix}$	$M_{\text{D}}\, \boldsymbol{v}_a \stackrel{!}{=} \boldsymbol{0}_b$
$\mathcal{M}_2$ (u): $a > b$	$a - b$	$\boldsymbol{v}_{\text{ker}} = \begin{pmatrix} \boldsymbol{v}_a \\ \boldsymbol{0}_b \end{pmatrix}$	$M_{\text{D}}\, \boldsymbol{v}_a \stackrel{!}{=} \boldsymbol{0}_b$
$\mathcal{M}_2$ (u): $a < b$	$b - a$	$\boldsymbol{v}_{\text{ker}} = \begin{pmatrix} \boldsymbol{0}_a \\ \boldsymbol{v}_b \end{pmatrix}$	$M_{\text{D}}^{\intercal}\, \boldsymbol{v}_b \stackrel{!}{=} \boldsymbol{0}_a$
$\mathcal{M}_3$ (u): $a > b$	$a - b$	$\boldsymbol{v}_{\text{ker}} = \begin{pmatrix} \boldsymbol{v}_a \\ \boldsymbol{0}_s \\ \boldsymbol{0}_t \end{pmatrix} \equiv \begin{pmatrix} \boldsymbol{v}_a \\ \boldsymbol{0}_b \end{pmatrix}$	$M_{\text{D}}\, \boldsymbol{v}_a \stackrel{!}{=} \boldsymbol{0}_b$
$\mathcal{M}_3$ (o*): $a < s$	$s - a$	$\boldsymbol{v}_{\text{ker}} = \begin{pmatrix} \boldsymbol{0}_a \\ \boldsymbol{v}_s \\ \boldsymbol{0}_t \end{pmatrix}$	$M_{\text{Ds}}^{\intercal}\, \boldsymbol{v}_s \stackrel{!}{=} \boldsymbol{0}_a$

the eigenvalue spectrum of an m-dimensional square matrix M is given by the m roots λ_i with $i = 1, \ldots, m$ of the characteristic polynomial defined as

$$\chi_M(\lambda) = \det\left(\lambda \cdot \mathbb{1}_m - M\right) . \tag{B.42}$$

In the above equation $\mathbb{1}_m$ denotes the m-dimensional identity matrix. In the following we will analyze all possible matrix structures with respect to their eigenvalue spectrum. We will find that several structures can be related to other structures so they do not have to be discussed individually. In order to avoid multiple labels we will write $M_{\text{D}} \equiv C$ and $M_{\text{R}} \equiv B$ in this part. Important results, however, will be expressed in terms of M_{D} and M_{R}, again. In the following we will specify which matrix structures can be reduced to other structures. Once all structures have been categorized as either reducible or irreducible, we will discuss the expected eigenvalue spectrum for the latter class of matrices.

Reducible matrix structures

We start our discussion with the case of a general unsaturated matrix

$$M = \begin{pmatrix} 0 & C^{\intercal} \\ C & B \end{pmatrix} \tag{B.43}$$

with $a > b$ and B may be non-singular, singular or $B \equiv 0$. A brief investigation of structure in the above equation leads to the conclusion that any unsaturated case can be reduced to the corresponding saturated case. Putting $a = b + \beta$ and applying the second canonical form given in Eq. (B.31) to M directly yields

$$M = \begin{pmatrix} 0_\beta & 0 & 0 \\ 0 & 0 & (C'_{b\times b})^\intercal \\ 0 & C'_{b\times b} & B \end{pmatrix} \equiv \begin{pmatrix} 0_\beta & 0 \\ 0 & M' \end{pmatrix} , \tag{B.44}$$

where 0_β denotes a β-dimensional zero matrix. The matrix M obviously possesses $\beta = a - b$ vanishing eigenvalues and the submatrix M' is a saturated matrix, which is (non-)singular if and only if B is (non-)singular. Note that the number of vanishing eigenvalues is in perfect agreement with the non-trivial kernels of Table B.1. Furthermore, the relation of B and C for M is passed on to M', so if M realizes a Majorana scenario, so does M' (and equally for the Dirac and pseudo-Dirac cases). As anticipated we have reduced the unsaturated case to the saturated one. In Table B.2 we summarize the results for the general unsaturated reducible matrix structures.

Next, we turn our attention to the singular saturated and over-saturated Majorana cases with M given by the third matrix structure $\mathcal{M}_3$ defined in Eq. (B.34), and with $a \leq b$ and $B_t \gg C$. In this case we can apply the seesaw formula to M and obtain to leading order [90]

$$M' = \begin{pmatrix} A_a & (C_{s\times a})^\intercal & 0 \\ C_{s\times a} & 0 & 0 \\ 0 & 0 & B_t \end{pmatrix} \equiv \begin{pmatrix} M'' & 0 \\ 0 & B_t \end{pmatrix} \tag{B.45}$$

with $A_a = -(C_{t\times a})^\intercal B_t^{-1} C_{t\times a}$ and $\mathrm{rk}(A_a) = \min(a, t)$. Note that $A_a \ll C$. The matrix M' always possesses t eigenvalues with magnitude proportional to $B_t = M_{\mathrm{R}t}$. For the remaining $a + s$ eigenvalues we must distinguish two cases. If $a \leq t$, then A_a has full rank and the submatrix M'' realizes a non-singular pseudo-Dirac structure with dimensions (s, a). And if $a > t$, we have $\mathrm{rk}(A_a) = t$ so that M'' realizes a singular pseudo-Dirac structure with dimensions $(s, a-t, t)$. Hence, the spectrum of the remaining eigenvalues depends on the relation between a and t. Note that in the saturated case with $a = b$ we automatically have $a > t$ and $a > s$. Accordingly, the singular saturated Majorana case is always reduced to a singular over-saturated pseudo-Dirac substructure. In Table B.3 we list the results for the singular saturated and over-saturated Majorana reducible matrix structures.

These are all reducible structures. In summary we have found that any unsaturated structure can be reduced to a matrix with $a - b$ vanishing eigenvalues and a saturated $(b + b)$-dimensional substructure exhibiting the same scenario as the original matrix. Furthermore, we have shown that the singular saturated Majorana case can be reduced to a matrix with t eigenvalues of order $B_t = M_{\mathrm{R}t}$ and a singular over-saturated pseudo-Dirac substructure with dimensions $(s, a - t, t)$. The singular over-saturated Majorana case possesses t

Table B.2: Summary of general unsaturated reducible matrix structures. The second column characterizes the structure of the submatrix that is obtained after bringing the matrix into second canonical form. Note that all cases displayed possess $a-b$ vanishing eigenvalues independent of and in addition to the substructure (with $b = s + t$ in the singular cases).

reducible structure (dimensions)	substructure (dimensions)
non-sing. uM (a, b)	non-sing. sM (b, b)
non-sing. uD (a, b)	non-sing. sD (b, b)
non-sing. uPD (a, b)	non-sing. sPD (b, b)
sing. uM (a, s, t)	sing. sM ($s+t$, s, t)
sing. uPD (a, s, t)	sing. sPD ($s+t$, s, t)

Table B.3: Summary of singular reducible matrix structures in the saturated and over-saturated Majorana cases. In the second column we show the conditions that lead to the different substructures in the third column. Note that the condition in the saturated case is trivial since $a = s + t$ implies $a > s$. The substructures are obtained after applying the seesaw formula. Note that all cases displayed possess t eigenvalues of the order of $M_{\mathrm{R}t}$, independent of and in addition to the substructure.

red. structure (dimensions)	condition		substructure (dimensions)
sing. sM (a, s, t)	$a > s$ (trivial)		sing. oPD (s, $a-t$, t)
sing. oM (a, s, t)	$a > t$	$a < s$	sing. uPD (s, $a-t$, t)
		$a = s$	sing. sPD (s, $a-t$, t)
		$a > s$	sing. oPD (s, $a-t$, t)
	$a \leq t$	$a < s$	non-sing. uPD (s, a)
		$a = s$	non-sing. sPD (s, a)
		$a > s$	non-sing. oPD (s, a)

eigenvalues of order $B_t = M_{\mathrm{R}t}$, too, and the sub-matrix is either a non-singular pseudo-Dirac structure with dimensions (s, a) if $a \leq t$, or a singular pseudo-Dirac structure with dimensions (s, $a-t$, t) if $a > t$. Whether the pseudo-Dirac structures are unsaturated, saturated or over-saturated is determined by the relation between s and a. Next we discuss the irreducible structures.

Irreducible matrix structures

Before we start with the actual discussion of the irreducible matrix structures, let us anticipate that we have investigated the singular saturated and over-saturated pseudo-Dirac cases, but could not obtain a refined form of the characteristic polynomial. In these scenarios information about the eigenvalues strongly depends on the different relations between a, s and t.

The first analytically calculable structure we consider is the non-singular sat-

urated case with the symmetric $(a+a)\times(a+a)$ matrix

$$M = \begin{pmatrix} 0 & C^{\intercal} \\ C & B \end{pmatrix} \tag{B.46}$$

where B is either non-singular (Majorana and pseudo-Dirac cases) or $B \equiv 0$ (Dirac case). Note that in the saturated case M does not possess any vanishing eigenvalues since $a = b$ (see Table B.1). The matrix's characteristic polynomial is given by

$$\begin{aligned} \chi_M(\lambda) &= \det\left(\lambda \cdot \mathbb{1}_{2a} - M\right) = \det\begin{pmatrix} \lambda \cdot \mathbb{1}_a & -C^{\intercal} \\ -C & \lambda \cdot \mathbb{1}_a - B \end{pmatrix} \\ &= \lambda^a \det\left(\lambda \cdot \mathbb{1}_a - B - \lambda^{-1} C C^{\intercal}\right) \\ &= \det\left(\lambda^2 \cdot \mathbb{1}_a - \lambda\, B - C C^{\intercal}\right) , \end{aligned} \tag{B.47}$$

where in the second line we have used Eq. (B.10) with $\lambda \neq 0$. Comparing the first and third line of the above equation it is important to notice that we have traded a $2a$-dimensional eigenvalue problem linear in λ for an a-dimensional eigenvalue problem quadratic in λ.

Of course, we cannot give a general analytic expression for the roots of Eq. (B.47). However, the fact that the argument of the determinant is a quadratic polynomial tells us that the eigenvalues of M come in pairs. Additionally, we can give an estimate for the eigenvalue pairs in the different cases (M, D, PD) when we treat B and C as ordinary numbers for a moment. Then we obtain the general and exact solution

$$\lambda_{\pm} = \tfrac{B}{2} \pm \sqrt{\tfrac{B^2}{4} + C C^{\intercal}}\,. \tag{B.48}$$

For the Majorana case with $B \gg C$ the solutions in Eq. (B.48) become

$$\lambda_+ = B \equiv M_{\mathrm{R}}\,, \qquad\qquad \lambda_- = -\frac{C C^{\intercal}}{B} \equiv -\frac{M_{\mathrm{D}} M_{\mathrm{D}}^{\intercal}}{M_{\mathrm{R}}} \tag{B.49}$$

to leading order in consistency with the eigenvalues obtained from the well-know seesaw formula. In the Dirac case with $B = 0$ the solution is simply

$$\lambda_{\pm} = \pm\sqrt{C C^{\intercal}} \equiv \pm\sqrt{M_{\mathrm{D}} M_{\mathrm{D}}^{\intercal}}\,. \tag{B.50}$$

In the pseudo-Dirac case with $B \ll C$ we obtain

$$\lambda_{\pm} = \pm\sqrt{C C^{\intercal}} + \tfrac{B}{2} \equiv \pm\sqrt{M_{\mathrm{D}} M_{\mathrm{D}}^{\intercal}} + \tfrac{M_{\mathrm{R}}}{2} \tag{B.51}$$

to leading order. We take Eqs. (B.49) - (B.51) as symbolic solutions to the eigenvalue problem in the non-singular saturated cases.

In the non-singular over-saturated cases with $a < b = a + \alpha$ we use the second canonical form of Eq. (B.31), for which M is given by

$$M = \begin{pmatrix} 0 & \left(C'_{a\times a}\right)^{\mathsf{T}} & 0 \\ C'_{a\times a} & B'_{a\times a} & \left(B'_{\alpha\times a}\right)^{\mathsf{T}} \\ 0 & B'_{\alpha\times a} & B'_{\alpha\times\alpha} \end{pmatrix} \equiv \begin{pmatrix} 0 & (C')^{\mathsf{T}} \\ C' & B' \end{pmatrix} . \tag{B.52}$$

The $a + b$ eigenvalues of M are found by solving the equation

$$\chi_M(\lambda) = \lambda^{-\alpha} \det \left[\lambda^2 \cdot \mathbb{1}_{a+\alpha} - \lambda\, B' - \begin{pmatrix} C'_{a\times a} \left(C'_{a\times a}\right)^{\mathsf{T}} & 0 \\ 0 & 0 \end{pmatrix} \right] \stackrel{!}{=} 0 \,. \tag{B.53}$$

As in the saturated case we cannot derive a general solution to this eigenvalue problem. Still we can estimate which solutions to the above equation can be expected. Due to the singular form of the matrix-product $C' \cdot (C')^{\mathsf{T}}$ we estimate with the help of Eq. (B.53) that there are a eigenvalue pairs $\lambda_\pm$ solving the equation

$$\begin{aligned} \lambda^2 - \lambda B' - C'_{a\times a} \left(C'_{a\times a}\right)^{\mathsf{T}} &\stackrel{!}{=} 0 \\ \Rightarrow \;\; \lambda_\pm = \tfrac{B'}{2} &\pm \sqrt{\tfrac{B'^2}{4} + C' \left(C'\right)^{\mathsf{T}}} \,, \end{aligned} \tag{B.54}$$

and $\alpha = b - a$ single solutions to

$$\lambda - B' \stackrel{!}{=} 0 \,. \tag{B.55}$$

In order to validate these estimates we confirmed that they coincide with the exact solution in the most simple over-saturated case with $a = 1$ and $b = 2$, and assuming that B' is diagonal.

Again, we remark that Eqs. (B.54) and (B.55) are to be understood as symbolic solutions. Note that the solution in Eq. (B.54) has the same form as the solution in Eq. (B.48) in the saturated case (apart from the primes, which merely indicate the transformation to the canonical form). Accordingly, the solutions to Eq. (B.54) in the Majorana and in the pseudo-Dirac case are given by Eqs. (B.49) and (B.51), respectively. Remember that there is no over-saturated Dirac case.

In summary we have found that the eigenvalue spectrum of the non-singular over-saturated cases with $a < b = a + \alpha$ is given by a pairs of eigenvalues with the same form as in the corresponding saturated cases augmented by $\alpha = b - a$ single eigenvalues with solution given as in Eq. (B.55), i.e. with a characteristic mass scale of the order of $B^{(\prime)}$. In Table 5.1 we summarize our findings for all non-singular cases.

This page is intentionally left blank

Bibliography

[1] P. Humbert, M. Lindner, and J. Smirnov, "*The Inverse Seesaw in Conformal Electro-Weak Symmetry Breaking and Phenomenological Consequences*," JHEP **06** (2015) 035, arXiv:1503.03066 [hep-ph].

[2] P. Humbert, M. Lindner, S. Patra, and J. Smirnov, "*Lepton Number Violation within the Conformal Inverse Seesaw*," JHEP **09** (2015) 064, arXiv:1505.07453 [hep-ph].

[3] **ATLAS** Collaboration, G. Aad *et al.*, "*Observation of a new particle in the search for the Standard Model Higgs boson with the ATLAS detector at the LHC*," Phys. Lett. **B716** (2012) 1–29, arXiv:1207.7214 [hep-ex].

[4] **CMS** Collaboration, S. Chatrchyan *et al.*, "*Observation of a new boson at a mass of 125 GeV with the CMS experiment at the LHC*," Phys. Lett. **B716** (2012) 30–61, arXiv:1207.7235 [hep-ex].

[5] S. Weinberg, "*Implications of Dynamical Symmetry Breaking*," Phys. Rev. **D13** (1976) 974–996.

[6] S. Weinberg, "*Implications of Dynamical Symmetry Breaking: An Addendum*," Phys. Rev. **D19** (1979) 1277–1280.

[7] E. Gildener, "*Gauge Symmetry Hierarchies*," Phys. Rev. **D14** (1976) 1667.

[8] L. Susskind, "*Dynamics of Spontaneous Symmetry Breaking in the Weinberg-Salam Theory*," Phys. Rev. **D20** (1979) 2619–2625.

[9] G. 't Hooft, C. Itzykson, A. Jaffe, H. Lehmann, P. K. Mitter, I. M. Singer, and R. Stora, "*Recent Developments in Gauge Theories. Proceedings, Nato Advanced Study Institute, Cargese, France, August 26 - September 8, 1979*," NATO Sci. Ser. B **59** (1980) pp.1–438.

[10] **ATLAS, CMS** Collaboration, G. Aad *et al.*, "*Combined Measurement of the Higgs Boson Mass in pp Collisions at $\sqrt{s} = 7$ and 8 TeV with the ATLAS and CMS Experiments*," Phys. Rev. Lett. **114** (2015) 191803, arXiv:1503.07589 [hep-ex].

[11] J. Wess and B. Zumino, "*Supergauge Transformations in Four-Dimensions*," Nucl. Phys. **B70** (1974) 39–50.

[12] A. Salam and J. A. Strathdee, "*Supergauge Transformations*," Nucl. Phys. **B76** (1974) 477–482.

[13] A. Strumia, "*Theory Summary of Moriond Electro-Weak 2015*," arXiv:1504.08331 [hep-ph].

[14] A. Pich, "*ICHEP 2014 Summary: Theory Status after the First LHC Run*," in *37th International Conference on High Energy Physics (ICHEP 2014) Valencia, Spain, July 2-9, 2014*. 2015. arXiv:1505.01813 [hep-ph].

[15] R. Jackiw and K. Johnson, "*Dynamical Model of Spontaneously Broken Gauge Symmetries*," Phys. Rev. **D8** (1973) 2386–2398.

[16] J. M. Cornwall and R. E. Norton, "*Spontaneous Symmetry Breaking Without Scalar Mesons*," Phys. Rev. **D8** (1973) 3338–3346.

[17] E. Eichten and F. Feinberg, "*Dynamical Symmetry Breaking of Nonabelian Gauge Symmetries*," Phys. Rev. **D10** (1974) 3254–3279.

[18] D. B. Kaplan and H. Georgi, "*SU(2) x U(1) Breaking by Vacuum Misalignment*," Phys. Lett. **B136** (1984) 183–186.

[19] M. J. Dugan, H. Georgi, and D. B. Kaplan, "*Anatomy of a Composite Higgs Model*," Nucl. Phys. **B254** (1985) 299–326.

[20] K. Agashe, R. Contino, and A. Pomarol, "*The Minimal composite Higgs model*," Nucl. Phys. **B719** (2005) 165–187, arXiv:hep-ph/0412089 [hep-ph].

[21] N. Arkani-Hamed, S. Dimopoulos, and G. R. Dvali, "*The Hierarchy problem and new dimensions at a millimeter*," Phys. Lett. **B429** (1998) 263–272, arXiv:hep-ph/9803315 [hep-ph].

[22] N. Arkani-Hamed, S. Dimopoulos, and G. R. Dvali, "*Phenomenology, astrophysics and cosmology of theories with submillimeter dimensions and TeV scale quantum gravity*," Phys. Rev. **D59** (1999) 086004, arXiv:hep-ph/9807344 [hep-ph].

[23] W. A. Bardeen, "*On naturalness in the standard model*," in *Ontake Summer Institute on Particle Physics Ontake Mountain, Japan, August 27-September 2, 1995*. 1995. http://lss.fnal.gov/archive/1995/conf/Conf-95-391-T.pdf.

[24] H. Aoki and S. Iso, "*Revisiting the Naturalness Problem – Who is afraid of quadratic divergences? –*," Phys. Rev. **D86** (2012) 013001, arXiv:1201.0857 [hep-ph].

[25] K. G. Wilson and J. B. Kogut, "*The Renormalization group and the epsilon expansion*," Phys. Rept. **12** (1974) 75–200.

[26] S. L. Glashow, "*Partial Symmetries of Weak Interactions*," Nucl. Phys. **22** (1961) 579–588.

[27] S. Weinberg, "*A Model of Leptons*," Phys. Rev. Lett. **19** (1967) 1264–1266.

[28] A. Salam, "*Weak and Electromagnetic Interactions*," Conf. Proc. **C680519** (1968) 367–377.

[29] F. Englert and R. Brout, "*Broken Symmetry and the Mass of Gauge Vector Mesons*," Phys. Rev. Lett. **13** (1964) 321–323.

[30] P. W. Higgs, "*Broken symmetries, massless particles and gauge fields*," Phys. Lett. **12** (1964) 132–133.

[31] P. W. Higgs, "*Broken Symmetries and the Masses of Gauge Bosons*," Phys. Rev. Lett. **13** (1964) 508–509.

[32] M. Lindner, "*Implications of Triviality for the Standard Model*," Z. Phys. **C31** (1986) 295.

[33] G. Degrassi, S. Di Vita, J. Elias-Miro, J. R. Espinosa, G. F. Giudice, G. Isidori, and A. Strumia, "*Higgs mass and vacuum stability in the Standard Model at NNLO*," JHEP **08** (2012) 098, arXiv:1205.6497 [hep-ph].

[34] S. Alekhin, A. Djouadi, and S. Moch, "*The top quark and Higgs boson masses and the stability of the electroweak vacuum*," Phys. Lett. **B716** (2012) 214–219, arXiv:1207.0980 [hep-ph].

[35] I. Masina, "*Higgs boson and top quark masses as tests of electroweak vacuum stability*," Phys. Rev. **D87** (2013) no. 5, 053001, arXiv:1209.0393 [hep-ph].

[36] S. R. Coleman and E. J. Weinberg, "*Radiative Corrections as the Origin of Spontaneous Symmetry Breaking*," Phys. Rev. **D7** (1973) 1888–1910.

[37] K. Fujikawa, "*Heavy Fermions in the Standard Sequential Scheme*," Prog. Theor. Phys. **61** (1979) 1186.

[38] K. A. Meissner and H. Nicolai, "*Effective action, conformal anomaly and the issue of quadratic divergences*," Phys. Lett. **B660** (2008) 260–266, arXiv:0710.2840 [hep-th].

[39] M. Holthausen, K. S. Lim, and M. Lindner, "*Planck scale Boundary Conditions and the Higgs Mass*," JHEP **02** (2012) 037, arXiv:1112.2415 [hep-ph].

[40] K. A. Meissner and H. Nicolai, "*Conformal Symmetry and the Standard Model*," Phys. Lett. **B648** (2007) 312–317, arXiv:hep-th/0612165 [hep-th].

[41] R. Foot, A. Kobakhidze, and R. R. Volkas, "*Electroweak Higgs as a pseudo-Goldstone boson of broken scale invariance*," Phys. Lett. **B655** (2007) 156–161, arXiv:0704.1165 [hep-ph].

[42] R. Foot, A. Kobakhidze, K. McDonald, and R. Volkas, "*Neutrino mass in radiatively-broken scale-invariant models*," Phys. Rev. **D76** (2007) 075014, arXiv:0706.1829 [hep-ph].

[43] W.-F. Chang, J. N. Ng, and J. M. S. Wu, "*Shadow Higgs from a scale-invariant hidden U(1)(s) model*," Phys. Rev. **D75** (2007) 115016, arXiv:hep-ph/0701254 [HEP-PH].

[44] T. Hambye and M. H. G. Tytgat, "*Electroweak symmetry breaking induced by dark matter*," Phys. Lett. **B659** (2008) 651–655, arXiv:0707.0633 [hep-ph].

[45] K. A. Meissner and H. Nicolai, "*Conformal invariance from non-conformal gravity*," Phys. Rev. **D80** (2009) 086005, arXiv:0907.3298 [hep-th].

[46] M. Holthausen, M. Lindner, and M. A. Schmidt, "*Radiative Symmetry Breaking of the Minimal Left-Right Symmetric Model*," Phys. Rev. **D82** (2010) 055002, arXiv:0911.0710 [hep-ph].

[47] S. Iso, N. Okada, and Y. Orikasa, "*Classically conformal B^- L extended Standard Model*," Phys. Lett. **B676** (2009) 81–87, arXiv:0902.4050 [hep-ph].

[48] S. Iso, N. Okada, and Y. Orikasa, "*The minimal B-L model naturally realized at TeV scale*," Phys. Rev. **D80** (2009) 115007, arXiv:0909.0128 [hep-ph].

[49] L. Alexander-Nunneley and A. Pilaftsis, "*The Minimal Scale Invariant Extension of the Standard Model*," JHEP **09** (2010) 021, arXiv:1006.5916 [hep-ph].

[50] R. Foot, A. Kobakhidze, and R. R. Volkas, "*Cosmological constant in scale-invariant theories*," Phys. Rev. **D84** (2011) 075010, arXiv:1012.4848 [hep-ph].

[51] C. Englert, J. Jaeckel, V. V. Khoze, and M. Spannowsky, "*Emergence of the Electroweak Scale through the Higgs Portal*," JHEP **04** (2013) 060, arXiv:1301.4224 [hep-ph].

[52] V. V. Khoze, "*Inflation and Dark Matter in the Higgs Portal of Classically Scale Invariant Standard Model*," JHEP **11** (2013) 215, arXiv:1308.6338 [hep-ph].

[53] Y. Kawamura, "*Naturalness, Conformal Symmetry and Duality*," PTEP **2013** (2013) no. 11, 113B04, arXiv:1308.5069 [hep-ph].

[54] S. Abel and A. Mariotti, "*Novel Higgs Potentials from Gauge Mediation of Exact Scale Breaking*," Phys. Rev. **D89** (2014) no. 12, 125018, arXiv:1312.5335 [hep-ph].

[55] R. Foot, A. Kobakhidze, K. L. McDonald, and R. R. Volkas, "*Poincare protection for a natural electroweak scale*," Phys. Rev. **D89** (2014) no. 11, 115018, arXiv:1310.0223 [hep-ph].

[56] A. Farzinnia, H.-J. He, and J. Ren, "*Natural Electroweak Symmetry Breaking from Scale Invariant Higgs Mechanism*," Phys. Lett. **B727** (2013) 141–150, arXiv:1308.0295 [hep-ph].

[57] M. Heikinheimo, A. Racioppi, M. Raidal, C. Spethmann, and K. Tuominen, "*Physical Naturalness and Dynamical Breaking of Classical Scale Invariance*," Mod. Phys. Lett. **A29** (2014) 1450077, arXiv:1304.7006 [hep-ph].

[58] J. Smirnov, "*Regularization of Vacuum Fluctuations and Frame Dependence*," arXiv:1402.1490 [hep-th].

[59] A. Salvio and A. Strumia, "*Agravity*," JHEP **06** (2014) 080, arXiv:1403.4226 [hep-ph].

[60] M. Lindner, S. Schmidt, and J. Smirnov, "*Neutrino Masses and Conformal Electro-Weak Symmetry Breaking*," JHEP **1410** (2014) 177, arXiv:1405.6204 [hep-ph].

[61] A. Farzinnia and J. Ren, "*Higgs Partner Searches and Dark Matter Phenomenology in a Classically Scale Invariant Higgs Boson Sector*," Phys. Rev. **D90** (2014) no. 1, 015019, arXiv:1405.0498 [hep-ph].

[62] H. Okada, T. Toma, and K. Yagyu, "*Inert Extension of the Zee-Babu Model*," Phys. Rev. **D90** (2014) 095005, arXiv:1408.0961 [hep-ph].

[63] S. Benic and B. Radovcic, "*Majorana dark matter in a classically scale invariant model*," JHEP **01** (2015) 143, arXiv:1409.5776 [hep-ph].

[64] P. H. Chankowski, A. Lewandowski, K. A. Meissner, and H. Nicolai, "*Softly broken conformal symmetry and the stability of the electroweak scale*," Mod. Phys. Lett. **A30** (2015) no. 02, 1550006, arXiv:1404.0548 [hep-ph].

[65] J. Guo, Z. Kang, P. Ko, and Y. Orikasa, "*Accidental dark matter: Case in the scale invariant local B-L model*," Phys. Rev. **D91** (2015) no. 11, 115017, arXiv:1502.00508 [hep-ph].

[66] K. Kannike, G. HÃ¼tsi, L. Pizza, A. Racioppi, M. Raidal, A. Salvio, and A. Strumia, "*Dynamically Induced Planck Scale and Inflation*," JHEP **05** (2015) 065, arXiv:1502.01334 [astro-ph.CO].

[67] H. Davoudiasl and C. Zhang, "*750 GeV messenger of dark conformal symmetry breaking*," Phys. Rev. **D93** (2016) no. 5, 055006, arXiv:1512.07672 [hep-ph].

[68] R. Jinno and M. Takimoto, "*Probing classically conformal $B-L$ model with gravitational waves*," arXiv:1604.05035 [hep-ph].

[69] A. J. Helmboldt, P. Humbert, M. Lindner, and J. Smirnov, "*Minimal Conformal Extensions of the Higgs Sector*," arXiv:1603.03603 [hep-ph].

[70] C. Sutton, *Spaceship neutrino*. Press Syndicate of the University of Cambridge, 1992. http://www.cambridge.org/uk/catalogue/catalogue.asp?isbn=0521364043.

[71] W. Pauli, "*Dear radioactive ladies and gentlemen*," Phys. Today **31N9** (1978) 27.

[72] C. L. Cowan, F. Reines, F. B. Harrison, H. W. Kruse, and A. D. McGuire, "*Detection of the free neutrino: A Confirmation*," Science **124** (1956) 103–104.

[73] R. Davis, Jr., D. S. Harmer, and K. C. Hoffman, "*Search for neutrinos from the sun*," Phys. Rev. Lett. **20** (1968) 1205–1209.

[74] **Super-Kamiokande** Collaboration, Y. Fukuda *et al.*, "*Evidence for oscillation of atmospheric neutrinos*," Phys. Rev. Lett. **81** (1998) 1562–1567, arXiv:hep-ex/9807003 [hep-ex].

[75] **KamLAND** Collaboration, K. Eguchi *et al.*, "*First results from KamLAND: Evidence for reactor anti-neutrino disappearance*," Phys. Rev. Lett. **90** (2003) 021802, arXiv:hep-ex/0212021 [hep-ex].

[76] **K2K** Collaboration, M. H. Ahn *et al.*, "*Indications of neutrino oscillation in a 250 km long baseline experiment*," Phys. Rev. Lett. **90** (2003) 041801, arXiv:hep-ex/0212007 [hep-ex].

[77] S. Weinberg, "*Baryon and Lepton Nonconserving Processes*," Phys. Rev. Lett. **43** (1979) 1566–1570.

[78] P. Minkowski, "$\mu \to e\gamma$ *at a Rate of One Out of* 10^9 *Muon Decays?*," Phys. Lett. **B67** (1977) 421–428.

[79] M. Gell-Mann, P. Ramond, and R. Slansky, "*Complex Spinors and Unified Theories*," Conf. Proc. **C790927** (1979) 315–321, arXiv:1306.4669 [hep-th].

[80] R. N. Mohapatra and G. Senjanovic, "*Neutrino Mass and Spontaneous Parity Violation*," Phys. Rev. Lett. **44** (1980) 912.

[81] T. Yanagida, "*Horizontal Symmetry and Masses of Neutrinos*," Prog. Theor. Phys. **64** (1980) 1103.

[82] R. N. Mohapatra and J. W. F. Valle, "*Neutrino Mass and Baryon Number Nonconservation in Superstring Models*," Phys. Rev. **D34** (1986) 1642.

[83] M. C. Gonzalez-Garcia and J. W. F. Valle, "*Fast Decaying Neutrinos and Observable Flavor Violation in a New Class of Majoron Models*," Phys. Lett. **B216** (1989) 360.

[84] F. Deppisch and J. Valle, "*Enhanced lepton flavor violation in the supersymmetric inverse seesaw model*," Phys.Rev. **D72** (2005) 036001, arXiv:hep-ph/0406040 [hep-ph].

[85] M. E. Peskin and D. V. Schroeder, *An Introduction to quantum field theory*. 1995.

[86] L. H. Ryder, *Quantum Field Theory*. Cambridge University Press, 1996.

[87] **Particle Data Group** Collaboration, K. A. Olive *et al.*, "*Review of Particle Physics*," Chin. Phys. **C38** (2014) 090001.

[88] R. N. Mohapatra and P. B. Pal, "*Massive neutrinos in physics and astrophysics. Second edition*," World Sci. Lect. Notes Phys. **60** (1998) 1–397. [World Sci. Lect. Notes Phys.72,1(2004)].

[89] K. Dick, M. Lindner, M. Ratz, and D. Wright, "*Leptogenesis with Dirac neutrinos*," Phys. Rev. Lett. **84** (2000) 4039–4042, arXiv:hep-ph/9907562 [hep-ph].

[90] W. Grimus and L. Lavoura, "*The Seesaw mechanism at arbitrary order: Disentangling the small scale from the large scale*," JHEP **11** (2000) 042, arXiv:hep-ph/0008179 [hep-ph].

[91] G. Lazarides, Q. Shafi, and C. Wetterich, "*Proton Lifetime and Fermion Masses in an SO(10) Model*," Nucl. Phys. **B181** (1981) 287–300.

[92] R. N. Mohapatra and G. Senjanovic, "*Neutrino Masses and Mixings in Gauge Models with Spontaneous Parity Violation*," Phys. Rev. **D23** (1981) 165.

[93] R. Foot, H. Lew, X. G. He, and G. C. Joshi, "*Seesaw Neutrino Masses Induced by a Triplet of Leptons*," Z. Phys. **C44** (1989) 441.

[94] E. Ma, "*Pathways to naturally small neutrino masses*," Phys. Rev. Lett. **81** (1998) 1171–1174, arXiv:hep-ph/9805219 [hep-ph].

[95] R. N. Mohapatra, "*Mechanism for Understanding Small Neutrino Mass in Superstring Theories*," Phys. Rev. Lett. **56** (1986) 561–563.

[96] R. Johnson, S. Ranfone, and J. Schechter, "*The Neutrino Seesaw in SO(10)*," Phys. Lett. **B179** (1986) 355.

[97] S. L. Glashow, "*A Novel neutrino mass hierarchy*," Phys. Lett. **B256** (1991) 255–257.

[98] M. Fukugita and T. Yanagida, "*Partially Broken Seesaw Mechanism*," Phys. Rev. Lett. **66** (1991) 2705–2707.

[99] E. K. Akhmedov, M. Lindner, E. Schnapka, and J. W. F. Valle, "*Dynamical left-right symmetry breaking*," Phys. Rev. **D53** (1996) 2752–2780, arXiv:hep-ph/9509255 [hep-ph].

[100] S. M. Barr, "*A Different seesaw formula for neutrino masses*," Phys. Rev. Lett. **92** (2004) 101601, arXiv:hep-ph/0309152 [hep-ph].

[101] C. H. Albright and S. M. Barr, "*Leptogenesis in the type III seesaw mechanism*," Phys. Rev. **D69** (2004) 073010, arXiv:hep-ph/0312224 [hep-ph].

[102] R. Allahverdi, B. Dutta, and R. N. Mohapatra, "*Schizophrenic Neutrinos and ν-less Double Beta Decay*," Phys. Lett. **B695** (2011) 181–184, arXiv:1008.1232 [hep-ph].

[103] A. Kusenko, F. Takahashi, and T. T. Yanagida, "*Dark Matter from Split Seesaw*," Phys. Lett. **B693** (2010) 144–148, arXiv:1006.1731 [hep-ph].

[104] F. Bonnet, M. Hirsch, T. Ota, and W. Winter, "*Systematic study of the d=5 Weinberg operator at one-loop order*," JHEP **07** (2012) 153, arXiv:1204.5862 [hep-ph].

[105] G. Danby, J. M. Gaillard, K. A. Goulianos, L. M. Lederman, N. B. Mistry, M. Schwartz, and J. Steinberger, "*Observation of High-Energy Neutrino Reactions and the Existence of Two Kinds of Neutrinos*," Phys. Rev. Lett. **9** (1962) 36–44.

[106] **DONUT** Collaboration, K. Kodama *et al.*, "*Observation of tau neutrino interactions*," Phys. Lett. **B504** (2001) 218–224, arXiv:hep-ex/0012035 [hep-ex].

[107] **SLD Electroweak Group, DELPHI, ALEPH, SLD, SLD Heavy Flavour Group, OPAL, LEP Electroweak Working Group, L3** Collaboration, S. Schael *et al.*, "*Precision electroweak measurements on*

the Z resonance," Phys. Rept. **427** (2006) 257–454, arXiv:hep-ex/0509008 [hep-ex].

[108] **Planck** Collaboration, P. Ade *et al.*, "*Planck 2013 results. XVI. Cosmological parameters*," Astron.Astrophys. **571** (2014) A16, arXiv:1303.5076 [astro-ph.CO].

[109] J. Kopp, P. A. N. Machado, M. Maltoni, and T. Schwetz, "*Sterile Neutrino Oscillations: The Global Picture*," JHEP **05** (2013) 050, arXiv:1303.3011 [hep-ph].

[110] C. Kraus *et al.*, "*Final results from phase II of the Mainz neutrino mass search in tritium beta decay*," Eur. Phys. J. **C40** (2005) 447–468, arXiv:hep-ex/0412056 [hep-ex].

[111] **KATRIN** Collaboration, A. Osipowicz *et al.*, "*KATRIN: A Next generation tritium beta decay experiment with sub-eV sensitivity for the electron neutrino mass. Letter of intent*," arXiv:hep-ex/0109033 [hep-ex].

[112] **KATRIN** Collaboration, J. Angrik *et al.*, "*KATRIN design report 2004*,".

[113] N. Palanque-Delabrouille *et al.*, "*Constraint on neutrino masses from SDSS-III/BOSS Lyα forest and other cosmological probes*," JCAP **1502** (2015) no. 02, 045, arXiv:1410.7244 [astro-ph.CO].

[114] N. Palanque-Delabrouille *et al.*, "*Neutrino masses and cosmology with Lyman-alpha forest power spectrum*," JCAP **1511** (2015) no. 11, 011, arXiv:1506.05976 [astro-ph.CO].

[115] M. C. Gonzalez-Garcia, M. Maltoni, and T. Schwetz, "*Global Analyses of Neutrino Oscillation Experiments*," arXiv:1512.06856 [hep-ph].

[116] B. Pontecorvo, "*Mesonium and anti-mesonium*," Sov. Phys. JETP **6** (1957) 429. [Zh. Eksp. Teor. Fiz.33,549(1957)].

[117] Z. Maki, M. Nakagawa, and S. Sakata, "*Remarks on the unified model of elementary particles*," Prog. Theor. Phys. **28** (1962) 870–880.

[118] L. Wolfenstein, "*Neutrino Oscillations in Matter*," Phys. Rev. **D17** (1978) 2369–2374.

[119] L. Wolfenstein, "*Neutrino Oscillations and Stellar Collapse*," Phys. Rev. **D20** (1979) 2634–2635.

[120] S. P. Mikheev and A. Yu. Smirnov, "*Resonance Amplification of Oscillations in Matter and Spectroscopy of Solar Neutrinos*," Sov. J. Nucl. Phys. **42** (1985) 913–917. [Yad. Fiz.42,1441(1985)].

[121] S. P. Mikheev and A. Yu. Smirnov, "*Resonant amplification of neutrino oscillations in matter and solar neutrino spectroscopy*," Nuovo Cim. **C9** (1986) 17–26.

[122] F. R. Klinkhamer and N. S. Manton, "*A Saddle Point Solution in the Weinberg-Salam Theory*," Phys. Rev. **D30** (1984) 2212.

[123] G. 't Hooft, "*Computation of the Quantum Effects Due to a Four-Dimensional Pseudoparticle*," Phys. Rev. **D14** (1976) 3432–3450. [Erratum: Phys. Rev.D18,2199(1978)].

[124] D. S. Gorbunov and V. A. Rubakov, *Introduction to the theory of the early universe: Hot big bang theory*. World Scientific, Hackensack, 2011.

[125] A. D. Sakharov, "*Violation of CP Invariance, c Asymmetry, and Baryon Asymmetry of the Universe*," Pisma Zh. Eksp. Teor. Fiz. **5** (1967) 32–35. [Usp. Fiz. Nauk161,61(1991)].

[126] M. Fukugita and T. Yanagida, "*Baryogenesis Without Grand Unification*," Phys. Lett. **B174** (1986) 45–47.

[127] H. V. Klapdor-Kleingrothaus, I. V. Krivosheina, A. Dietz, and O. Chkvorets, "*Search for neutrinoless double beta decay with enriched Ge-76 in Gran Sasso 1990-2003*," Phys. Lett. **B586** (2004) 198–212, arXiv:hep-ph/0404088 [hep-ph].

[128] H. V. Klapdor-Kleingrothaus and I. V. Krivosheina, "*The evidence for the observation of 0nu beta beta decay: The identification of 0nu beta beta events from the full spectra*," Mod. Phys. Lett. **A21** (2006) 1547–1566.

[129] B. Schwingenheuer, "*Status and prospects of searches for neutrinoless double beta decay*," Annalen Phys. **525** (2013) 269–280, arXiv:1210.7432 [hep-ex].

[130] **GERDA** Collaboration, M. Agostini *et al.*, "*Results on Neutrinoless Double-β Decay of ^{76}Ge from Phase I of the GERDA Experiment*," Phys.Rev.Lett. **111** (2013) no. 12, 122503, arXiv:1307.4720 [nucl-ex].

[131] A. S. Barabash, "*Precise half-life values for two neutrino double beta decay*," Phys. Rev. **C81** (2010) 035501, arXiv:1003.1005 [nucl-ex].

[132] J. Schechter and J. W. F. Valle, "*Neutrinoless Double beta Decay in SU(2) x U(1) Theories*," Phys. Rev. **D25** (1982) 2951.

[133] M. Duerr, M. Lindner, and A. Merle, "*On the Quantitative Impact of the Schechter-Valle Theorem*," JHEP **06** (2011) 091, arXiv:1105.0901 [hep-ph].

[134] H. PÃ¤s and W. Rodejohann, "*Neutrinoless Double Beta Decay*," New J. Phys. **17** (2015) no. 11, 115010, arXiv:1507.00170 [hep-ph].

[135] G. Racah, "*On the symmetry of particle and antiparticle*," Nuovo Cim. **14** (1937) 322–328.

[136] W. H. Furry, "*On transition probabilities in double beta-disintegration*," Phys. Rev. **56** (1939) 1184–1193.

[137] H. Pas, M. Hirsch, H. V. Klapdor-Kleingrothaus, and S. G. Kovalenko, "*Towards a superformula for neutrinoless double beta decay*," Phys. Lett. **B453** (1999) 194–198.

[138] H. Pas, M. Hirsch, H. V. Klapdor-Kleingrothaus, and S. G. Kovalenko, "*A Superformula for neutrinoless double beta decay. 2. The Short range part*," Phys. Lett. **B498** (2001) 35–39, arXiv:hep-ph/0008182 [hep-ph].

[139] A. Halprin, S. T. Petcov, and S. P. Rosen, "*Effects of Light and Heavy Majorana Neutrinos in Neutrinoless Double Beta Decay*," Phys. Lett. **B125** (1983) 335.

[140] F. Simkovic, J. Vergados, and A. Faessler, "*Few active mechanisms of the neutrinoless double beta-decay and effective mass of Majorana neutrinos*," Phys. Rev. **D82** (2010) 113015, arXiv:1006.0571 [hep-ph].

[141] A. Faessler, A. Meroni, S. T. Petcov, F. Simkovic, and J. Vergados, "*Uncovering Multiple CP-Nonconserving Mechanisms of $(\beta\beta)_{0\nu}$ Decay*," Phys. Rev. **D83** (2011) 113003, arXiv:1103.2434 [hep-ph].

[142] A. Faessler, G. L. Fogli, E. Lisi, A. M. Rotunno, and F. Simkovic, "*Multi-Isotope Degeneracy of Neutrinoless Double Beta Decay Mechanisms in the Quasi-Particle Random Phase Approximation*," Phys. Rev. **D83** (2011) 113015, arXiv:1103.2504 [hep-ph].

[143] A. Meroni, S. T. Petcov, and F. Simkovic, "*Multiple CP Non-conserving Mechanisms of $\beta\beta$-Decay and Nuclei with Largely Different Nuclear Matrix Elements*," JHEP **02** (2013) 025, arXiv:1212.1331 [hep-ph].

[144] S. Pascoli, M. Mitra, and S. Wong, "*Effect of cancellation in neutrinoless double beta decay*," Phys. Rev. **D90** (2014) no. 9, 093005, arXiv:1310.6218 [hep-ph].

[145] F. Zwicky, "*Die Rotverschiebung von extragalaktischen Nebeln*," Helv. Phys. Acta **6** (1933) 110–127.

[146] V. C. Rubin and W. K. Ford, Jr., "*Rotation of the Andromeda Nebula from a Spectroscopic Survey of Emission Regions*," Astrophys. J. **159** (1970) 379–403.

[147] K. G. Begeman, A. H. Broeils, and R. H. Sanders, "*Extended rotation curves of spiral galaxies: Dark haloes and modified dynamics*," Mon. Not. Roy. Astron. Soc. **249** (1991) 523. http://mnras.oxfordjournals.org/content/249/3/523.

[148] L. V. E. Koopmans and T. Treu, "*The structure and dynamics of luminous and dark matter in the early-type lens galaxy of 0047-281 at z=0.485*," Astrophys. J. **583** (2003) 606–615, arXiv:astro-ph/0205281 [astro-ph].

[149] D. Clowe, A. Gonzalez, and M. Markevitch, "*Weak lensing mass reconstruction of the interacting cluster 1E0657-558: Direct evidence for the existence of dark matter*," Astrophys. J. **604** (2004) 596–603, arXiv:astro-ph/0312273 [astro-ph].

[150] M. Markevitch, A. H. Gonzalez, D. Clowe, A. Vikhlinin, L. David, W. Forman, C. Jones, S. Murray, and W. Tucker, "*Direct constraints on the dark matter self-interaction cross-section from the merging galaxy cluster 1E0657-56*," Astrophys. J. **606** (2004) 819–824, arXiv:astro-ph/0309303 [astro-ph].

[151] **SDSS** Collaboration, M. Tegmark *et al.*, "*Cosmological parameters from SDSS and WMAP*," Phys. Rev. **D69** (2004) 103501, arXiv:astro-ph/0310723 [astro-ph].

[152] J. L. Feng, "*Dark Matter Candidates from Particle Physics and Methods of Detection*," Ann. Rev. Astron. Astrophys. **48** (2010) 495–545, arXiv:1003.0904 [astro-ph.CO].

[153] J. Silk *et al.*, *Particle Dark Matter: Observations, Models and Searches*. 2010.

[154] **XENON100** Collaboration, E. Aprile *et al.*, "*Dark Matter Results from 225 Live Days of XENON100 Data*," Phys. Rev. Lett. **109** (2012) 181301, arXiv:1207.5988 [astro-ph.CO].

[155] **LUX** Collaboration, D. S. Akerib *et al.*, "*Improved WIMP scattering limits from the LUX experiment*," Phys. Rev. Lett. **116** (2016) no. 16, 161301, arXiv:1512.03506 [astro-ph.CO].

[156] **XENON1T** Collaboration, E. Aprile, "*The XENON1T Dark Matter Search Experiment*," Springer Proc. Phys. **148** (2013) 93–96, arXiv:1206.6288 [astro-ph.IM].

[157] P. Bode, J. P. Ostriker, and N. Turok, "*Halo formation in warm dark matter models*," Astrophys. J. **556** (2001) 93–107, arXiv:astro-ph/0010389 [astro-ph].

[158] S. H. Hansen, J. Lesgourgues, S. Pastor, and J. Silk, "*Constraining the window on sterile neutrinos as warm dark matter*," Mon. Not. Roy. Astron. Soc. **333** (2002) 544–546, arXiv:astro-ph/0106108 [astro-ph].

[159] E. Gildener and S. Weinberg, "*Symmetry Breaking and Scalar Bosons*," Phys. Rev. **D13** (1976) 3333.

[160] A. Abada and M. Lucente, "*Looking for the minimal inverse seesaw realisation*," Nucl. Phys. **B885** (2014) 651–678, arXiv:1401.1507 [hep-ph].

[161] J. A. Casas and A. Ibarra, "*Oscillating neutrinos and muon —> e, gamma*," Nucl. Phys. **B618** (2001) 171–204, arXiv:hep-ph/0103065 [hep-ph].

[162] S. Antusch, C. Biggio, E. Fernandez-Martinez, M. B. Gavela, and J. Lopez-Pavon, "*Unitarity of the Leptonic Mixing Matrix*," JHEP **10** (2006) 084, arXiv:hep-ph/0607020 [hep-ph].

[163] E. Akhmedov, A. Kartavtsev, M. Lindner, L. Michaels, and J. Smirnov, "*Improving Electro-Weak Fits with TeV-scale Sterile Neutrinos*," JHEP **05** (2013) 081, arXiv:1302.1872 [hep-ph].

[164] S. Antusch and O. Fischer, "*Non-unitarity of the leptonic mixing matrix: Present bounds and future sensitivities*," JHEP **10** (2014) 094, arXiv:1407.6607 [hep-ph].

[165] W. Loinaz, N. Okamura, S. Rayyan, T. Takeuchi, and L. C. R. Wijewardhana, "*The NuTeV anomaly, lepton universality, and nonuniversal neutrino gauge couplings*," Phys. Rev. **D70** (2004) 113004, arXiv:hep-ph/0403306 [hep-ph].

[166] **MEG** Collaboration, J. Adam *et al.*, "*New constraint on the existence of the $\mu^+ \to e^+\gamma$ decay*," Phys. Rev. Lett. **110** (2013) 201801, arXiv:1303.0754 [hep-ex].

[167] T.-P. Cheng and L.-F. Li, *Gauge theory of elementary particle physics*. Oxford University Press Inc., New York, 1984.

[168] T.-P. Cheng and L.-F. Li, "*Muon Number Nonconservation Effects in a Gauge Theory with V A Currents and Heavy Neutral Leptons*," Phys. Rev. **D16** (1977) 1425.

[169] S. T. Petcov, "*The Processes mu –> e Gamma, mu –> e e anti-e, Neutrino' –> Neutrino gamma in the Weinberg-Salam Model with Neutrino Mixing*," Sov. J. Nucl. Phys. **25** (1977) 340. [Erratum: Yad. Fiz.25,1336(1977)].

[170] W. J. Marciano and A. I. Sanda, "*Exotic Decays of the Muon and Heavy Leptons in Gauge Theories*," Phys. Lett. **B67** (1977) 303–305.

[171] B. W. Lee and R. E. Shrock, "*Natural Suppression of Symmetry Violation in Gauge Theories: Muon - Lepton and Electron Lepton Number Nonconservation*," Phys. Rev. **D16** (1977) 1444.

[172] A. M. Baldini *et al.*, "*MEG Upgrade Proposal*," arXiv:1301.7225 [physics.ins-det].

[173] **SINDRUM** Collaboration, U. Bellgardt *et al.*, "*Search for the Decay mu+ → e+ e+ e-*," Nucl. Phys. **B299** (1988) 1.

[174] A. Blondel *et al.*, "*Research Proposal for an Experiment to Search for the Decay $\mu \to eee$*," arXiv:1301.6113 [physics.ins-det].

[175] T. Asaka, S. Blanchet, and M. Shaposhnikov, "*The nuMSM, dark matter and neutrino masses*," Phys. Lett. **B631** (2005) 151–156, arXiv:hep-ph/0503065 [hep-ph].

[176] S. Tremaine and J. E. Gunn, "*Dynamical Role of Light Neutral Leptons in Cosmology*," Phys. Rev. Lett. **42** (1979) 407–410.

[177] A. Boyarsky, O. Ruchayskiy, and D. Iakubovskyi, "*A Lower bound on the mass of Dark Matter particles*," JCAP **0903** (2009) 005, arXiv:0808.3902 [hep-ph].

[178] K. Abazajian and S. M. Koushiappas, "*Constraints on Sterile Neutrino Dark Matter*," Phys. Rev. **D74** (2006) 023527, arXiv:astro-ph/0605271 [astro-ph].

[179] A. Boyarsky, O. Ruchayskiy, D. Iakubovskyi, and J. Franse, "*Unidentified Line in X-Ray Spectra of the Andromeda Galaxy and Perseus Galaxy Cluster*," Phys. Rev. Lett. **113** (2014) 251301, arXiv:1402.4119 [astro-ph.CO].

[180] S. Dodelson and L. M. Widrow, "*Sterile-neutrinos as dark matter*," Phys. Rev. Lett. **72** (1994) 17–20, arXiv:hep-ph/9303287 [hep-ph].

[181] A. Abada, G. Arcadi, and M. Lucente, "*Dark Matter in the minimal Inverse Seesaw mechanism*," JCAP **1410** (2014) 001, arXiv:1406.6556 [hep-ph].

[182] H. Pilkuhn, *The Interactions of Hadrons*. North-Holland Publishing Company, Amsterdam, 1967.

[183] D. Berdine, N. Kauer, and D. Rainwater, "*Breakdown of the Narrow Width Approximation for New Physics*," Phys. Rev. Lett. **99** (2007) 111601, arXiv:hep-ph/0703058 [hep-ph].

[184] F. M. L. Almeida, Jr., Y. D. A. Coutinho, J. A. Martins Simoes, and M. A. B. do Vale, "*On a signature for heavy Majorana neutrinos in hadronic collisions*," Phys. Rev. **D62** (2000) 075004, arXiv:hep-ph/0002024 [hep-ph].

[185] J. Kersten and A. Yu. Smirnov, "*Right-Handed Neutrinos at CERN LHC and the Mechanism of Neutrino Mass Generation*," Phys. Rev. **D76** (2007) 073005, arXiv:0705.3221 [hep-ph].

[186] A. Das and N. Okada, "*Inverse seesaw neutrino signatures at the LHC and ILC*," Phys. Rev. **D88** (2013) 113001, arXiv:1207.3734 [hep-ph].

[187] A. Das, P. S. Bhupal Dev, and N. Okada, "*Direct bounds on electroweak scale pseudo-Dirac neutrinos from $\sqrt{s} = 8$ TeV LHC data*," Phys. Lett. **B735** (2014) 364–370, arXiv:1405.0177 [hep-ph].

[188] **CMS** Collaboration, C. Collaboration, "*Search for physics beyond the standard model in events with two opposite-sign same-flavor leptons, jets, and missing transverse energy in pp collisions at sqrt[s] = 8 TeV*," CMS-PAS-SUS-12-019 (2014) . https://cds.cern.ch/record/1751493.

[189] **CMS** Collaboration, V. Khachatryan *et al.*, "*Search for heavy neutrinos and* W *bosons with right-handed couplings in proton-proton collisions at $\sqrt{s} = 8$ TeV*," Eur. Phys. J. **C74** (2014) no. 11, 3149, arXiv:1407.3683 [hep-ex].

[190] P. S. B. Dev, A. Pilaftsis, and U.-k. Yang, "*New Production Mechanism for Heavy Neutrinos at the LHC*," Phys. Rev. Lett. **112** (2014) no. 8, 081801, arXiv:1308.2209 [hep-ph].

[191] A. Djouadi, "*Decays of the Higgs bosons*," in *Quantum effects in the minimal supersymmetric standard model. Proceedings, International Workshop, MSSM, Barcelona, Spain, September 9-13, 1997*. 1997. arXiv:hep-ph/9712334 [hep-ph].

[192] C. Anastasiou, S. Buehler, F. Herzog, and A. Lazopoulos, "*Inclusive Higgs boson cross-section for the LHC at 8 TeV*," JHEP **04** (2012) 004, arXiv:1202.3638 [hep-ph].

[193] **ATLAS** Collaboration, T. A. collaboration, "*Measurement of top-quark pair differential cross-sections in the l+jets channel in pp collisions at $\sqrt{s} = 7$ TeV using the ATLAS detector*," ATLAS-CONF-2013-099 (2013) . https://cds.cern.ch/record/1600778.

[194] **CMS** Collaboration, S. Chatrchyan *et al.*, "*Searches for new physics using the $t\bar{t}$ invariant mass distribution in pp collisions at $\sqrt{s}$=8 TeV*," Phys. Rev. Lett. **111** (2013) no. 21, 211804, arXiv:1309.2030 [hep-ex]. [Erratum: Phys. Rev. Lett.112,no.11,119903(2014)].

[195] **CMS** Collaboration, "*Projected Performance of an Upgraded CMS Detector at the LHC and HL-LHC: Contribution to the Snowmass Process*," in *Community Summer Study 2013: Snowmass on the Mississippi (CSS2013) Minneapolis, MN, USA, July 29-August 6, 2013*. 2013. arXiv:1307.7135.

[196] **CMS** Collaboration, C. Collaboration, "*Inclusive W/Z cross section at 8 TeV*," CMS-PAS-SMP-12-011 (2012) . https://cds.cern.ch/record/1460098.

[197] **ATLAS** Collaboration, T. A. collaboration, "*Search for high-mass states with one lepton plus missing transverse momentum in pp collisions at $\sqrt{s} = 8$ TeV with the ATLAS detector*," ATLAS-CONF-2014-017 (2014) . https://cds.cern.ch/record/1692660.

[198] M. Viel, J. Lesgourgues, M. G. Haehnelt, S. Matarrese, and A. Riotto, "*Constraining warm dark matter candidates including sterile neutrinos and light gravitinos with WMAP and the Lyman-alpha forest*," Phys. Rev. **D71** (2005) 063534, arXiv:astro-ph/0501562 [astro-ph].

[199] K. Abazajian, "*Linear cosmological structure limits on warm dark matter*," Phys. Rev. **D73** (2006) 063513, arXiv:astro-ph/0512631 [astro-ph].

[200] U. Seljak, A. Makarov, P. McDonald, and H. Trac, "*Can sterile neutrinos be the dark matter?*," Phys. Rev. Lett. **97** (2006) 191303, arXiv:astro-ph/0602430 [astro-ph].

[201] K. A. Olive and M. S. Turner, "*Cosmological Bounds on the Masses of Stable, Right-handed Neutrinos*," Phys. Rev. **D25** (1982) 213.

[202] R. J. Scherrer and M. S. Turner, "*Decaying Particles Do Not Heat Up the Universe*," Phys. Rev. **D31** (1985) 681.

[203] F. Bezrukov, H. Hettmansperger, and M. Lindner, "*keV sterile neutrino Dark Matter in gauge extensions of the Standard Model*," Phys. Rev. **D81** (2010) 085032, arXiv:0912.4415 [hep-ph].

[204] M. Nemevsek, G. Senjanovic, and Y. Zhang, "*Warm Dark Matter in Low Scale Left-Right Theory*," JCAP **1207** (2012) 006, arXiv:1205.0844 [hep-ph].

[205] J. McDonald, "*Thermally generated gauge singlet scalars as selfinteracting dark matter*," Phys. Rev. Lett. **88** (2002) 091304, arXiv:hep-ph/0106249 [hep-ph].

[206] L. J. Hall, K. Jedamzik, J. March-Russell, and S. M. West, "*Freeze-In Production of FIMP Dark Matter*," JHEP **03** (2010) 080, arXiv:0911.1120 [hep-ph].

[207] A. Merle, V. Niro, and D. Schmidt, "*New Production Mechanism for keV Sterile Neutrino Dark Matter by Decays of Frozen-In Scalars*," JCAP **1403** (2014) 028, arXiv:1306.3996 [hep-ph].

[208] M. Klasen and C. E. Yaguna, "*Warm and cold fermionic dark matter via freeze-in*," JCAP **1311** (2013) 039, arXiv:1309.2777 [hep-ph].

[209] X. Chu, T. Hambye, and M. H. G. Tytgat, "*The Four Basic Ways of Creating Dark Matter Through a Portal*," JCAP **1205** (2012) 034, arXiv:1112.0493 [hep-ph].

[210] Z. Kang, "*Upgrading sterile neutrino dark matter to FImP using scale invariance*," Eur. Phys. J. **C75** (2015) no. 10, 471, arXiv:1411.2773 [hep-ph].

[211] P. Gondolo and G. Gelmini, "*Cosmic abundances of stable particles: Improved canalysis*," Nucl. Phys. **B360** (1991) 145–179.

[212] H. V. Klapdor-Kleingrothaus *et al.*, "*Latest results from the Heidelberg-Moscow double beta decay experiment*," Eur. Phys. J. **A12** (2001) 147–154, arXiv:hep-ph/0103062 [hep-ph].

[213] **IGEX** Collaboration, C. E. Aalseth *et al.*, "*The IGEX Ge-76 neutrinoless double beta decay experiment: Prospects for next generation experiments*," Phys. Rev. **D65** (2002) 092007, arXiv:hep-ex/0202026 [hep-ex].

[214] C. E. Aalseth *et al.*, "*The IGEX experiment revisited: A Response to the critique of Klapdor-Kleingrothaus, Dietz and Krivosheina*," Phys. Rev. **D70** (2004) 078302, arXiv:nucl-ex/0404036 [nucl-ex].

[215] **EXO** Collaboration, M. Auger *et al.*, "*Search for Neutrinoless Double-Beta Decay in ^{136}Xe with EXO-200*," Phys.Rev.Lett. **109** (2012) 032505, arXiv:1205.5608 [hep-ex].

[216] **KamLAND-Zen** Collaboration, A. Gando *et al.*, "*Limit on Neutrinoless $\beta\beta$ Decay of ^{136}Xe from the First Phase of KamLAND-Zen and Comparison with the Positive Claim in ^{76}Ge*," Phys.Rev.Lett. **110** (2013) no. 6, 062502, arXiv:1211.3863 [hep-ex].

[217] J. C. Helo, M. Hirsch, and S. Kovalenko, "*Heavy neutrino searches at the LHC with displaced vertices*," Phys. Rev. **D89** (2014) 073005, arXiv:1312.2900 [hep-ph].

[218] E. Izaguirre and B. Shuve, "*Multilepton and Lepton Jet Probes of Sub-Weak-Scale Right-Handed Neutrinos*," Phys. Rev. **D91** (2015) no. 9, 093010, arXiv:1504.02470 [hep-ph].

[219] P. Fileviez Perez, T. Han, and T. Li, "*Testability of Type I Seesaw at the CERN LHC: Revealing the Existence of the B-L Symmetry*," Phys. Rev. **D80** (2009) 073015, arXiv:0907.4186 [hep-ph].

[220] **ATLAS** Collaboration, G. Aad *et al.*, "*Search for high-mass dilepton resonances in pp collisions at $\sqrt{s} = 8$ TeV with the ATLAS detector*," Phys. Rev. **D90** (2014) no. 5, 052005, arXiv:1405.4123 [hep-ex].

[221] **CMS** Collaboration, V. Khachatryan *et al.*, "*Search for physics beyond the standard model in dilepton mass spectra in proton-proton collisions at $\sqrt{s} = 8$ TeV*," JHEP **04** (2015) 025, arXiv:1412.6302 [hep-ex].

[222] T. A. collaboration, "*Search for new phenomena in the dilepton final state using proton-proton collisions at $\sqrt{s} = 13$ TeV with the ATLAS detector*," ATLAS-CONF-2015-070 (2015) . https://cds.cern.ch/record/2114842.

[223] C.-Y. Chen and P. S. B. Dev, "*Multi-Lepton Collider Signatures of Heavy Dirac and Majorana Neutrinos*," Phys. Rev. **D85** (2012) 093018, arXiv:1112.6419 [hep-ph].

[224] **CMS** Collaboration, S. Chatrchyan *et al.*, "*Search for new physics in events with same-sign dileptons and jets in pp collisions at $\sqrt{s} = 8$ TeV*," JHEP **01** (2014) 163, arXiv:1311.6736. [Erratum: JHEP01,014(2015)].

[225] **Virgo, LIGO Scientific** Collaboration, B. P. Abbott *et al.*, "*Observation of Gravitational Waves from a Binary Black Hole Merger*," Phys. Rev. Lett. **116** (2016) no. 6, 061102, arXiv:1602.03837 [gr-qc].

[226] Z.-z. Xing, "*Massive and Massless Neutrinos on Unbalanced Seesaws*," Chin. Phys. **C32** (2008) 96–99, arXiv:0706.0052 [hep-ph].

[227] E. J. Chun, C. W. Kim, and U. W. Lee, "*Three neutrino Delta m**2 scales and singular seesaw mechanism*," Phys. Rev. **D58** (1998) 093003, arXiv:hep-ph/9802209 [hep-ph].

[228] Y. Chikira, N. Haba, and Y. Mimura, "*The Singular seesaw mechanism with hierarchical Dirac neutrino mass*," Eur. Phys. J. **C16** (2000) 701–705, arXiv:hep-ph/9808254 [hep-ph].

[229] A. Davidson, L. Michel, M. L. Sage, and K. C. Wali, "*Quark mass hierarchies from universal seesaw mechanism*," Phys. Rev. **D49** (1994) 1378–1388.

[230] K. L. McDonald, B. H. J. McKellar, and A. Mastrano, "*(3+2) neutrino scheme from a singular double seesaw mechanism*," Phys. Rev. **D70** (2004) 053012, arXiv:hep-ph/0401241 [hep-ph].

[231] V. Berezinsky, M. Narayan, and F. Vissani, "*Low scale gravity as the source of neutrino masses?*," JHEP **04** (2005) 009, arXiv:hep-ph/0401029 [hep-ph].

[232] M. Lindner, T. Ohlsson, and G. Seidl, "*Seesaw mechanisms for Dirac and Majorana neutrino masses*," Phys. Rev. **D65** (2002) 053014, arXiv:hep-ph/0109264 [hep-ph].

[233] J.-w. Mei and Z.-z. Xing, "*Radiative corrections to neutrino mixing and CP violation in the minimal seesaw model with leptogenesis*," Phys. Rev. **D69** (2004) 073003, arXiv:hep-ph/0312167 [hep-ph].

[234] P. H. Frampton, S. L. Glashow, and T. Yanagida, "*Cosmological sign of neutrino CP violation*," Phys. Lett. **B548** (2002) 119–121, arXiv:hep-ph/0208157 [hep-ph].

[235] S. Bosch, *Lineare Algebra*. Springer-Verlag Berlin Heidelberg, 3 ed., 2006. http://dx.doi.org/10.1007/3-540-29885-1.